SAN DIEGO STATE UNIVERSITY

AND

UNIVERSITY OF CALIFORNIA, SANTA BARBARA

Satellite-derived estimates of herbaceous fractional cover and its influence on fire regime in San Diego County, California, USA shrublands

A Dissertation submitted in partial satisfaction of the

requirements for the degree Doctor of Philosophy

in Geography

by

Krista R. L. West

Committee in charge:

Professor Douglas Stow, Chair, San Diego State University

Professor John O'Leary, San Diego State University

Professor Dar Roberts, University of California, Santa Barbara

Professor Leila Carvalho, University of California, Santa Barbara

Dr. Alexandra Syphard, SDSU Adjunct, Conservation Biology Institute

December 2023

The dissertation of Krista R. L. West is approved.

_____

John O'Leary

_____

Dar Roberts

_____

Leila Carvalho

_____

Alexandra Syphard

_____

Douglas Stow, Committee Chair

December 2023

Satellite-derived estimates of herbaceous fractional cover and its influence on fire regime in San Diego County, California, USA shrublands

ACKNOWLEDGEMENTS

I would like to express my deepest gratitude to my committee for imparting their wisdom, guidance, patience, and encouragement. Doug Stow introduced me to spectral mixture analysis, taught me how to think through research objectives, and challenged me to approach each component of this work critically. I am thankful for the countless hours he spent discussing the perils of herbaceous vegetation in wildfire-prone San Diego County, and for his encouragement to never stop asking questions. Dar Roberts, who has inspired me since my undergraduate years in the Department of Geography at UCSB, shared his expertise of remote sensing approaches and passion for working on projects that will benefit communities at risk of wildfire. John O'Leary taught me about Southern California's shrubland communities and led me on a hike to see the different growth form types firsthand. Leila Carvalho opened my eyes to the world of multi-temporal analyses and broadened my appreciation of Santa Ana winds to include their northern counterpart, Sundowner winds. Alexandra Syphard helped me begin to decipher the myriad of effects that fuels, topography, and weather play on wildfires.

I am extremely grateful for the members of the SDSU and UCSB Departments of Geography who helped me navigate the Joint Doctoral Program (JDP) process. Fernando Bosco and Piotr Jankowski, who both served in the roles of Department Chair and JDP Director at SDSU during my time in the program, were always available to offer mentorship. Candra Young, Anna Daniels, Patti O'Leary, Marcus Chiu, Pete Coulter, and Harry Johnson (SDSU) were extremely helpful in answering all my logistical and technical

questions (and there were many). I also appreciate the help provided by Trisalyn Nelson, Alan Murray, Stuart Sweeney, Dan Montello, Consuelo Rivera, and Kathryn Ficke (UCSB).

Generous financial support was provided by the SDSU Department of Geography; a SDSU University Graduate Fellowship; California Strategic Growth Council's Climate Change Research Program, funded by the California Climate Investments initiative (Agreement #CCRP0061) with the Climate Science Alliance and Connecting Wildlands and Communities project; NASA Earth Science Applications: Equity and Environmental Justice (Data Integration Project #21-EEJ21-0037); the SDSU William and Vivian Finch Award for Remote Sensing, a Remote Sensing Scholarship from the American Society for Photogrammetry and Remote Sensing Pacific Southwest Region; and a Doctoral Scholarship from the United States Geospatial Intelligence Foundation.

I could not have undertaken this journey without my spouse, Dave, who provided endless encouragement, joined me in rugged terrain for field work, and recognized the difference between needing a nudge back to my computer or lacing up our shoes for a run. Special thanks to my parents, Bob and Pam, who instilled in me a love for the outdoors, reading maps, and poring over images of the Earth from above (as well as for teaching me that being a Geography major involved much more than just memorizing country names and state capitols). Each opportunity I've pursued since my undergraduate years has introduced me to new ways to view the world, and I am forever grateful for every person who has inspired me along the way.

VITA OF KRISTA R. L. WEST
December 2023

EDUCATION

Bachelor of Arts in Geography, University of California, Santa Barbara, June 2008 (minor: Geological Sciences)
Master of Science in Remote Sensing Intelligence, Naval Postgraduate School, September 2012
Doctor of Philosophy in Geography, San Diego State University and University of California, Santa Barbara, December 2023 (expected)

PROFESSIONAL EMPLOYMENT

2008-12: Research Associate, Department of Physics, Remote Sensing Center, Naval Postgraduate School
2012-13: Intelligence Specialist, Hyperspectral Imagery Program Manager/Tactician, 497th Operations Support Squadron (OSS), Weapons and Tactics Flight, Distributed Ground State-One (DGS-1)
2014-14: Documentation Specialist, Senior Consultant, Booz Allen Hamilton
2014-15: Business Systems Analyst, Senior Consultant, Booz Allen Hamilton
2015-16: Instructor of Geosciences, Department of Economics and Geosciences (DFEG), United States Air Force Academy (USAFA)
2016-19: Remote Sensing Scientist and Account Manager, Intterra
2019-20: Doctoral Research Associate, San Diego State University Research Foundation
2020-21: Research Fellow, San Diego State University Research Foundation
2021-22: Doctoral Teaching Associate (Instructor of Record), Department of Geography, San Diego State University, Remote Sensing of Environment Laboratory (GEOG 591L) and Geographic Information Science and Spatial Reasoning (GEOG 104)
2022-23: Graduate Assistant, Department of Geography, San Diego State University
2021-present: Remote Sensing Scientist, Solis Applied Science

REFEREED JOURNAL PUBLICATIONS

Kanaev, A. V., Daniel, B. J., Neumann, J. G., Kim, A. M., & **Lee, K. R.** (2011). Object level HSI-LIDAR data fusion for automated detection of difficult targets. *Optics Express, 19(1)*, 20916-20929, DOI: 10.1364/OE.19.020916.

Bachmann, C. M., Montes, M. J., Parrish, C. E., Fusina, R. A., Nichols, C. R., Li, R., Hallenborg, E., Jones, C. A., **Lee, K.**, Sellars, J., White, S. A., & Fry, J. C. (2012). A dual-spectrometer approach to reflectance measurements under sub-optimal sky conditions. *Optics Express, 20(8)*, 8959-8973, DOI: 10.1364/OE.20.008959.

Storey, E., **West, K. R. L.**, & Stow, D. (2020). Utility and optimization of LANDSAT-derived burned area maps for southern California. *International Journal of Remote Sensing, 42(2)*, 486-505, DOI: 10.1080/01431161.2020.1809741.

Roja, I. M., Jennings, M. K., Conlisk, E., Syphard, A. D., Mikesell, J., Kinoshita, A. M., **West, K.**, Stow, D., Storey, E., De Guzman, M. E., Foote, D., Warneke, A., Pairis, A., Ryan, S., Flint, L. E., & Lewison, R. L. (2021). A landscape-scale framework to identify refugia from multiple stressors. *Conservation Biology*, 1-11. DOI: 10.111/cobi.13834

CONFERENCE PROCEEDINGS

Benham, L., Chester, W. K., Eisberg, A., Iyer, S., **Lee, K.**, Marra, J., Schmidt, C., & Skiles, J. W. (2008). Integrating data from NASA missions into NOAA's Pacific Region Integrated Climatology Information Products (PRICIP). AGU.

Benham, L., Chester, W. K., Eisberg, A., Iyer, S., **Lee, K.**, Marra, J., Schmidt, C., & Skiles, J. W. (2009). Integrating data from NASA missions into NOAA's Pacific Region Integrated Climatology Information Products (PRICIP). ASPRS.

Puetz, A. M., **Lee, K.**, & Olsen, R. C. (2009). WorldView-2 data simulation and analysis results. Proc. of SPIE, 7334: Algorithms and Technologies for Multispectral, Hyperspectral, and Ultraspectral Imagery XV, DOI: 10.1117/12.818187.

Kim, A. M., **Lee, K. R.**, Olsen, R. C., & Jablonski, D. (2010). Using panchromatic imagery in place of multispectral imagery for kelp detection in water. Proc. of SPIE, 7678: Ocean Sensing and Monitoring II, DOI: 10.1117/12.850352.

Fusina, R. A., Fry, J. C., Nichols, C. R., Bachmann, C. M., Li, R., Sellars, J., Parrish, C., Montes, M. J., Gross, C., White, S. A., **Lee, K.**, & Jones, C. A. (2010). Geodatabase development to support hyperspectral imagery exploitation. IGARSS, DOI: 10.1109/IGARSS.2010.5654182.

Bachmann, C. M., Nichols, C. R., Montes, M. J., Fusina, R. A., Li, R., Gross, C., Fry, J. C., Parrish, C., Sellars, J., White, S. A., Jones, C. A., & **Lee K.** (2010). Coastal characterization from hyperspectral imagery: An intercomparison of retrieval properties from three coast types. IGARSS, DOI: 10.1109/IGARSS.2010.5650660.

Lee, K. R., Kim, A. M., Olsen, R. C., & Kruse, F. A. (2011). Using WorldView-2 to determine bottom-type and bathymetry. Proc. of SPIE, 8030: Ocean Sensing and Monitoring III, DOI: 10.1117/12.883578.

Mancini, S., Olsen, R. C., Abileah, R., & **Lee, K. R.** (2012). Automating nearshore bathymetry extraction from wave motion in satellite optical imagery. Proc. of SPIE, 8390: Algorithms and Technologies for Multispectral, Hyperspectral, and Ultraspectral Imagery XVIII, DOI: 10.1117/12.945940.

Lee, K. R., Olsen, R. C., & Kruse, F. A. (2012). Using multi-angle WorldView-2 imagery to determine ocean depth near the island of Oahu, Hawaii. Proc. of SPIE, 8390: Algorithms

and Technologies for Multispectral, Hyperspectral, and Ultraspectral Imagery XVIII, DOI: 10.1117/12.918716.

Lee, K. R., Olsen, R. C., & Kruse, F. A. (2012). Determining bathymetry near Oahu, Hawaii ising WorldView-2 imagery acquired at multiple angles. OSA Optical Remote Sensing of the Environment, DOI: 10.1364/ORSE.2012.RM2E.2.

Lee, K. R., Olsen, R. C., Kruse, F. A., & Kim, A. M. (2013). Using multi-angle WorldView-2 imagery to determine bathymetry near Oahu, Hawaii. Proc. of SPIE, 8743: Algorithms and Technologies for Multispectral, Hyperspectral, and Ultraspectral Imagery XIX, DOI: 10.1117/12.2015660.

NAVAL RESEARCH LAB (NRL) REPORTS

Bachmann, C. M., Montes, M. J., Fusina, R. A., Li, R., Gray, D., Korwan, D., Gross, C., Fry, J. C., Nichols, C. R., Ezrine, D. F., Miller, W. D., Jones, C., **Lee, K. R.**, Wende, J., & McConnon, C. (2012). Mariana Islands-Hyperspectral airborne remote environmental sensing experiment 2010. NRL/MR/7230-12-9405.

Bachmann, C. M., Fusina, R. A., Montes, M. J., Li, R., Gross, C., Nichols, C.R., Fry, J. C., Parrish, C., Sellars, J., White, S. A., Jones, C., & **Lee, K. R.** (2012). Talisman-Saber 2009 remote sensing experiment. NRL/MR/7230-12-9404.

CONFERENCE PRESENTATIONS

Puetz, A. M., **Lee, K.**, & Olsen, R. C. (2009). WorldView-2 data simulation and analysis results. Proc. of SPIE, 7334: Algorithms and Technologies for Multispectral, Hyperspectral, and Ultraspectral Imagery XV.

Kim, A. M., **Lee, K. R.**, Olsen, R. C., & Jablonski, D. (2010). Using panchromatic imagery in place of multispectral imagery for kelp detection in water. Proc. of SPIE, 7678: Ocean Sensing and Monitoring II.

Lee, K. R., Kim, A. M., Olsen, R. C., & Kruse, F. A. (2011). Using WorldView-2 to determine bottom-type and bathymetry. Proc. of SPIE, 8030: Ocean Sensing and Monitoring III.

Lee, K. R., Olsen, R. C., & Kruse, F. A. (2012). Using multi-angle WorldView-2 imagery to determine ocean depth near the island of Oahu, Hawaii. Proc. of SPIE, 8390: Algorithms and Technologies for Multispectral, Hyperspectral, and Ultraspectral Imagery XVIII.

Lee, K. R., Olsen, R. C., & Kruse, F. A. (2012). Determining bathymetry near Oahu, Hawaii using WorldView-2 imagery acquired at multiple angles. OSA Optical Remote Sensing of the Environment.

West, K., Stow, D., Sousa, D., & Roberts, D. (2022). Spectral unmixing techniques examined for analysis of herbaceous fractional cover in wildfire-prone shrublands in Southern California, USA. San Diego State University Student Research Symposium.

PAPERS PRESENTED AT SCIENTIFIC MEETINGS (NO PROCEEDINGS PAPER)

Bachmann, C. M., Montes, M. J., Fusina, R. A., Li, R., Gross, C., Nichols, C. R., Fry, J. C., Parrish, C., White, S., Sellars, J., Jones, C., **Lee, K.**, & Hallenborg, E. (2009). Estimation of beach properties and shallow water bathymetry from hyperspectral imagery. GeoTech.

Lee, K. R., Bachman, C. M., Fusina, R. A., Montes, M. J., Li, R., Fry, J. C., Nichols, C. R., Parrish, C., & Sellars, J. (2010). Coastal vegetation mapping from hyperspectral imagery. OSA Optical Remote Sensing of the Environment.

Bachmann, C. M., Nichols, C. R., Montes, M. J., Fusina, R. A., Fry, J. C., Li, R., Gray, D., Korwan, D., Parrish, C., Sellars, J., White, S. A., Woolard, J., **Lee, K. R.**, McConnon, C., & Wende, J. (2010). Coastal characterization from hyperspectral imagery. OSA Optical Remote Sensing of the Environment.

Lee, K. R., Olsen, R. C., & Kruse, F. A. (2011). Using multi-angle WorldView-2 imagery to determine ocean depth near Oahu, HI. ENVI Classified User Symposium (ENVIUS West).

West, K. R. L., Stow, D. A., Sousa, D. J., Roberts, D. A., & O'Leary, J. F. (2023). Unmixing techniques for herbaceous vegetation mapping in Southern California: Landsat spectral unmixing analysis for mapping herbaceous fractional cover in wildfire-prone shrublands of San Diego County, California, USA. American Association of Geographers (AAG).

CONFERENCE POSTERS

Benham, L., Chester, W. K., Eisberg, A., **Lee, K.**, & Iyer, S. (2008). Integrating data from NASA missions into NOAA's Pacific Region Integrated Climatology Information Products (PRICIP) project. NASA Ames Research Center.

Lee, K. R., Bachman, C. M., Fusina, R. A., Montes, M. J., Li, R., Fry, J. C., Nichols, C. R., Parrish, C., & Sellars, J. (2010). Coastal vegetation mapping from hyperspectral imagery. OSA Optical Remote Sensing of the Environment.

Lee, K. R., Olsen, R. C., & Kruse, F. A. (2012). Using WorldView-2 Imagery Acquired at Multiple Angles to Determine Ocean Depth Near Oahu, Hawai'i. Ocean Sciences Meeting.

AWARDS

Akella Family Scholarship, Department of Geography, University of California, Santa Barbara, 2007

DGS-1 497th OSS Civilian of the Quarter, 2013

DGS-1 497th Intelligence, Surveillance, and Reconnaissance Civilian of the Quarter, 2013

USAFA Social Sciences Division Civilian of the Quarter, 2015

USAFA DFEG Geosciences Core Instructor of the Semester, 2015

USAFA DFEG Teacher-Research Excellence (T-REx) Award, 2016

University Graduate Fellowship, San Diego State Graduate and Research Affairs, 2020

William and Vivian Finch Award for Remote Sensing, Department of Geography, San Diego State University, 2021

Remote Sensing Scholarship, Pacific Southwest Region, American Society for Photogrammetry and Remote Sensing, 2021

Doctoral Scholarship, United States Geospatial Intelligence Foundation, 2021

Student Paper Competition: Second Place, Remote Sensing Specialty Group, American Association of Geographers, 2023

FIELDS OF STUDY

Major Field: Geography

Studies in Remote Sensing with Professors Douglas Stow and Dar Roberts

Studies in Landscape Ecology with Professor John O'Leary

Studies in Time-Series Analysis with Professor Leila Carvalho

Studies in Fire Ecology with Dr. Alexandra Syphard

ABSTRACT

Satellite-derived estimates of herbaceous fractional cover and its influence on fire regime in San Diego County, California, USA shrublands

by

Krista R. L. West

Expanding invasive herbaceous vegetation (non-native grasses and forbs or herbs) is replacing portions of native shrublands in San Diego County, California, USA through a grass-fire cycle, which contributes to an increased risk of wildfire ignition and spread as well as a changing fire regime. Despite the association between herb abundance and wildfire risk, remote sensing and image processing approaches for quantification of fractional herb cover in shrublands are not well established, nor is the association between herb fraction and proportion of ignitions. In this research, I comparatively assess the accuracy of herb cover estimation and mapping based on three spectral unmixing models applied to Landsat-derived spectral reflectance and spectral vegetation index data from multiple 2020 dates. Based on the model and methods that most accurately and reliably represent herb cover, I then reconstruct the spatial-temporal distribution of herb growth using Landsat images from 1988, 1997, and 2011 and assess the extent to which herb cover has expanded and replaced woody vegetation cover (1988 to 2020). Finally, I combine the herb cover maps with historical ignition points to evaluate the spatial association between herb fractions and

locations where fires initially ignited and spread (1992 to 2020). When compared to generated reference data, results demonstrate the parsimonious spectral unmixing approach applied to a fall date estimates herb cover at the 10% accuracy level and more accurately than the more sophisticated unmixing models. Absolute change estimates derived from the earliest and most recent herb cover maps show approximately 25% of the study area exhibited an increase in herb cover > 20%, and roughly 5% experienced a decrease in herb < -20%, with the greatest concentration of change occurring in wildland-urban interface areas. Factors most strongly associated with substantial increase in herb cover include fire return interval, drought, proximity to development, and elevation. The results of evaluating historical ignitions in herbs show the largest proportion of ignitions occurred in areas with > 20% herbaceous fractional cover. Results from this study will enable improved detection of sensitive habitats by satellite for wildfire-prone communities and help identify target areas for mitigating and combating the grass-fire cycle.

TABLE OF CONTENTS

LIST OF FIGURES

LIST OF TABLES

I. Introduction

A. Motivation for Research

Non-native grasses and forbs (invasive herbaceous vegetation growth forms or herbs) have fueled some of the world's most destructive and deadliest wildfires. Invasive herbs contribute to the positive feedback loop called the grass-fire cycle (D'Antonio & Vitousek, 1992; Halsey & Syphard, 2015; Keeley, 2001). This occurs when herbs invade, expand, and convert native shrublands and forest ecosystems following a landscape disturbance like wildfire. The presence of herbs, which are fine plant structures that become flammable fuels when dry and dead, can lead to more frequent and intense fires that spread rapidly and widely among high fuel loads, particularly during a high temperature and low humidity extreme wind event. Ultimately, replacement of the native vegetation by invasive herbs can have far-reaching impacts – loss of ecological services; decrease in biodiversity due to threats to endemic and endangered flora and fauna; increase in a landscape's flammability; and post-fire susceptibility to further herb invasion (Syphard *et al.*, 2018; Syphard *et al.*, 2019). Detection of herbs at a regional level, particularly when combined with historical wildfire data and knowledge about changing climate, can aid pre-fire mitigation and post-fire vegetation recovery efforts. Observation of herbaceous vegetation change over time can inform fire regime change monitoring.

In this dissertation, I apply and validate herbaceous vegetation cover mapping and change monitoring approaches based on Landsat multispectral satellite image data. This is achieved by mapping and reconstructing the distribution of herbaceous vegetation in relation to wildland areas and the wildland-urban interface (WUI) of San Diego County, California,

USA based on a time sequence derived by spectral unmixing techniques. I combine the resulting herb cover maps with historical wildfire ignition data to analyze the association between herb fractional cover and the proportion of ignitions. I identify the herb interval classes in which a disproportionate number of ignitions occurred. As populations in WUI areas continue to increase, it is critical that additional research be performed and that products be created and shared with first responders, policy makers, and WUI residents.

B. Overview of Chapters

In Chapter II, "Landsat spectral unmixing analysis for mapping herbaceous fractional cover in wildfire-prone San Diego County, California, USA shrublands (2020)," I comparatively assess the accuracy of herb cover estimation and mapping based on three different unmixing models applied to Landsat satellite multispectral image data from multiple dates in 2020. The models include spectral mixture analysis (SMA), multiple endmember spectral mixture analysis (MESMA), and temporal mixture model (TMM) analysis. I evaluate single date, multi-date (intra-annual), and spectral reflectance and spectral vegetation index (normalized difference infrared index (NDII) and normalized difference vegetation index (NDVI)) combinations. I address the following research question: How well can remote sensing and image processing approaches be used to identify and quantify herbaceous vegetation cover in San Diego County?

I expand upon the work from Chapter II in Chapter III, "Spectral unmixing of a Landsat time sequence to reconstruct herbaceous fractional cover dynamics in wildfire-prone San Diego County, California, USA shrublands (1988-2020)." I reconstruct the spatial-temporal distribution of herb growth form cover using SMA applied to Landsat data over a 33-year period at nearly decadal intervals. I assess the accuracy of the herb cover change results, as

well as the degree of uncertainty. I address the following research questions: (1) When spectral unmixing models are applied to imagery covering a multi-decadal period in the San Diego County study area, how reliable and accurate are maps of herbaceous cover change? (2) Where within the study area did substantial change in herbaceous fractional cover occur and do areas of substantial change appear to coincide with wildfire frequency or drought effects occurring within the study period?

I combine historical ignition point data and the Landsat-derived, spectrally unmixed herbaceous cover maps from Chapter III to determine whether fires ignited in low, intermediate, or high herb fractional cover interval classes for Chapter IV, "Evaluation of herbaceous cover fraction and wildfire ignition association in San Diego County, California, USA shrublands (1992-2020)." I compare proportions of ignitions in Federal versus Non-Federal lands, and complete five exploratory analyses: all ignitions, human-caused ignitions, naturally-caused ignitions, ignitions resulting in a multi-date fire, and ignitions resulting in a large fire size. I address the following research question: Are differences in the spatial distribution of wildfire ignitions associated with differences in herbaceous fractional cover in San Diego County shrublands for 1992 to 2020?

In Chapter V, "Conclusion," I summarize the results of each preceding chapter based on the overall objectives. I highlight key contributions and findings of the results. I conclude with recommendations for next steps for future research directions.

II. Landsat spectral unmixing analysis for mapping herbaceous fractional cover in wildfire-prone San Diego County, California, USA shrublands (2020)

A. Introduction

In regions with Mediterranean-type climates, expansion of non-native grasses and forbs (invasive herbaceous vegetation or herbs) can lead to more frequent and intense wildfires that can spread rapidly and widely in landscapes with high fuel loads and fine fuel biomass (Balch *et al.*, 2013; Knapp, 1998; Link *et al.*, 2006). As a flammable and "flashy" fuel, herbs contribute to a positive feedback loop which has been named the grass-fire cycle (D'Antonio & Vitousek, 1992; Halsey & Syphard, 2015; Keeley, 2001). Invasion of non-native herbaceous vegetation following a wildfire or other landscape disturbance can cause a decline in native shrubs, trees, and herbs, which allows for additional non-native herbaceous cover expansion, and thereby increases the likelihood of future fire. Ultimately, invasive herbs can completely replace native vegetation (Syphard *et al.*, 2018), which can have far-reaching impacts via loss of ecological function, diminished ecosystem services, and increased flammability of the landscape (Syphard *et al.*, 2019). Habitat loss threatens endangered flora and fauna and leads to a decrease in biodiversity, and this change or disturbance in landscapes often leads to susceptibility of invasion by herbaceous species.

Native Southern California shrubland communities are populated by a morphological mixture of true shrubs and subshrubs (Keeley, 2000; Lippitt *et al.*, 2017; Pryde, 2004). True shrubs include chamise (*Adenostoma fasciculatum*) chaparral and mixed chaparral communities, and subshrubs found in coastal sage scrub (e.g., *Artemisia californica*,

Eriogonum fasciculatum, and *Salvia* species) communities. Chaparral is the evergreen sclerophyllous shrubland that dominates the cismontane side of coastal mountain ranges, growing mostly below 2,000 m in elevation (Keeley & Davis, 2007). Chaparral communities are closely associated with the Mediterranean-type climate pattern of winter rain and summer drought (Keeley & Davis, 2007). Sage scrub communities generally occur from sea level up to 500 m in elevation, where they intergrade with chaparral in an ecotone. Undisturbed sage scrub has an herbaceous understory of native grasses and forbs, whereas chaparral does not (Rundel, 2007). Both shrubland types are often replaced by mostly disturbance-dependent annual non-native grasslands following wildfire (Huenneke, 1989; Keeley & Davis, 2007). Repeated fires at short intervals are a common cause of conversion of interior sage scrub to grasslands dominated by non-native annual species (Rundel, 2007).

Herbs are vascular plants that lack perennial aboveground woody stems, with perennating buds borne at or below the ground surface, and include forbs, graminoids, and herbaceous vines (FGDC, 1997; Whittaker, 1975). In Southern California, the most common non-native herbs that invade disturbed shrublands include grasses like wild oats (*Avena fatua*), foxtail chess (*Bromus madritensis*), and ripgut (*Bromus diandrus*); and non-grass invaders like filaree (*Erodium* species), mustard (*Brassica* species), and various thistles. These invasive herbaceous annuals quickly fill in disturbed areas because they germinate earlier than native herbs following rainfall, grow faster, and have more aggressive seed dispersal mechanisms (Halsey, 2008). Balch *et al.* (2013) claimed that shrubland/grassland fires represent "the greatest hazard for fire management."

Plant phenology, defined as the seasonal change in biological life because of changing conditions (Dudley *et al.*, 2015; Lieth, 1974), can provide a useful source of information for

separating vegetation growth forms, particularly herbaceous and subshrub. Herbs and shrubs tend to have high reflectance in the near infrared (NIR) region of the electromagnetic spectrum during the wet season. During the dry season, herbs and bare ground have comparably high reflectance through the visible and NIR spectral range. Additionally, seasonal signals between wet and dry seasons (wet-to-dry and dry-to-wet transition periods) are evident in soil moisture timeseries (Araki *et al.*, 2022), which affects the aboveground vegetation and is critical for vegetation growth in water-limited Mediterranean-type landscapes. Thus, spectral separability between shrubs and herbs or herbs and bare ground can be problematic if data from only one season are used (Hamada *et al.*, 2009).

Spectral mixture analysis (SMA), also known as linear spectral unmixing, assumes that the ground area sampled by a pixel can be reasonably approximated by a fractional mixture of a small number of spectrally distinct materials (Adams *et al.*, 1986; Gillespie *et al.*, 1990; Roberts *et al.*, 1998; Settle & Drake, 1993; Smith *et al.*, 1990). SMA considers the radiance (or reflectance) of a mixed pixel to be an area-weighted linear combination of spectral endmember (EM) materials, plus error. An EM is a "pure" representation of a material and its spectrum (Adams *et al.*, 1993). An advantage of SMA is that it can be used to determine the fraction (abundance) of materials or land cover types within the ground resolution element (GRE) associated with an image pixel, compared to traditional classifiers that identify and assign a single material to a pixel (Lippitt *et al.*, 2017). SMA is also a biophysically based model (Adams *et al.*, 1993; Roberts *et al.*, 1998) that is computationally efficient and simplistic. However, a drawback of SMA is that only one set of EMs is used to model all pixels and so does not explicitly account for EM variability (Lippitt *et al.*, 2017). Vegetation fractions produced by SMA have been used to describe land cover change

(Dennison & Roberts, 2003; Nill *et al.*, 2022; Roberts *et al.*, 2002; Rogan *et al.*, 2002) and vegetation regeneration after disturbance (Dennison & Roberts, 2003; Riano *et al.*, 2002).

Multiple endmember spectral mixture analysis (MESMA) is an extension of SMA, in which the number and types of EM are allowed to vary on a per-pixel basis. It accounts for variability in the spectral dimensionality between pixels, and spectral variability within an EM class, reducing fraction errors resulting from the use of a single EM set (Roberts *et al.*, 1998). All possible two-, three-, four-, five-, and six-EM model combinations can be tested for each pixel, and then optimum models are selected based on the model with the lowest root mean square error (RMSE) that meets fraction and residual constraints (Roberts *et al.*, 1998). Vegetation fractions produced by MESMA have been used to estimate vegetation cover (Hamada *et al.*, 2011; Roberts *et al.*, 1998; Singh & Gray, 2020) and assess and monitor vegetation growth form change over time (Dudley *et al.*, 2015; Hamada *et al.*, 2012; Lippitt *et al.*, 2017).

Temporal mixture models (TMMs) extend the conceptual model of SMA to the temporal domain (Piwowar *et al.*, 1998; Quarmby, 1992; Quarmby *et al.*, 1992). Rather than representing each pixel spectrum as a linear combination of constituent EM materials, TMMs treat each pixel time series as a linear combination of EM processes (Small, 2012; Sousa & Small, 2019). TMMs have recently been applied to California oak woodlands (Sousa & Davis, 2020), but detailed accuracy assessment for herb cover mapping has yet to be performed. Vegetation fractions produced by TMM analyses have been used to map seasonal cloud forest/grassland systems (Sousa *et al.*, 2019), tropical mangrove forests (Small & Sousa, 2019), and agricultural dynamics (Jain *et al.*, 2013; Lobell & Asner, 2004; Quarmby *et al.*, 1992; Sousa & Small, 2019).

The normalized difference infrared Index (NDII) computes the normalized spectral slope between NIR and shortwave infrared (SWIR) spectral regions. NDII has been found to be sensitive to the optical properties of soil (Hernández-Clemente *et al.*, 2009), plant tissue structure or biomass, and water content (Hardinsky *et al.*, 1983). NDII is computed as:

$$NDII = (SWIR - NIR) / (SWIR + NIR)$$

The normalized difference vegetation index (NDVI) computes the normalized spectral slope between red and NIR reflectance values (Rouse *et al.*, 1973). NDVI has been used for decades to monitor seasonal and inter-annual changes in vegetation growth and activity. As a normalized index, it reduces topographic illumination and atmospheric effects that may be present in satellite-derived surface reflectance (SR) data (Díaz-Delgado *et al.*, 2002; Jensen, 2016; Peña-Barragán *et al.*, 2011; Rouse *et al.*, 1973). NDVI is computed as:

$$NDVI = (NIR - Red) / (NIR + Red)$$

Spectral unmixing is fundamentally dependent upon EM selection. EMs may be selected geographically based on knowledge of the area being studied, through a process (such as in VIPER Tools for SMA or MESMA, or from the principal components analysis (PCA) output for TMMs), from simulated radiative transfer models, or from a spectral library built from spectra collected in a lab or on the ground during field work using portable spectroradiometers (Somers *et al.*, 2011).

The objective of this study was to develop and test three approaches for quantifying herbaceous vegetation cover in San Diego County, California, USA. SMA, MESMA, and TMMs were applied to single and multi-date (intra-annual) Landsat imagery. Multi-date image inputs for improvement of spectral unmixing accuracy when estimating herb cover, compared to single date SR and spectral index (NDII and NDVI) inputs alone, were

evaluated. In so doing, I sought to answer the following question: How well can remote sensing and image processing approaches be used to identify and quantify herbaceous vegetation cover in San Diego County?

B. Data and Methods

1. Study Area

The study domain is the 795,463 ha of the Southern California Mountains and Southern California/Northern Baja Coast U.S. Environmental Protection Agency (EPA) level III ecoregions (Griffith *et al.*, 2016; U.S. EPA, 2013) within San Diego County (Figure 1). Areas under built, urban, and agricultural land use were considered as "Developed" and masked from analysis, in addition to an area in the southeast portion of the study domain that is not covered by the Landsat scenes used in this study.

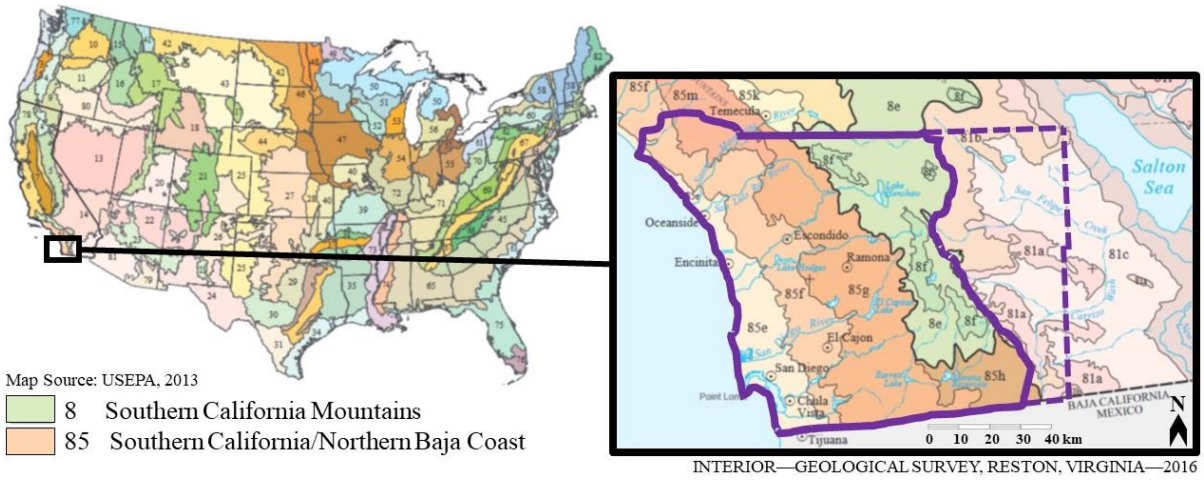

Figure 1. Study area location within San Diego County. Left: U.S. with the focus area delineated in black. Right: Department of the Interior (DOI)/U.S. Geological Survey (USGS)/U.S. Environmental Protection Agency (EPA) (Level III) Ecoregions with the 795,463 ha San Diego County study domain (delineated in solid purple) within the San Diego County extent (shown in dashed purple line).

The study domain has a semi-arid Mediterranean-type climate that experiences moderate winter precipitation (250 to 1,000 mm) and warm to hot, dry summer seasons (26 to 37 °C)

(Hamada *et al.*, 2009). The shrubland habitats cover a range of topographic variability that have experienced differences in land use and fire history (Lippitt *et al.*, 2017).

Growth form types in the wildland area include herbaceous, true shrubs, subshrubs, and trees, with bare ground (soil and rock substrate) also composing the GRE associated with a Landsat pixel. The California shrublands in this study area are commonly invaded by exotic herbs (Keeley, 2001; Park *et al.*, 2018), and thus have a mix of native and non-native herb species (D'Antonio *et al.*, 2007; Park *et al.*, 2018). Differentiation of non-native from native herbs was not attempted for this study, as their Landsat SR signatures are not generally separable (Olsson *et al.*, 2011).

2. Landsat Image Data

A single-year time series of NASA/USGS Landsat imagery was used to quantify herbaceous cover for the year 2020. All Landsat 8 Operational Land Imager (OLI) SR (Collection 2, Level-2, path/row 40/37) 30 m GRE data products from USGS EarthExplorer with less than 10% cloud cover were reviewed. Ten cloud-free images from eight months of 2020 were used (Table 1).

Table 1. Landsat 8 OLI image information for path/row 40/37 in 2020 selected for this study. Acquisition dates, land cloud cover percentages, sun elevation, and sun azimuth are reported.

Acquisition Date (YYYY/MM/DD)	Land Cloud Cover	Sun Elevation	Sun Azimuth
2020/01/18	0.35	31.58	153.38
2020/04/23	0.11	61.95	131.39
2020/06/10	0.03	68.57	112.56
2020/06/26	0.66	68.05	110.93
2020/08/29	0.06	58.64	135.55
2020/09/30	0.01	49.49	150.17
2020/10/16	0.08	44.31	155.08
2020/11/17	0.18	34.94	159.49
2020/12/03	0.03	31.71	159.30
2020/12/19	0.06	30.02	157.89

3. Aerial Image Data

Orthoimagery was used for reference data generation and accuracy assessment. National Agriculture Imagery Program (NAIP) four-band (visible and NIR) (0.6 m GRE) from spring 2020 from USGS EarthExplorer and Nearmap three-band (visible) data (as fine as 0.06 m GRE) from all seasons of 2020 were acquired (Table 2).

Table 2. NAIP and Nearmap orthoimage acquisition dates over the San Diego County study domain in 2020. Seasons are defined by meteorological start dates.

Orthoimagery	Spatial Resolution (m)	Acquisition Dates (YYYY/MM/DD)
NAIP	0.6	Spring: 2020/04/15, 2020/04/25, 2020/04/28, 2020/05/20, 2020/05/25
Nearmap	0.06	Winter: 2020/01/03, 2020/01/04, 2020/01/05, 2020/01/06, 2020/01/11 Spring: 2020/05/01, 2020/05/20 Summer: 2020/07/19 Fall: 2020/09/05, 2020/09/21, 2020/09/22

4. Map Data

National Land Cover Database (NLCD) 2019 data from USGS were used to create a mask of urban and developed land cover and surface water (lakes, reservoirs, and woody wetlands) classes prior to unmixing (Figure 2, right). Application of the NLCD cover mask to the Landsat data resulted in an area of 545,674 ha, hereafter referred to as the San Diego County study area.

Historical fire polygons from the California Department of Forestry and Fire Protection (CAL FIRE) Fire and Resource Assessment Program (FRAP) were used to identify areas that had burned within four years before and the year of image acquisition (2016 to 2020) (CAL FIRE FRAP, 2021). The five-year period was selected based on the regrowth trajectories and postfire recovery findings of chamise chaparral (Lippitt *et al.*, 2013; Storey *et al.*, 2016; Syphard *et al.*, 2019). Reference sampling grids were not generated at these burned locations (Figure 2, right). These burned land areas were not masked for unmixing.

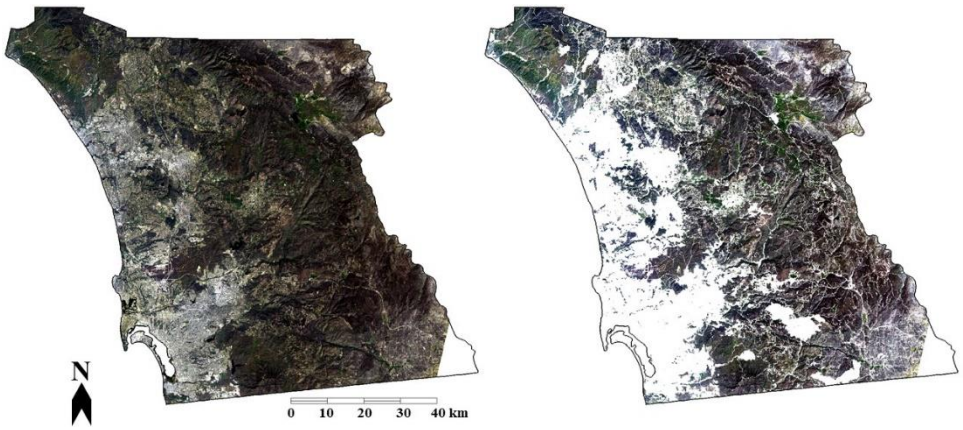

Figure 2. Study area location within San Diego County, California. Left: Landsat 8 OLI from 2020/04/23 acquired over the study domain (795,463 ha). Right: The study area with NLCD developed areas, surface water, the southeast portion not covered by Landsat (545,674 ha), and CAL FIRE FRAP burned areas from 2016 to 2020 masked (14,509 ha burned during this five-year period).

5. Field Data

To supplement the Landsat and aerial image data and provide context for reference data generation, true color geolocated field photos were acquired during the 2021 calendar year with an iPhone XS within Mission Trails Regional Park (MTRP) (Figure 3).

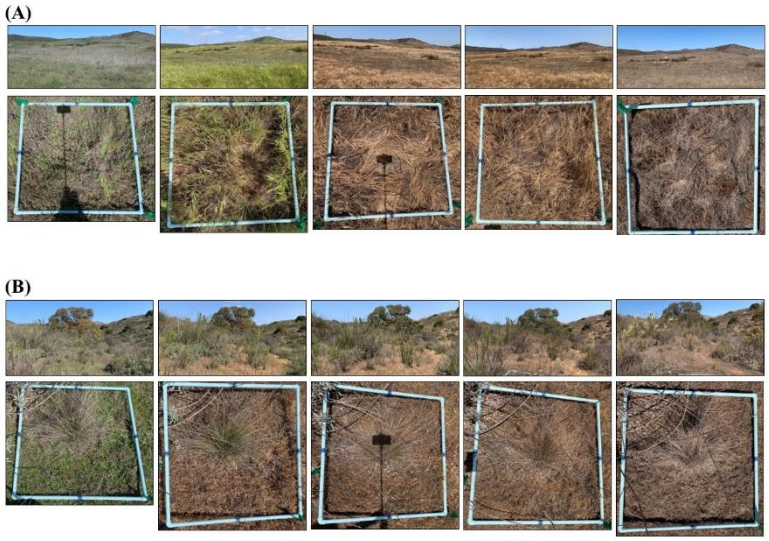

Figure 3. Field-level images captured from the same locations within MTRP over different dates in 2021 depicting phenological changes at a landscape-level view and overhead with a 1 m x 1 m quadrat for scale. (A) Images captured in a grassland area depict very high herbaceous fractional cover. (B) Images captured in an area with true and subshrub, as well as herb and bare ground. Dates (left to right, MM/DD): 03/19, 04/16, 05/08, 06/19, and 10/17.

6. Landsat Data Preparation

Image data preparation and mixture modeling were applied to the Landsat images using ENVI 5.6.3 + IDL 8.8.3 and ENVI Classic with VIPER Tools 2.0 software. Processed satellite, aerial, and map data were analyzed with ENVI and ArcGIS Pro 2.8.3 software.

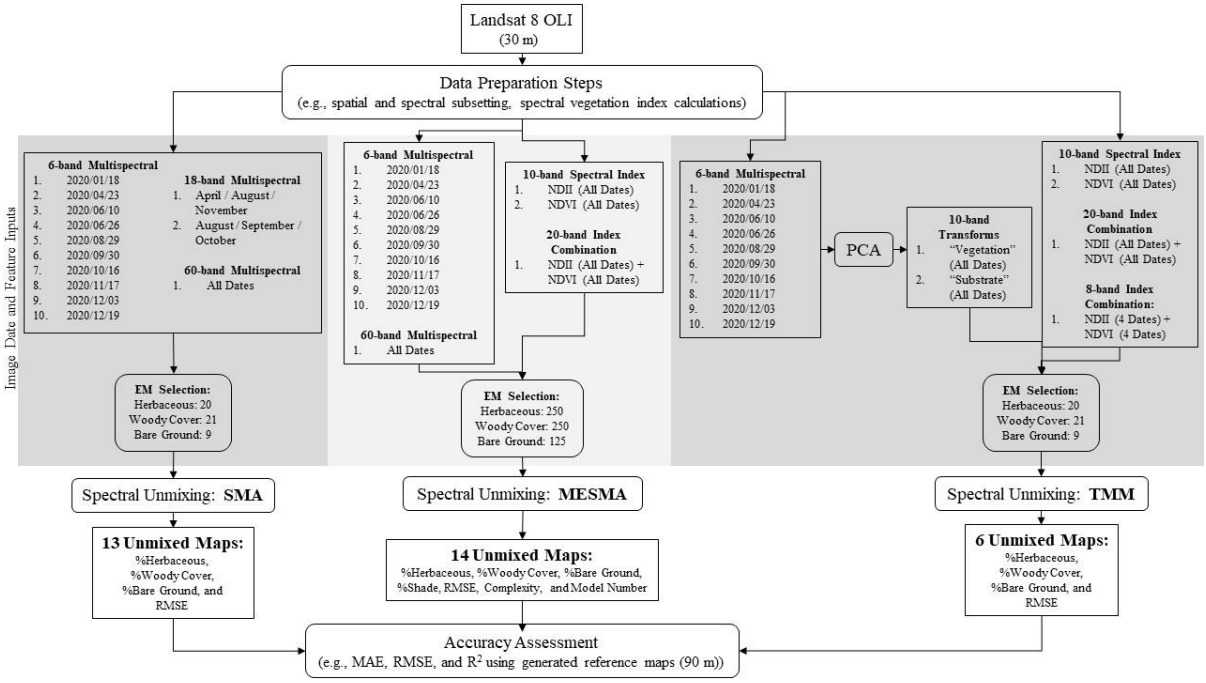

Figure 4. Image processing workflow. Lists of each image date and feature input that were tested, along with the number of EMs per model tested, are shown in the gray boxes. From left to right, SMA, MESMA, and TMM unmixing steps were used on the listed inputs, and a total of 33 unmixed maps were produced.

USGS-provided scale factors were applied to all Landsat SR images. Data were spatially subset to the smallest common areal extent of coverage (04/23) within the San Diego County study area. Data were spectrally subset to remove the Coastal band (resulting in six reflectance bands: Blue through SWIR 2 (0.433 to 1.390 μm)). Image date and feature inputs were prepared for use with two tactics (single date and multi-date time series) for three approaches (SMA, MESMA, and TMMs). Single date six-band multispectral data inputs were used with SMA and MESMA steps to unmix each date individually; multi-date stacks of spectral data were also unmixed. For multi-date spectral index inputs used with MESMA

and TMMs, band math was used to calculate and output NDII and NDVI data sets. Output values ranged between -1.00 and 1.00. All dates were stacked to create a multi-date NDII file, a multi-date NDVI file, and files that contained combined NDII and NDVI dates. Multispectral multi-date combinations were also created (Figure 4).

7. Spectral Unmixing

Regions of interest (ROIs) representing the purest pixels or pixel groups which primarily represent a single vegetation growth form type (herbaceous or woody cover (true shrub, subshrub, and tree)) and bare ground (soil and rock) were selected to derive EM signatures. Selection of the individual and grouped 30 m x 30 m pixel ROIs were based on visual interpretation of the Landsat, NAIP, and Nearmap images and the field sources, and by selecting apexes of feature space data clouds (Boardman, 1993; Peterson & Stow, 2003; Sousa & Davis, 2020). For SMA and TMMs, the same nine-to-21 pixels per land cover class were selected to derive EM signatures; the values of these pixels were averaged to create a single pixel EM per land cover type. For MESMA, ROI polygons totaling 125-to-250 pixels per land cover class were identified; a high number of pixels were used for the MESMA process to capture both within and between ROI variability to portray the true spectral diversity of each EM (Roberts *et al.*, 2019b). The ROIs were used to create a unique spectral library for each image date and set of feature inputs. A total of 33 Landsat multispectral band and spectral index combinations were tested as image date and feature inputs for the three different unmixing model approaches.

For SMA (Figure 4, left), each of the ten separate dates (six spectral bands each), two three-date multispectral combinations (18 spectral bands each), and a ten-date multispectral combination (60 spectral bands) were tested separately, resulting in 13 unmixed outputs.

Each image date and combination, and the set of spectral signatures for EMs for each data set, were selected as the inputs. A unit sum constraint with a weight of 1.00 (equating to 100% cover) was set.

For MESMA, VIPER Tools v. 2.0 (Roberts *et al.*, 2019a), an ENVI Classic add-on, was used to test two sets of feature inputs – multispectral image dates and a multi-date combination, and spectral index inputs and an index combination – resulting in 14 unmixed outputs (Figure 4, middle). For the first set, each of the ten separate dates (six spectral bands each) and the ten-date multispectral file (60 spectral bands) were modeled. For the second set, the band stacked ten-date NDII (ten bands), the band stacked ten-date NDVI (ten bands), and a combined ten-date NDII and NDVI (ten dates each, 20 bands total) data sets were modeled.

Each of the 14 image date and feature inputs were processed with VIPER Tools and the same steps were applied for each individual test. First, ROI metadata were created, and second, a spectral library using the ROI file with polygons per land cover type was created. Third, a square array was calculated for the spectral library and fraction constraints were set from -0.05 to 1.05 (equating to -5 to 105% cover) with a maximum allowable RMSE of 0.025. Fourth, a spectral library was optimized based on calculated metrics: Endmember Average RMSE (EAR) (Dennison & Roberts, 2003), Minimum Average Spectral Angle (MASA) (Dennison *et al.*, 2004), and Count Based (CoB) EM selection (Roberts *et al.*, 2003) (EAR/MASA/CoB (EMC)), resulting in one-to-three EMs per land cover type unique to each spectral band image date or spectral index input (for a total of three-to-nine EMs). It is possible for this selection strategy to result in the same EM for a land cover type, so fewer than three pixels per class may be selected. Fifth, spectral unmixing steps were used. For

each feature input, the scale factor was set to 1.00, the associated EMC spectral library was selected, three mixture model schemes of varying complexity (two-, three-, and four-EM models) with an absolute threshold of 0.001 were selected, and the unmixing constraints were set to -0.05 and 1.05 for fractional cover. All other options were left at the default values.

For TMMs, two sets of data were tested, resulting in six feature outputs (Figure 4, right). For one set, PCA was used on each of the ten multispectral dates to distill the spectral bands down, and from which the apexes of principal component data clouds in two-dimensional feature space were used to identify vegetation, substrate, and dark categories. Stacks of all the vegetation and substrate outputs (one band per each of the ten dates) were generated, resulting in two ten-date (ten bands) outputs: "Vegetation" and "Substrate." Due to spectral confusion of vegetation and herbaceous cover types compared to substrate, depending on the season, both were tested. The "Vegetation" and "Substrate" inputs were unmixed using the same location-based pixel EMs selected from the images for the previous SMA steps and a unit sum constraint with a weight of 1.00 was set.

The second set of inputs included the band stacked ten-date NDII and NDVI data sets, the combined ten-date NDII and NDVI (ten dates each, 20 bands total), and a stack of the four NDII and four NDVI outputs (four dates each, eight bands total) that had the strongest seasonal signals. Again, each test input was unmixed using the same location-based pixel EMs selected from the images for the previous SMA steps, and a unit sum constraint with a weight of 1.00 was set.

8. Reference Data Generation

Reference data used for accuracy assessment were generated by visual image interpretation of the multi-date NAIP and Nearmap orthoimagery. A 150-by-150 grouping of NAIP pixels equivalent to three-by-three Landsat pixels (90 m x 90 m or 0.81 ha) was used to estimate fractional cover. Hereafter, the three-by-three Landsat pixel equivalent is referred to as the sampling grid. Use of a sampling grid that is larger than a single Landsat pixel accounts for uncertainty in the co-registration of NAIP and Nearmap pixel groupings relative to Landsat pixels (Hogland & Affleck, 2019; Shih *et al.*, 2020). A regularly spaced grid was generated and overlaid on the Landsat data and 100 systematically aligned individual sampling grids from eight areas of interest (AOIs) (i.e., subareas within the study area, labeled based on nearby landscape features of interest) were created (Figure 5).

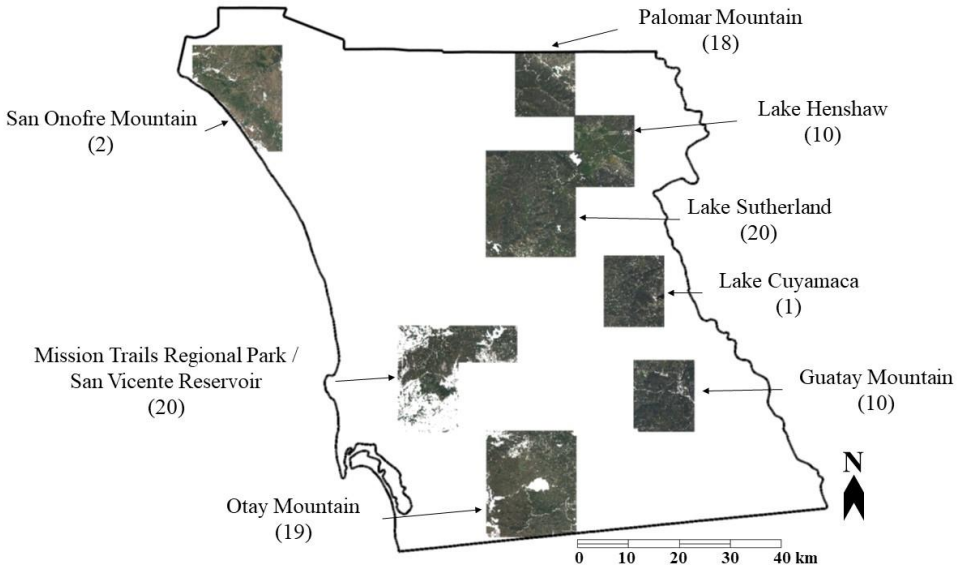

Figure 5. Locations of eight AOIs within the San Diego County study area used to assess the accuracy of herb fractional cover estimates. The number following each AOI label represents the number of 90 m x 90 m sampling grids used to generate reference data within that AOI. AOIs were selected based on the presence of locations with high herbaceous fractional cover, locations with a range of true shrub and subshrub growth form cover, accessibility for field work, and different time-since-burn dates. Image data: Spring 2020 NAIP airborne orthoimages with NLCD areas and 2016 to 2020 burned areas (CAL FIRE FRAP) masked.

Sampling grids included a variety of landscape cover types, different cover fraction values, and multiple slope aspects. Additionally, the sampling grids were representative of the full study area, had burned in a wildfire incident anywhere between zero and four times between 1910 and 2020, and were separated by a minimum distance of 100 m from one another. For each of the 100 sampling grids, a 100-point dot grid was created for visual image interpretation of the cover type located at each of the 100 points (Figure 6). Land cover type information for all points was recorded in an attribute table as herbaceous, woody cover, or bare ground, and fractional cover values per sampling grid were calculated.

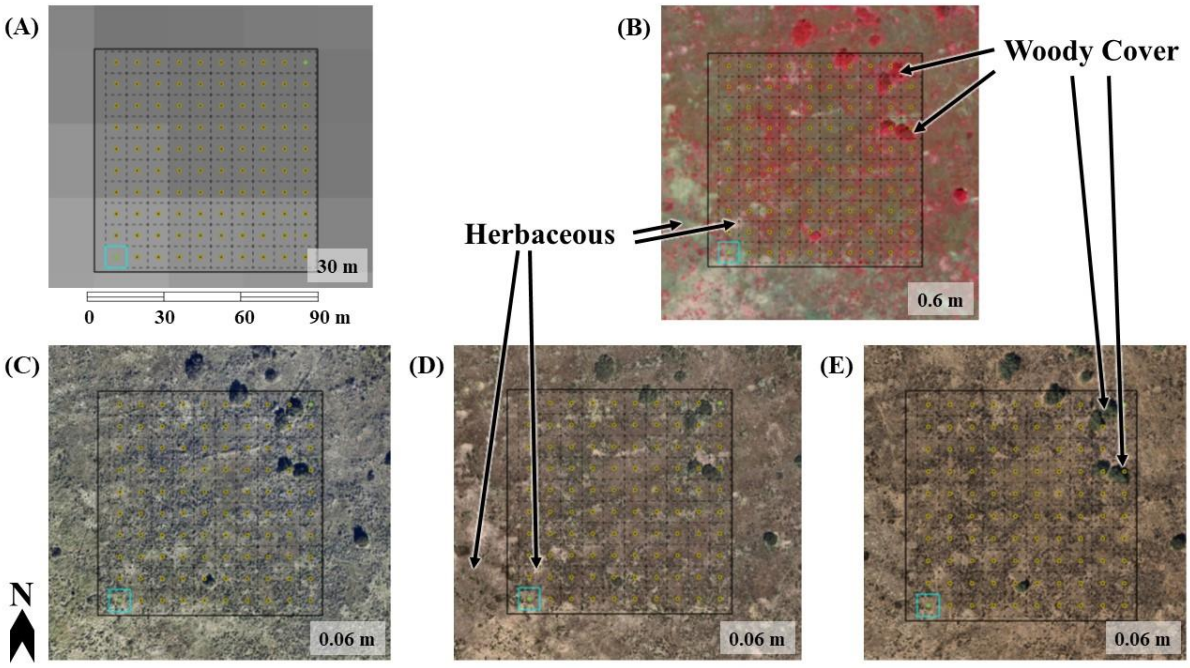

Figure 6. Examples of a single sampling grid with the 100-point dot grid and 2020 imagery. (A) The size of Landsat pixels within the sampling grid. (B) A false color NAIP image (MM/DD: 05/20). (C) through (E) True color Nearmap images (left to right, MM/DD): 01/04, 05/01, 09/22. Arrows point to examples of herbaceous vegetation and woody cover in the scene.

9. Accuracy Assessment

The accuracy of herbaceous cover proportions was quantified using the generated reference data. Each of the 33 resulting predicted cover fractions were assessed for accuracy

based on the following metrics: mean absolute error (MAE), RMSE, and coefficient of determination (R^2). Fractional cover values for individual Landsat pixels were aggregated to match the sampling grids. Simple linear regression models were run and scatterplots of unmixed results for %Herbaceous (the dependent, or modeled, variables) versus generated reference data for %Herbaceous (the independent, or interpreted, variables) were produced. A best fit line was calculated to assess systematic error and determine whether herb cover outputs were underpredicting or overpredicting herb cover (Lippitt *et al.*, 2017; Peterson & Stow, 2003; Uyeda *et al.*, 2016).

The spectral band, spectral index, or combination result from SMA, MESMA, or TMMs that had the lowest MAE and RMSE and highest R^2 values were selected for visual/descriptive analysis. Patterns of herbaceous cover were visually analyzed relative to the NAIP and Nearmap orthoimagery. The goal of this analysis was to determine whether the output map appeared reasonable based on the distribution and location of different land cover types and where the highest and lowest percentages of herb cover were located. Results were also compared to the Rangeland Analysis Platform's (RAP) vegetation cover product from 2020 (Jones *et al.*, 2018). RAP provides annual fractional cover estimates (1986 to 2022), and unmixed outputs from this study were compared to the RAP estimates for annual forbs and grasses, perennial forbs and grasses, and litter (combined and considered to be herbaceous growth forms) (Allred *et al.*, 2021; Jones *et al.*, 2018; Jones *et al.*, 2021).

C. Results

Following the steps in the workflow (Figure 4), 33 sets of fractional cover maps were produced: 13 from SMA, 14 from MESMA, and six from TMMs. The outputs of all

unmixing approaches were maps of %Herbaceous for the entire San Diego County study area for 2020, at a GRE of 30 m, with land use/land cover areas not of interest masked. Accuracy and error statistics are presented in Tables 3 through 6 for each of the three unmixing approaches and include the raw values, raw values with min-max normalization applied, and raw values constrained to range from 0.00 to 1.00 (0 to 100% cover). Mixture model output values were not fully constrained to the set unit sum constraint of 1.00 (100% for SMA and TMMs) or -0.05 to 1.05 (-5 to 105% for MESMA). As each image date and feature input set resulted in a different range of output values, the values from each output data set were converted to a value between 0.00 and 1.00 (0 to 100%) using a min-max normalization method using the formula:

$$Normalized\ Value = \frac{(Original\ Value - Minimum\ Value)}{(Maximum\ Value - Minimum\ Value)}$$

(Jin *et al.*, 2015a). Also, output values for each image date and feature input were constrained – negative values were set to 0.00, values greater than 1.00 were set to a maximum value of 1.00, and all other values between 0.00 and 1.00 were not adjusted.

Constrained herbaceous cover outputs from each SMA image date are displayed in Figure 7, and the associated output values are listed in Table 3. Herbaceous cover was most accurately estimated by the SMA model's constrained 2020/08/29 date with MAE = 8.85%, RMSE = 12.02%, and R^2 = 0.85 (Table 3, Figure 8).

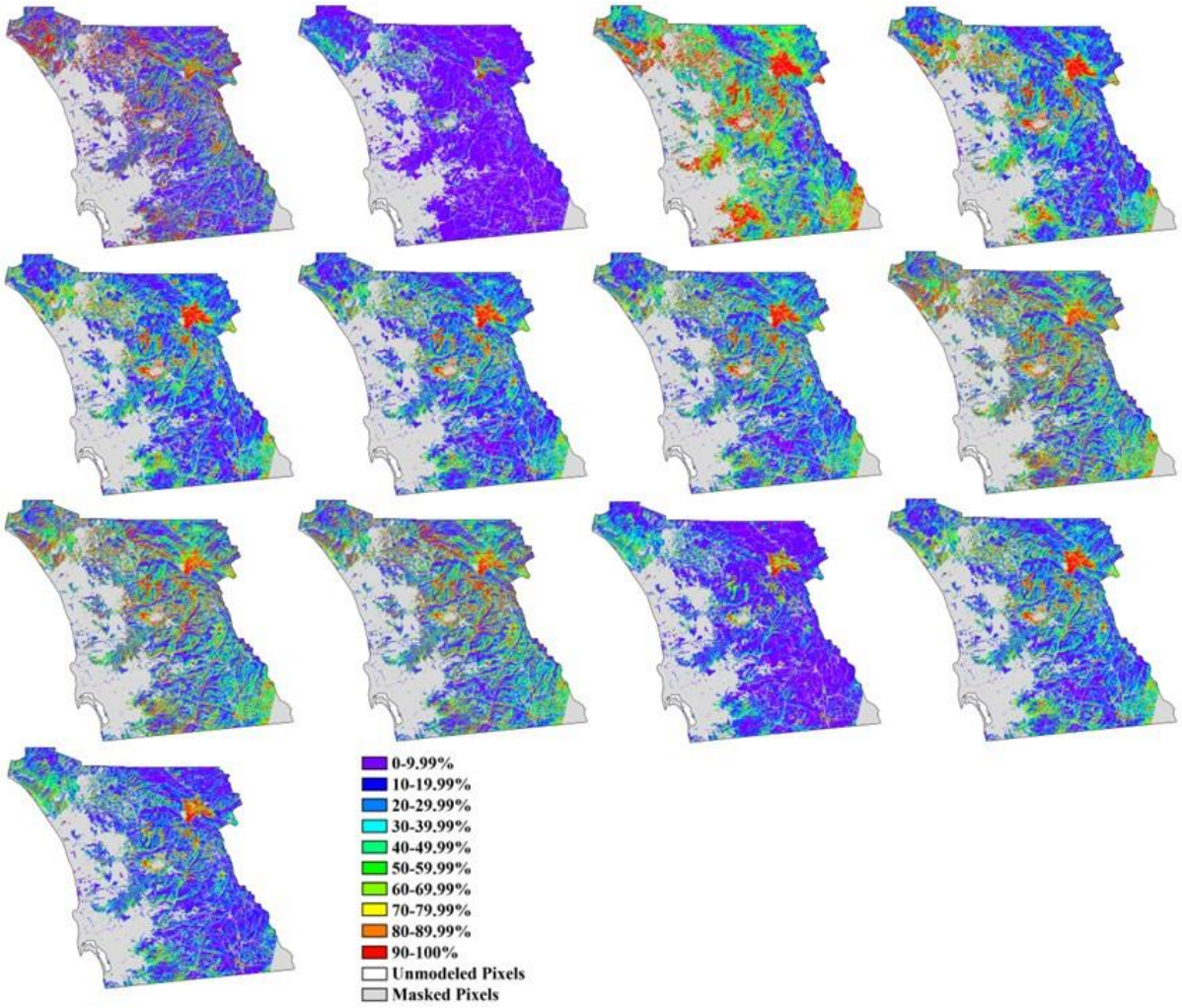

Figure 7. Herbaceous fractional cover maps from the SMA model with constrained output values. First row, left to right (MM/DD): 01/18, 04/23, 06/10, 06/26. Second row, left to right: 08/29, 09/30, 10/16, 11/17. Third row, left to right: 12/03, 12/19, April/August/November, August/September/October. Fourth row: All Dates.

Table 3. Herbaceous fractional cover error results for SMA image date inputs. MAE, RMSE, and R^2 results are displayed for the raw output values, raw values with min-max normalization applied, and raw values constrained to 0.00 to 1.00. The lowest error magnitudes for each output representation and date are highlighted.

Image Dates	Raw			Normalized			Constrained		
	MAE	RMSE	R^2	MAE	RMSE	R^2	MAE	RMSE	R^2
2020/01/18	33.79%	43.97%	0.32	21.84%	26.15%	0.32	20.17%	29.90%	0.29
2020/04/23	37.63%	42.69%	0.57	15.21%	20.13%	0.57	21.05%	29.23%	0.51
2020/06/10	31.94%	36.79%	0.76	16.36%	19.66%	0.76	26.88%	32.95%	0.62
2020/06/26	13.79%	17.71%	0.83	10.81%	13.73%	0.83	11.25%	15.14%	0.81
2020/08/29	10.76%	13.82%	0.83	11.96%	14.25%	0.83	8.85%	12.02%	0.85
2020/09/30	11.16%	14.95%	0.79	14.68%	16.98%	0.79	9.26%	13.14%	0.81
2020/10/16	12.95%	16.55%	0.75	16.21%	18.89%	0.75	10.91%	14.77%	0.77
2020/11/17	21.01%	25.16%	0.50	26.26%	30.27%	0.50	19.32%	24.19%	0.52
2020/12/03	21.36%	25.46%	0.48	26.78%	31.07%	0.48	18.90%	23.87%	0.50
2020/12/19	22.86%	27.99%	0.43	25.56%	29.68%	0.43	18.95%	24.86%	0.45
April/August/ November	17.17%	21.39%	0.76	12.05%	15.89%	0.76	13.08%	18.64%	0.78
August/September/ October	11.37%	14.95%	0.78	14.71%	16.94%	0.78	9.58%	13.30%	0.81
All Dates	14.83%	18.88%	0.70	15.90%	18.64%	0.70	11.78%	16.21%	0.74

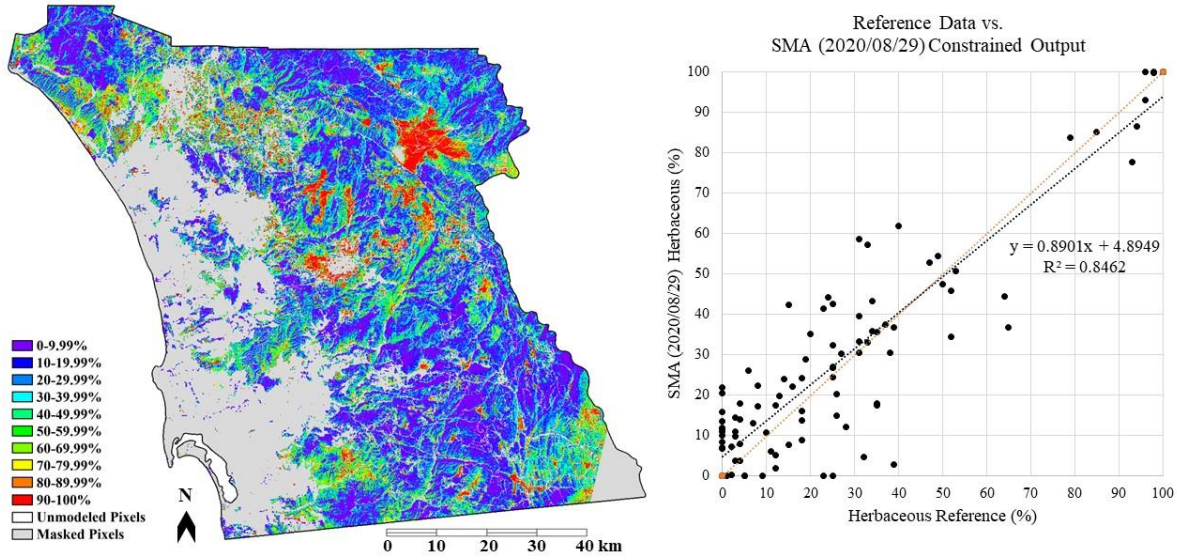

Figure 8. Left: Herbaceous fractional cover map from the SMA model and the constrained 2020/08/29 image date. Right: Scatterplot associated with the constrained 2020/08/29 output. The orange dotted 1:1 line communicates this model and output accurately and systematically estimated herb cover.

Constrained herbaceous cover outputs from each MESMA image date and feature input are displayed in Figure 9, and the associated output values are listed in Table 4. The feature input that yielded the highest accuracy from the MESMA model was the combination of all ten dates (All Dates) with constrained MAE = 14.42%, RMSE = 18.14%, and R^2 = 0.64

(Table 4, Figure 10). However, the output maps with the highest R^2 values were those from the 2020/06/26 and 2020/08/29 image dates (0.66).

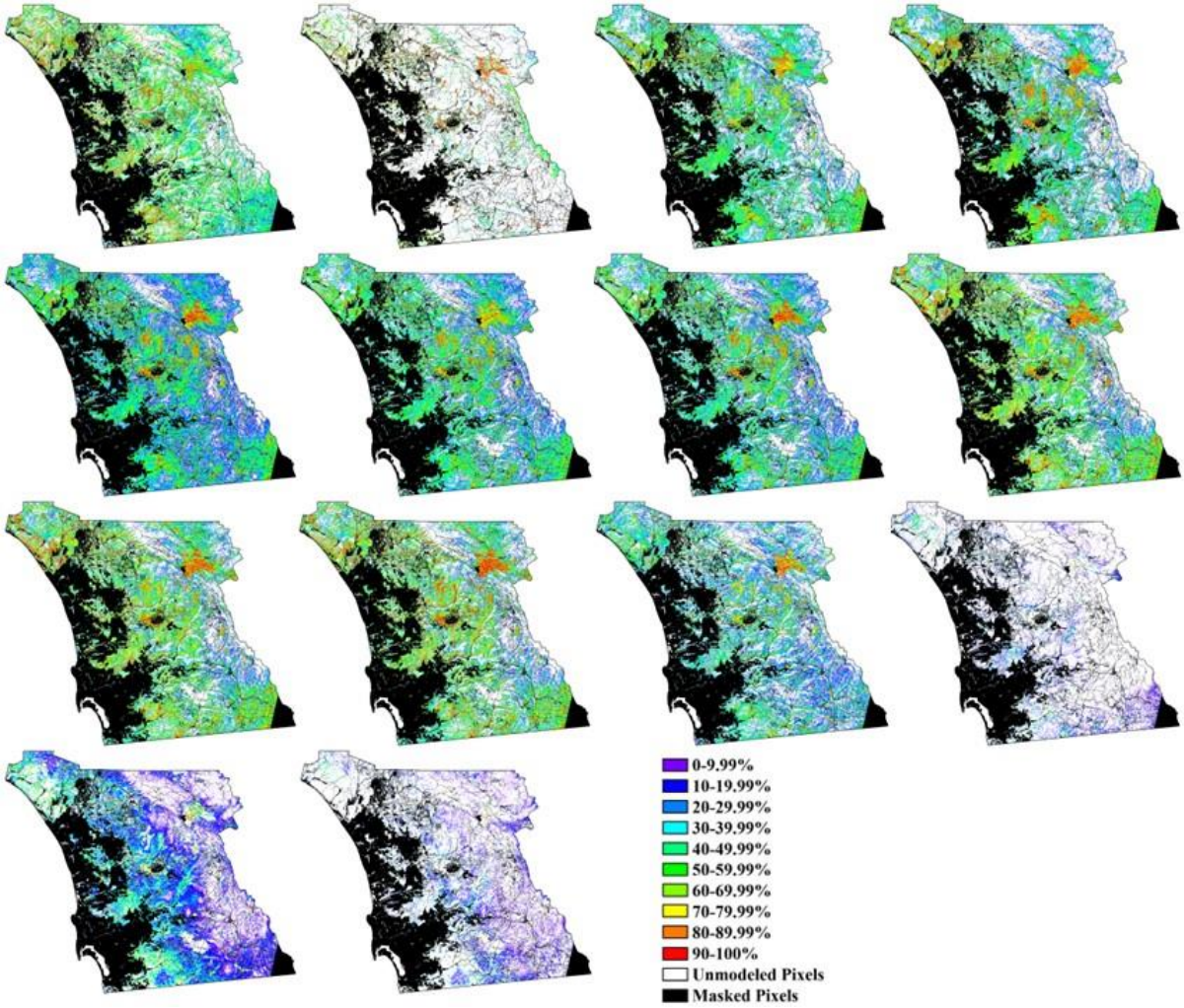

Figure 9. Herbaceous fractional cover maps from the MESMA model with constrained output values. First row, left to right (MM/DD): 01/18, 04/23, 06/10, 06/26. Second row, left to right: 08/29, 09/30, 10/16, 11/17. Third row, left to right: 12/03, 12/19, All Dates, NDII. Fourth row, left to right: NDVI, NDII+NDVI.

Table 4. Herbaceous fractional cover error results for MESMA image date inputs. MAE, RMSE, and R^2 results are displayed for the raw output values, raw values with min-max normalization applied, and raw values constrained to 0.00 to 1.00. The lowest error magnitudes for each output representation and date are highlighted.

Image Dates & Feature Inputs	Raw			Normalized			Constrained		
	MAE	RMSE	R^2	MAE	RMSE	R^2	MAE	RMSE	R^2
2020/01/18	26.65%	32.02%	0.25	28.06%	33.89%	0.25	26.65%	32.02%	0.25
2020/04/23	23.53%	31.30%	0.31	23.33%	31.44%	0.31	23.53%	31.30%	0.31
2020/06/10	19.24%	23.19%	0.56	21.35%	25.49%	0.56	19.15%	23.18%	0.57
2020/06/26	17.20%	21.18%	0.66	18.66%	22.72%	0.66	17.17%	21.17%	0.66
2020/08/29	16.34%	19.64%	0.66	16.83%	20.42%	0.66	16.34%	19.64%	0.66
2020/09/30	17.92%	21.56%	0.58	19.96%	24.61%	0.58	17.92%	21.56%	0.58
2020/10/16	16.14%	20.09%	0.62	18.99%	23.51%	0.62	16.05%	20.08%	0.62
2020/11/17	21.46%	25.84%	0.57	22.19%	27.00%	0.57	21.46%	25.84%	0.57
2020/12/03	21.47%	26.07%	0.53	22.97%	28.61%	0.53	21.47%	26.07%	0.53
2020/12/19	22.34%	27.41%	0.49	22.72%	28.14%	0.49	22.34%	27.41%	0.49
All Dates	14.51%	18.15%	0.64	15.40%	18.92%	0.64	14.42%	18.14%	0.64
NDII	23.76%	37.27%	0.07	21.18%	34.49%	0.07	23.27%	37.09%	0.06
NDVI	18.41%	30.52%	0.13	20.28%	30.45%	0.13	18.08%	30.42%	0.12
NDII+NDVI	26.44%	39.69%	0.00	27.18%	37.80%	0.00	26.12%	39.62%	0.01

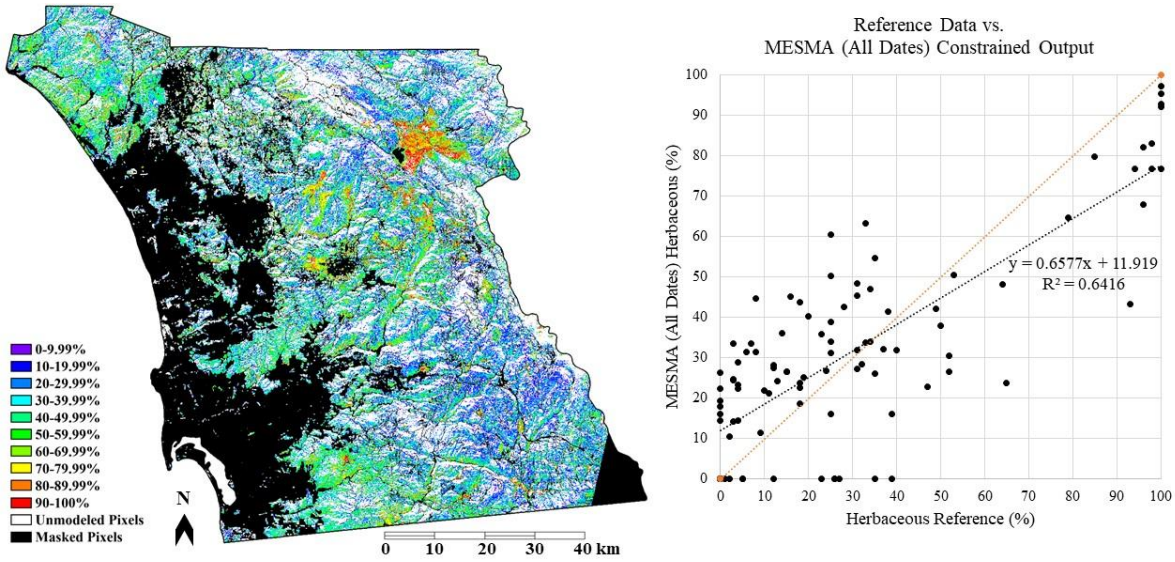

Figure 10. Left: Herbaceous fractional cover map from the MESMA model and the constrained ten date (All Dates) feature input. Right: Scatterplot associated with the constrained All Dates output. The orange dotted 1:1 line communicates this model and output's underestimation of herb, particularly when herb cover was greater than 35%.

The percentage of sampling grids modeled by MESMA ranged from 23% to 94%, depending on the image date or feature input. When unmodeled sampling grids were omitted from the calculations, the feature input that yielded the lowest RMSE and highest R^2 values

of 20.03% and 0.70 was the combination of all ten dates (All Dates) with values constrained (Table 5, Figure 11). Eighty-two percent of the All Dates sampling grids were modeled.

Table 5. Herbaceous fractional cover error results for MESMA image date inputs. MAE, RMSE, and R^2 results are displayed for the raw output values, raw values with min-max normalization applied, and raw values constrained to 0.00 to 1.00. Sampling grids that were unmodeled by MESMA were omitted from the calculations. The lowest error magnitudes for each output representation and date are highlighted.

Image Dates & Feature Inputs	Percent of Modeled Sampling Grids	Raw			Normalized			Constrained		
		MAE	RMSE	R^2	MAE	RMSE	R^2	MAE	RMSE	R^2
2020/01/18	87%	29.76%	34.33%	0.18	31.38%	36.33%	0.18	29.76%	34.33%	0.18
2020/04/23	23%	25.84%	65.26%	0.50	24.95%	65.56%	0.50	25.84%	65.26%	0.50
2020/06/10	89%	20.86%	24.58%	0.59	23.30%	27.10%	0.59	20.76%	24.57%	0.60
2020/06/26	89%	18.99%	22.45%	0.66	20.64%	24.10%	0.66	18.95%	22.44%	0.66
2020/08/29	93%	17.17%	20.36%	0.69	17.69%	21.18%	0.69	17.17%	20.36%	0.69
2020/09/30	31%	19.28%	22.60%	0.60	21.53%	25.80%	0.60	19.28%	22.60%	0.60
2020/10/16	94%	17.11%	20.72%	0.61	19.95%	24.23%	0.61	17.01%	20.71%	0.62
2020/11/17	91%	23.62%	27.09%	0.56	24.46%	29.25%	0.57	23.62%	28.06%	0.57
2020/12/03	88%	24.24%	27.79%	0.50	25.94%	30.50%	0.50	24.24%	27.79%	0.50
2020/12/19	90%	24.67%	28.89%	0.46	25.08%	29.66%	0.46	24.67%	28.89%	0.46
All Dates	82%	15.24%	20.05%	0.70	16.41%	21.30%	0.70	15.14%	20.03%	0.70
NDII	45%	16.07%	55.55%	0.56	12.99%	55.35%	0.56	14.95%	56.02%	0.55
NDVI	83%	13.03%	33.50%	0.53	15.67%	34.70%	0.53	12.64%	33.39%	0.54
NDII+NDVI	45%	12.60%	59.16%	0.24	19.33%	61.16%	0.25	11.91%	58.42%	0.25

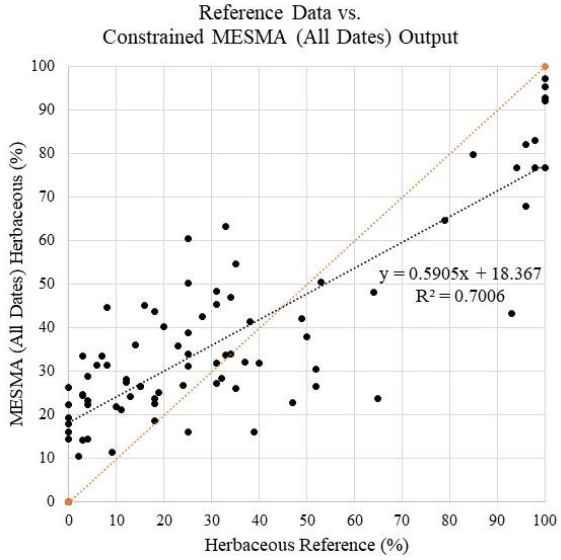

Figure 11. Scatterplot associated with the constrained All Dates output. Sampling grids that were unmodeled by MESMA were omitted from the calculations. The orange dotted 1:1 line communicates this model and output's underestimation of herb, particularly when herb cover was greater than 45%.

Constrained herbaceous cover outputs from each TMM feature input are displayed in Figure 12, and the associated output values are listed in Table 6. The TMM model's feature input that yielded the lowest error output was the substrate band stack ("Substrate") with constrained MAE = 11.21%, RMSE = 17.97%, and R^2 = 0.75 (Table 6, Figure 13).

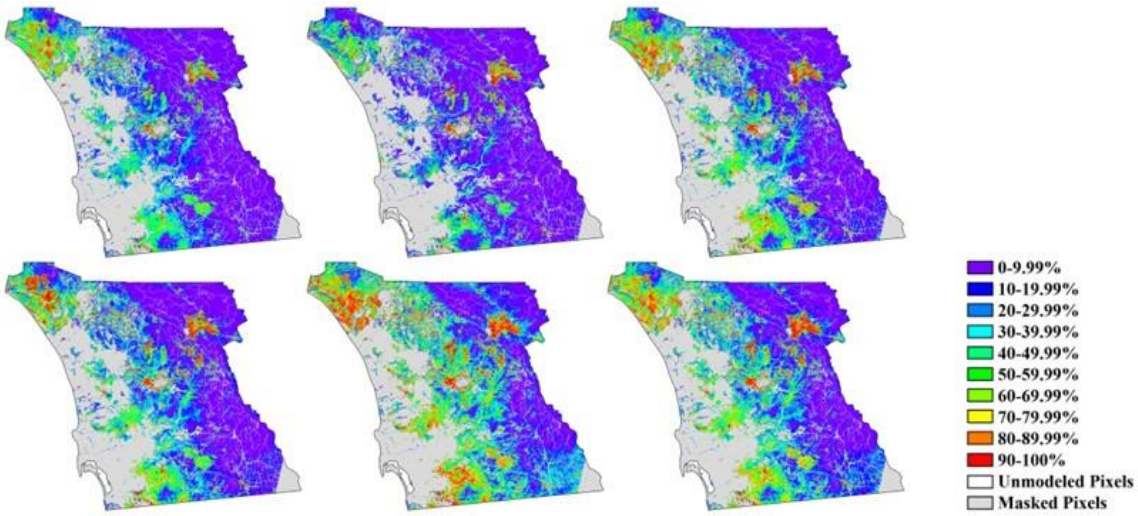

Figure 12. Herbaceous fractional cover maps from the TMM model with constrained output values. First row, left to right: "Vegetation," "Substrate," and NDII. Second row, left to right: NDVI, NDII+NDVI, and NDII(4)+NDVI(4).

Table 6. Herbaceous fractional cover error results for TMM feature inputs. MAE, RMSE, and R^2 results are displayed for the raw output values, raw values with min-max normalization applied, and raw values constrained to 0.00 to 1.00. The lowest error magnitudes for each output representation and date are highlighted.

Feature Inputs	Raw			Normalized			Constrained		
	MAE	RMSE	R^2	MAE	RMSE	R^2	MAE	RMSE	R^2
"Vegetation"	18.77%	28.23%	0.42	29.59%	33.09%	0.42	13.78%	20.66%	0.57
"Substrate"	15.17%	22.33%	0.68	13.73%	18.04%	0.68	11.21%	17.97%	0.75
NDII	19.95%	26.46%	0.49	21.42%	25.55%	0.49	15.30%	21.86%	0.54
NDVI	17.54%	24.63%	0.56	24.30%	28.47%	0.56	13.36%	19.64%	0.63
NDII+NDVI	22.02%	27.12%	0.50	25.22%	29.31%	0.50	20.06%	26.11%	0.51
NDII(4)+NDVI(4)	17.75%	23.03%	0.59	19.31%	23.09%	0.59	15.47%	21.57%	0.61

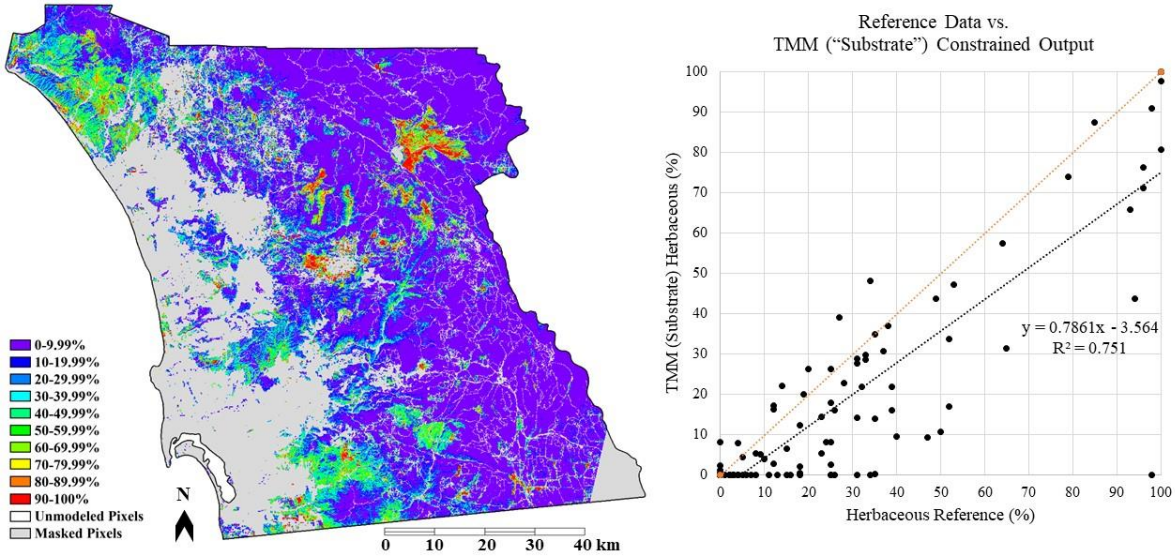

Figure 13. Left: Herbaceous fractional cover map from the TMM model and the constrained "Substrate" band stack. Right: Scatterplot associated with the constrained "Substrate" output. The orange dotted 1:1 line communicates the underestimation of herb cover for this model and feature outputs.

D. Discussion

1. Unmixing Model Approaches

The herbaceous fractional cover maps from each unmixing model type that yielded the lowest error (Figures 8, 10, and 13) visually portray the spatial distribution of herb cover in the San Diego County study area in a realistic manner. The single date SMA model (2020/08/29) (Figure 8) yielded the lowest MAE and RMSE and highest R^2 and is emphasized in this discussion.

When identical single date versus multi-date input results were compared, the influence of EM selection and differences in unmixing approaches on accuracy were isolated. For example, the 2020/08/29 image output yielded MAE = 8.85%, RMSE = 12.02%, and R^2 = 0.85 from the SMA model (Table 3) and MAE = 17.17%, RMSE = 20.36%, and R^2 = 0.69 from the MESMA model with unmodeled sampling grids omitted (Table 5). The All Dates

combination output yielded values of MAE = 11.78%, RMSE = 16.21%, and R^2 = 0.74 from the SMA model (Table 3) and MAE = 15.14%, RMSE = 20.03%, and R^2 = 0.70 from the MESMA model with sampling grids omitted (Table 5). The NDVI feature output yielded values of MAE = 12.64%, RMSE = 33.39%, and R^2 = 0.54 from the MESMA model with unmodeled sampling grids omitted (Table 5) and MAE = 13.36%, RMSE = 19.64%, and R^2 = 0.63 from the TMM model (Table 6).

Lower accuracy cover estimates from the MESMA model may be due to the constraints that were set, which resulted in a high number of unmodeled pixels. Additionally, MESMA yields high accuracy outputs for areas exhibiting considerable spectral variability between and within EM classes (e.g., urban areas), but less well when the contrast between EMs is low (Hamada *et al.*, 2011; Powell *et al.*, 2007; Roberts *et al.*, 1998; Shih *et al.*, 2020). When materials on the ground have only a modest amount of spectral contrast, MESMA often models the surface as consisting of only one cover type and shade.

TMM accuracy may be limited due to topographic effects, as well as "phenological mimicking." Phenological mimicking can be considered the analog of "spectral mimicking" (Adams and Gillespie, 2006) in the temporal domain (Sousa & Davis, 2020). Like any phenology-based approach to vegetation mapping that relies on a time-varying "greenness" metric, TMMs will be limited by the statistical separability (or lack thereof) among the temporal variations in photosynthetic vegetation in the spatial and temporal domain of the study.

Reference herbaceous cover data generated from visual interpretation of ultra-high GRE orthoimagery were compared to the 2020 herb cover estimates from RAP, which yielded MAE = 14.01%, RMSE = 16.41%, and R^2 = 0.83, respectively. RAP overestimated herb

cover values from 0 to 40% and underestimated herb cover from 65 to 100%. These lower accuracy estimates compared to the more accurate unmixing model estimates may be due to a limited number of San Diego County study area plot-level measurements used to calibrate the machine learning model implemented by RAP (Jones *et al.*, 2018). Like machine learning processes, datasets and parameters should be validated after each adjustment in EM selection based on independent testing (reference) data (Allred *et al.*, 2021; Jones *et al.*, 2018). Unlike machine learning, SMA methods require substantially less training data and effort and can still produce accurate fractional cover estimates without the need to generate large amounts of reference data for training.

2. Feature Input Effects

The SMA model's constrained single date image input from fall may have yielded the highest accuracy estimates because EMs were meticulously selected to represent the purest examples of land cover types in terms of complete ground cover and at the apexes of spectral feature space. When the SMA model multi-date features were tested, the high spectral contrast and separability were diminished by the addition of image date inputs with low spectral contrast. MESMA EMC metrics for spectral library selection steps, which are designed to identify the most separable EMs (Dennison *et al.*, 2004, Dennison & Roberts, 2003; Roberts *et al.*, 2003), appeared to be robust for models based on multiple date inputs that captured vegetation phenology signals.

Multispectral SR bands from single summer and fall dates yielded more accurate results than SVIs used as feature inputs. However, combinations of single date reflectance bands (e.g., April/August/November, All Dates) yielded results that were comparable to SVI inputs. Both models that tested single date SR image inputs (SMA and MESMA) resulted in

error values most likely caused by seasonal differences. Approximately 93% of average annual precipitation in the San Diego County study area occurs between October and April (Lippitt *et al.*, 2017), and herbs typically senesce and die by summer. The 01/08, 04/23, 06/10, 11/17, 12/03, and 12/19 image dates yielded the outputs with the highest error values stemming from seasonal spectral confusion between land cover types and terrain shadow variability throughout the year.

MESMA models and TMMs that incorporated multi-date SVI feature inputs, particularly NDVI which tracks vegetation growth and activity, resulted in more accurate herb cover estimates than those for single date SR image inputs (e.g., winter image dates when terrain shadowing was more pervasive). Herb cover distributions appear to follow topographic patterns, apparently due to the different vegetation growth form types and densities growing on north- versus south-facing slopes. Other SVIs besides NDII and NDVI may be worth testing as feature inputs.

3. Spatial Patterns of Herbaceous Cover

Differences in spatial patterns of herb cover were observed due to the biophysical geographic characteristics of individual AOIs. Accuracy of the SMA product that yielded the lowest error values is summarized for each AOI (Figure 5) that contained ten or more sampling grids in Table 7.

Table 7. Herbaceous, woody cover, and bare ground fractional cover averages and error results for the SMA model and constrained 2020/08/29 herbaceous output for each AOI. The number following each AOI label represents the number of 90 m x 90 m sampling grids used to generate reference data from within that AOI.

AOI	Average %Herbaceous	Average %Woody Cover	Average %Bare Ground	MAE	RMSE	R^2
Lake Henshaw (10)	63.50%	29.20%	7.30%	4.95%	8.29%	0.97
Palomar Mountain (18)	23.95%	69.85%	6.20%	5.77%	8.09%	0.94
Guatay Mountain (10)	18.20%	71.90%	9.90%	7.77%	9.39%	0.95
Mission Trails Regional Park/San Vicente Reservoir (20)	28.35%	56.90%	14.50%	7.43%	9.94%	0.83
Lake Sutherland (20)	19.25%	67.80%	12.95%	11.11%	13.94%	0.76
Otay Mountain (19)	31.63%	59.47%	8.89%	13.72%	17.17%	0.60

The most accurate estimates resulted for the Lake Henshaw and Palomar Mountain AOIs which were relatively homogeneous in growth form composition. The Lake Henshaw AOI is predominantly composed of grassland and the Palomar Mountain AOI is dominated by woody cover, with low herb cover. Lands covered by the Lake Henshaw sampling grids have not experienced a recorded wildfire since prior to 1910, and only two of 18 Palomar Mountain sampling grids have burned, most recently in 1984 (CAL FIRE FRAP, 2021). The SMA products for the Guatay Mountain and MTRP/San Vicente Reservoir AOIs were only slightly lower in accuracy. Both AOIs have similar peak elevations and are dominated by woody cover but contain open grasslands with greater heterogeneity in growth form cover than the Lake Henshaw and Palomar Mountain AOIs. Lake Sutherland and Otay Mountain SMA products exhibited the least accurate cover estimates and were the most heterogeneous of all AOIs. They were also the most recently burned, with 15 of 20 Lake Sutherland sampling grids burned in 2007 and ten of 19 Otay Mountain sampling grids burned in 2003 (five of which burned again in 2007) (CAL FIRE FRAP, 2021).

To my knowledge, this is the first study to focus exclusively on herbaceous fractional cover in San Diego County shrublands using unmixing model approaches – SMA, MESMA, and TMM. Results from this work may be applied to climate-vegetation zones that are

affected by rapid transformation of growth form cover (Báez & Collins, 2008) as well as locations impacted by grass-fire cycles. Examples include Mediterranean-type climates where non-native herbs are encroaching upon native shrubs and trees. Conversely, shrubs are invading native grasslands in other biogeographic provinces, such as grasslands in the northern Chihuahuan Desert In New Mexico (Báez and Collins, 2008), in South Dakota (South Dakota Grassland Coalition), and in prairies of Alberta, Canada (Zapisocki *et al.*, 2022). These methods may enable monitoring of changes of growth form cover by satellite for wildfire-prone communities and support adaptive management practices for mitigating and combating the grass-fire cycle.

E. Conclusions

With a focus on herbaceous cover estimation and mapping, this study successfully explored the accuracy of three unmixing methodologies applied to NASA/USGS Landsat 8 OLI SR data acquired over San Diego County shrublands. The SMA model and the constrained 2020/08/29 image output yielded the most accurate results of MAE = 8.85%, RMSE = 12.02%, and R^2 = 0.85. This simple and parsimonious approach, with the specific parameters tested, yielded a slightly higher accuracy than did more complex unmixing models and feature inputs. An unmixing approach provides a framework for quantifying, mapping, reconstructing, and monitoring herbaceous vegetation cover on a regular basis; representing output cover products with 10% interval classes would be appropriate given the levels of error and uncertainty that were quantified in this study.

Extraction of pure spectral signatures of herbaceous cover for EMs from a 30 m GRE image was challenging (Hamada *et al.*, 2011), and this undoubtedly affected the accuracy results. SMA requires either an authoritative and validated spectral library, or knowledge of

the landscape and/or access to high GRE orthoimagery acquired from multiple seasons to identify growth forms remotely for accurate EM selection. The MESMA model's EM selection process is less critical since it is recommended that many ROIs are selected for the EMC part of the process. However, results from the MESMA model demonstrated the degree to which a spectral mixture can be modeled by a small number of EMC-selected EMs, as well as demonstrated that no single set of EMs can adequately describe every spectrum in the image (Roberts *et al.*, 1998). Because of this, the creation of the combined true shrub, subshrub, and tree – Woody Cover – land cover class may have negatively impacted the processes and resulting values. The multi-date feature input approach of TMMs ensured seasonality was incorporated in the analysis, but selection of substrate, vegetation, and dark spectra from the principal components point cloud proved to be difficult to capture in a consistent way that could be compared between feature input types. However, the "Substrate" output likely yielded the highest accuracy of the TMM outputs due to the spectral similarity between herbaceous and bare ground in late summer and early fall, and may be considered for future herbaceous identification work, particularly when temporal EMs are selected from point clouds as opposed to geographic knowledge (as was the case with this work).

Both the high GRE NAIP and Nearmap orthoimage-based reference data and moderate GRE Landsat fractions are model-based estimates, and measurements of comparative model agreement, as opposed to predicted outputs compared to "ground truth." Assessing the accuracy of the reference data with field-based estimates could be beneficial yet labor intensive.

The results of this study indicate potential for application of the SMA model to longer time scale assessments. In Chapter III, this approach will be applied to a long time (multi-decadal) sequence of Landsat data to analyze herbaceous cover change and evidence of the effects of the grass-fire cycle in the San Diego County study area.

III. Spectral unmixing of a Landsat time sequence to reconstruct herbaceous fractional cover dynamics in wildfire-prone San Diego County, California, USA shrublands (1988-2020)

A. Introduction

Wildfire is a natural element in a Mediterranean-type ecosystem, but is nonetheless a landscape disturbance and, when the land is altered beyond its characteristic range of variability, a combination of vegetation community reassembly, invasion, conversion, or replacement may occur over time. Post-fire succession in previously disturbed shrublands, whether due to mechanical disturbances or shorter fire return intervals, often starts with non-native grasses and forbs (herbaceous vegetation or herbs). These invasive vegetation types tend to recover quickly after disturbances because of their ability to colonize open spaces (Christensen, 1994; D'Antonio & Vitousek, 1992). Vegetation communities composed of high fractions of herbaceous vegetation, and particularly herbs that have senesced or dried, may tolerate and enhance fire effects (D'Antonio & Vitousek, 1992). Post-fire grass invasion can set a grass-fire cycle in motion where an invasive grass colonizes an area following a wildfire or other landscape disturbance, causes a decline in native shrubs and trees, and provides the fine fuel necessary for the ignition and spread of subsequent fires. Successive fires in an area then increase in frequency, area, and possibly intensity over time. Grasslands invading shrublands are the cause of significant negative ecosystem effects (Brooks *et al.*, 2004; Mack *et al.*, 2001) and can alter ecosystem processes over large areas because they could feed back to alter other components of global change (e.g., climate, atmospheric composition, land use) (D'Antonio & Vitousek, 1992). Additionally, wildfires

pose a risk to the growing human population and structures, particularly in wildland-urban interface (WUI) areas (Radeloff *et al.*, 2018). For these reasons, it is important to identify and monitor areas that experience expansion of invasive herb cover, and particularly locations that have type converted from native shrubland- to non-native herb-dominated areas over time.

Typically, vegetation development and change are studied by long-term observations of individual sites. In the past, vegetation change was analyzed for proximal sites of differing stand ages, by inferring development sequences from differences in cover (Lippitt *et al.*, 2013; McMichael *et al.*, 2004; Uyeda *et al.*, 2016). However, the challenge with this method is that inter-site differences that are unrelated to site age may mistakenly be interpreted as developmental and, therefore, data collected in this way must be interpreted cautiously (Kellman, 1980). Other studies avoided the issue of inference from different stand ages by studying long-term change for specific locations through analysis of random sample points to infer the rate or extent of change (Syphard *et al.*, 2019). Using a time sequence of aerial photographs, Syphard *et al.* (2019) quantified fractional cover change of woody and herb growth forms at 25% cover intervals between 1953 and 2016 across 916 randomly sampled plots in San Diego County (the same study area used for this study). Shrub conversion and decline were related to a range of explanatory variables (i.e., fire frequency, proximity to human disturbance, and biophysical landscape characteristics). Substantial net woody cover loss was reported and, of the plots that were more than 75% woody cover in 1953, 59% experienced a decline with a mean woody cover loss of 22.5%. Of those, 28% were heavily type-converted to the point that herbaceous vegetation covered more than 50% of the plot. Major driver variables for woody conversion and decline were fire intervals shorter than 15

years, the total number of fires, actual evapotranspiration, and elevation (Syphard *et al.*, 2019). However, these methods do not output regional change cover maps.

Unlike methods using local observations over time, remote sensing offers an approach to effectively monitor a Mediterranean-type shrubland ecoregion across large landscapes, particularly with the long time series of moderate spatial resolution imagery and large extent provided by the Landsat archive. Landsat time series have been used to analyze pre- and post-fire data to monitor regeneration of woody fractional vegetation cover (FVC) (Clemente *et al.*, 2009; Storey *et al.*, 2021). Clemente *et al.* (2009) used image data to monitor post-fire regeneration in a Mediterranean semiarid and subhumid study area in Beas de Granada, Spain. Landsat images acquired before and after a 1993 wildfire incident were compared to field survey data collected in 2000 and again in 2005. Ground data were used to calculate FVC as the percentage of vegetation occupying a unit area and were related to seven Landsat-derived vegetation indices and compared through a Pearson correlation matrix. The spectral post-fire analysis revealed that regeneration was related to gradual spectral changes over time within different vegetation communities, and the proposed linear regression model could derive accurate FVC estimates from Normalized Difference Vegetation Index (NDVI) data (Clemente *et al.*, 2009). Storey *et al.* (2021) used high spatial resolution aerial imagery to calibrate fractional shrub cover estimates derived from Landsat Surface Reflectance (SR) NDVI trajectories over southern California from 1984 through 1988 and 2014 through 2018. Change in shrub cover was evaluated for stands that experienced different fire return intervals, numbers of fires, and environmental settings, and a substantial fraction of chaparral was determined to have degraded because of fire (Storey *et al.*, 2021).

Although trend analyses based on spectral features and vegetation indices, such as NDVI, have been used to reveal patterns of vegetation green up and dry down, spectral indices have limitations in that their relationship to biophysical properties are empirical. Park *et al.* (2018) used NDVI to provide a high-resolution approach for assessing the distribution and relative cover by herbs into woody cover but found the model may overlook some differences in the extent of seasonal changes in NDVI among different species within each cover type. Variation in seasonal NDVI and the lack of interspecific discrimination was attributed to the tendency of the method to underpredict fractional herb cover in highly invaded areas and overpredict herb cover in areas with extremely low herb cover. These limitations may represent some inherent constraint in using seasonally based vegetation mapping with data such as that from Landsat (Park *et al.*, 2018). Therefore, a vegetation cover mapping approach that can be used to estimate continuous cover fractions of distinct surface types at a sub-pixel level is more appropriate for landscape-scale change detection among cover types.

Spectral mixture analysis (SMA), or linear spectral unmixing, is an image processing approach for estimating material cover fractions based on the assumption that the ground area sampled by a pixel, the ground resolution element (GRE), can be reasonably approximated by a fractional mixture of a small number of spectrally distinct materials (Adams *et al.*, 1986; Gillespie *et al.*, 1990; Roberts *et al.*, 1998; Settle & Drake, 1993; Smith *et al.*, 1990). Endmembers (EMs) representing homogeneous, or "pure," materials and their spectra are fundamental inputs in the SMA process. During the unmixing process, the radiance (or reflectance) of a mixed GRE is considered to be an area-weighted linear combination of spectral EM materials, plus error (e.g., Adams *et al.*, 1993). EMs may be

selected based on geographic knowledge of the study area, or through a process such as in VIPER Tools for SMA or multiple endmember spectral mixture analysis (MESMA), from an existing spectral library built from field or laboratory spectroradiometer measurements, or from simulated radiative transfer models (Dennison & Roberts, 2003; Somers *et al.*, 2011).

SMA is an important tool for remote sensing of vegetation analysis (Dennison & Roberts, 2003) and since SMA can be used to provide a full spectrum measurement of vegetation response, SMA fractions are often more robust for fractional cover determination than traditional vegetation indices (Dennison & Roberts, 2003; Elmore *et al.*, 2000; Peddle *et al.*, 2001; Riano *et al.*, 2002). Vegetation fractions produced by SMA have been used to describe land cover change (Dennison & Roberts, 2003; Nill *et al.*, 2022; Roberts *et al.*, 2002; Rogan *et al.*, 2002) and vegetation regeneration after disturbance (Dennison & Roberts, 2003; Riano *et al.*, 2002). The usefulness of accurate quantification of fractional cover using SMA is further corroborated when applied to multitemporal image data sets for the purpose of tracking vegetation change over time.

Multitemporal image data captured throughout the intra-annual phenological cycle are useful for identification of vegetation at the growth form level, partly due to the changing spectral response of vegetation due to phenology (Dudley *et al.*, 2015; Lieth, 1974). Plant phenology, defined as the seasonal change in biological life as a result of changing environmental conditions (Dudley *et al.*, 2015; Lieth, 1974), provides information that can be used to ascertain details about broad plant species composition and vegetation health (Dudley *et al.*, 2015). Multitemporal imagery has been used to quantify herbaceous

expansion and change over time (Balch *et al.*, 2013; Jones *et al.*, 2018; Lippitt *et al.*, 2017; Park *et al.*, 2018).

In Mediterranean-type ecosystems, landscape disturbances often modify a vegetation species' relative abundance rather than composition such that recovery involves the return to initial abundances (Clemente *et al.*, 2009; Lavorel, 1999; Storey *et al.*, 2016; Storey *et al.*, 2021). A spectral unmixing method is appropriate for identification and observation of FVC change through time because landcover classifications are constrained by the observational unit of a GRE, which almost exclusively represents a mix of several distinct surface materials (Keshava & Mustard, 2002; Nill *et al.*, 2022). Therefore, the objective of this study was to reconstruct and analyze the spatial-temporal patterns of herbaceous growth form cover for a shrubland study area in San Diego County, California, USA using SMA applied to four Landsat multispectral images captured over a 33-year period (1988 to 2020) at nearly decadal intervals. The rationale for use of SMA for this objective, as opposed to another unmixing approach like MESMA or temporal mixture models, was based on results from Chapter II, in which I found the SMA model to output slightly higher herb cover accuracy as well as provide a parsimonious modeling approach. The output of four herb cover maps was evaluated, and the difference between an early and current year were analyzed. The accuracy of the herb cover change results, as well as the degree of uncertainty, were assessed using the reference data, according to mean absolute error (MAE), root mean square error (RMSE), and coefficient of determination (R^2) metrics. The reliability of the herb cover change estimates was addressed and locations with high amounts of change over time were identified. Specifically, I asked the following research questions:

1. When spectral unmixing models are applied to imagery covering a multi-decadal period in the San Diego County study area, how reliable and accurate are maps of herbaceous cover change?
2. Where within the study area did substantial change in herbaceous fractional cover occur and do areas of substantial change appear to coincide with wildfire frequency or drought effects occurring within the study period?

B. Data and Methods

1. Study Area

The study domain is the 783,290 ha of the Southern California Mountains and Southern California/Northern Baja Coast U.S. Environmental Protection Agency (EPA) level III ecoregions within San Diego County (Griffith *et al.*, 2016; U.S. EPA, 2013) (Figure 14). Areas under urban, built, and agricultural land use were considered as "Developed" and masked from analysis, along with an area in the southeast portion of the study domain that is not covered by the Landsat scenes used in this study.

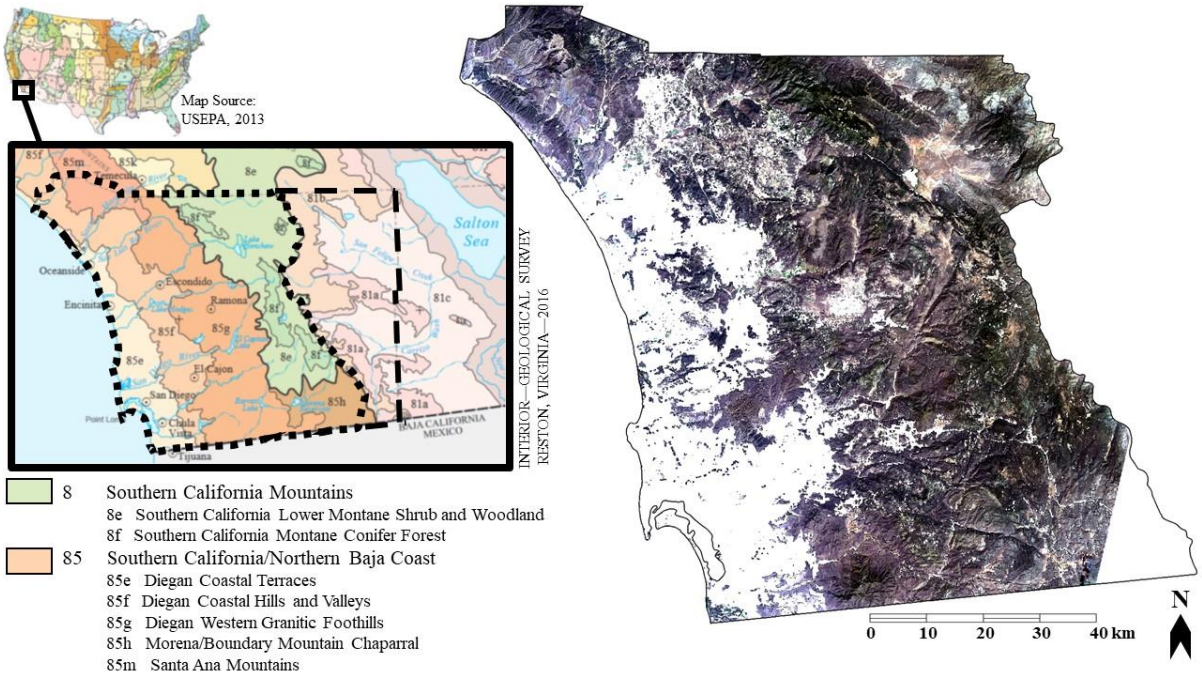

Figure 14. Study area location within San Diego County, California. Left: Department of Interior (DOI)/U.S. Geological Survey (USGS) (Level III and IV) Ecoregions with the San Diego County study domain (delineated in black dotted line) within the San Diego County extent (shown in dashed black line) (804,116 ha). Right: Landsat 8 OLI image data from (YYYY/MM/DD) 2020/08/29 acquired over the study domain with NLCD developed areas, surface water, and the southeast portion not covered by Landsat masked (532,167 ha).

The San Diego County study area has a semi-arid Mediterranean-type climate that experiences warm to hot, dry summer seasons (26˚ to 37 °C) and moderate winter precipitation (250 to 1,000 mm) (Hamada *et al.*, 2009). The shrubland communities cover a variable range of topography and have experienced different land uses over time (Lippitt *et al.*, 2017). Growth form types in the wildland area include herbaceous and woody cover (true shrubs, subshrubs, and trees), with bare ground (soil and rock substrate) also composing a Landsat GRE. California shrublands are commonly invaded by non-native herbs (Keeley, 2001; Park *et al.*, 2018) but may include pockets of native herb species (D'Antonio *et al.*, 2007; Park *et al.*, 2018). However, differentiation of invasive from native herb species was not attempted for this study, as their Landsat SR signatures are not generally separable (Olsson *et al.*, 2011).

To characterize the patterns and dynamics of land cover in the San Diego County shrublands, fractional cover of three classes was estimated.

1. Herbaceous: Comprises largely invasive grass and forb species that are annuals, with some perennial bunchgrasses (Bartolome *et al.*, 2007; Heady, 1956). Annual grassland varies on at least three important scales: intra-annual change within a growing season, differences between years, and directional change over many years (Bartolome, 1989; Bartolome *et al.*, 2007). Rainfall and air temperature are the primary drivers of change at the two smaller temporal scales (Bartolome *et al.*, 2007; Jackson & Bartolome, 2002), and anthropogenically influenced factors are often the driver of long-term changes (Bartolome *et al.*, 2007).
2. Woody Cover: Includes true shrub (e.g., chamise (*Adenostoma fasciculatum*)) chaparral and mixed chaparral communities (Keeley, 2000; Pryde, 2004), subshrub (e.g., coastal sage scrub (e.g., *Artemisia californica*, *Eriogonum fasciculatum*, and *Salvia* species)) communities (Rundel, 2007), and trees (e.g., open oak woodlands in riparian areas and canyons, and oak woodlands and montane coniferous forests in higher elevations) (Arroyo *et al.*, 1995, Davis & Richardson, 1995; Di Castri *et al.*, 1981).
3. Bare Ground: Encompasses soil and rock substrate.

Fuel-driven wildfires are common in central and northern California conifer forests where lightning is the more frequent cause of ignitions compared to human ignitions (Keeley & Syphard, 2018). However, lightning in San Diego County is less common, particularly closer to the coast, so the natural fire regime is one of infrequent wildfires that likely ignited in higher-elevation montane forests and burned into shrublands. Now, human-

caused ignitions account for 99% of all fires that occur in coastal California, north and south (Keeley & Syphard, 2018), which has decreased the intervals between fires. San Diego County may be characterized by periodic fuel- or wind-driven wildfires (Keeley & Syphard, 2019). Large, high-intensity crown fires (in this domain, crown fires may burn in true and subshrubs, and not just trees) driven by hot, dry Santa Ana wind events typically occur in autumn, and smaller fires tend to burn in summer seasons (Jin *et al.*, 2015b; Syphard *et al.*, 2019). Between 1984 and 2020, 522 wildfire incidents were recorded in the Southern California Ecoregion, which burned 516,500 ha (CAL FIRE FRAP, 2021). Conversion of native shrubs to herbs has been documented in parts of San Diego County (Keeley & Brennan, 2012; Lippitt *et al.*, 2013, Syphard *et al.*, 2019).

2. Landsat Image Data

The NASA/U.S. Geological Survey (USGS) Landsat program offers the longest continuous record of image data acquired from space, which makes it the ideal source for estimating and mapping herbaceous cover change over large extents and relatively long durations. All Landsat 5 Thematic Mapper (TM), Landsat 7 Enhanced Thematic Mapper Plus (ETM+), and Landsat 8 Operational Land Imager (OLI) SR (Collection 2, Level-2, path/row 40/37) 30 m GRE data products from USGS EarthExplorer with < 10% cloud cover and a fall season date were reviewed. Fall dates were selected because of the seasonal and spectral differences observed between the mostly senesced herbaceous and mostly evergreen woody vegetation (as described in Chapter II). Landsat 7 ETM+ data after 2002 were not considered because of the Scan Line Corrector failure (which creates “No Data” gaps) (Shih *et al.*, 2020). Image dates were selected based on three factors: (1) exhibition of similar annual precipitation amounts near the long-term annual mean precipitation value,

according to records for a weather station centrally located within the Southern California Ecoregion (Descanso, CA) (Figure 15); (2) the temporal bounds defined by the historical period of existing Landsat SR data between 1984 and present (Jones *et al.*, 2018); and (3) the available fall dates within that period of data. Landsat imagery was acquired for four dates, 1988/09/22, 1997/10/17, 2011/10/08, and 2020/08/29 (Figure 15, Table 8).

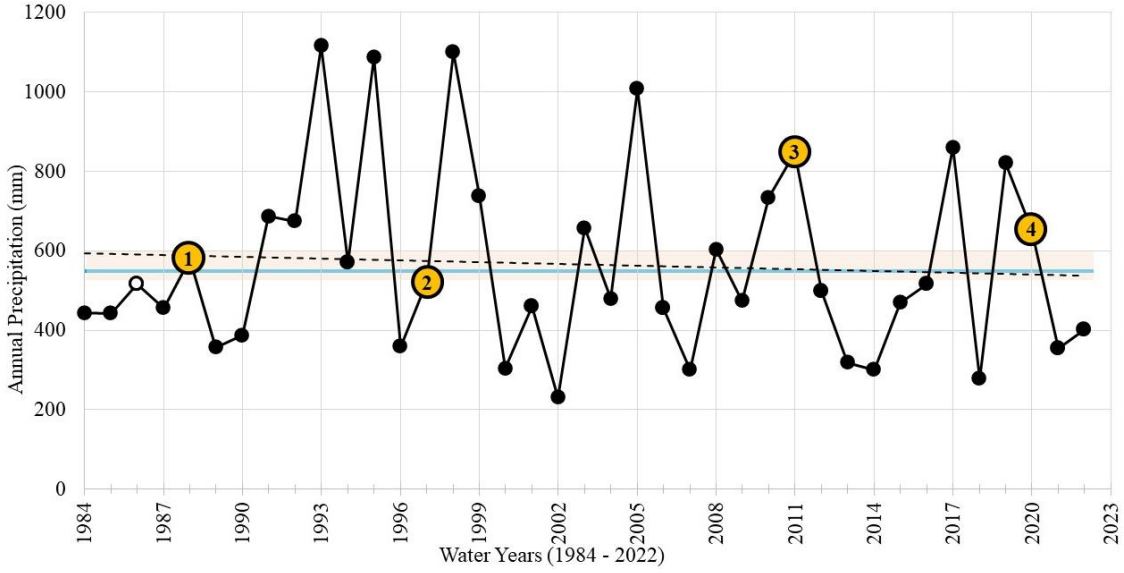

Figure 15. Annual water year (WY: October through September) precipitation data from the Descanso Station, San Diego County. Y-axis: Annual precipitation data (mm) (sources: https://www.wrcc.dri.edu/cgi-bin/cliMAIN.pl?ca2406 and https://raws.dri.edu/cgi-bin/rawMAIN.pl?cactus). X-axis: WY (1984 through 2022). The solid blue line represents the average annual precipitation value, the dotted black line represents the trendline, and the orange bar visually communicates the change-over-time in the trendline for 1984 through 2022. The hollow black dot represents a year with incomplete total values (e.g., months' worth of missing data). Numbered gold dots represent the years selected for study: (1) 1988 (578.87 mm), (2) 1997 (521.72 mm), (3) 2011 (847.85 mm), and (4) 2020 (653.03 mm).

Table 8. Landsat 5 TM and 8 OLI image information for path/row 40/37 selected for this study. Acquisition dates, land cloud cover percentages, solar elevation, and solar azimuth are reported.

Landsat Sensor	Acquisition Date	Land Cloud Cover	Solar Elevation	Solar Azimuth
5 TM	1988/09/22	0.00	48.23	137.013
5 TM	1997/10/17	0.00	41.42	146.98
5 TM	2011/10/08	0.00	45.92	148.56
8 OLI	2020/08/29	0.06	58.64	135.55

3. Aerial Image Data

Aerial image data were used primarily to generate reference data, which were used for accuracy assessment. Three-band (color infrared (CIR)) digital orthophoto quadrangles (DOQ) (1 m GRE) from summer 1996 and fall 1997, the earliest dates of digital multispectral orthoimagery available, were acquired from USGS EarthExplorer. Four-band (visible and near infrared (NIR)) National Agriculture Imagery Program (NAIP) orthoimagery (0.6 m GRE) from spring 2020 were acquired from USGS EarthExplorer. Three-band (visible) Nearmap orthoimagery (as fine as 0.06 m GRE) from all seasons of 2020 were also acquired. Orthoimage acquisition dates are listed in Table 9.

Table 9. DOQ, NAIP, and Nearmap orthoimage acquisition dates over the San Diego County study domain in 1996, 1997, and 2020. Seasons are defined by meteorological start dates.

Orthoimagery	Spatial Resolution (m)	Acquisition Dates (YYYY/MM/DD)
DOQ	1.0	Summer: 1996/06/04 Fall: 1996/09/26, 1996/09/27, 1996/09/30, 1997/10/16
NAIP	0.6	Spring: 2020/04/15, 2020/04/25, 2020/04/28, 2020/05/20, 2020/05/25
Nearmap	0.06	Winter: 2020/01/03, 2020/01/04, 2020/01/05, 2020/01/06, 2020/01/10, 2020/01/11 Spring: 2020/05/01, 2020/05/02, 2020/05/16, 2020/05/20 Summer: 2020/07/19 Fall: 2020/09/05, 2020/09/21, 2020/09/22, 2020/10/08, 2020/10/16

4. Ancillary Data

USGS National Land Cover Database (NLCD) 2019 data were used to create a mask of urban and built land cover (developed and cultivated crops) and surface water (lakes, reservoirs, and woody wetlands) classes. Land cover masks were applied prior to the implementation of unmixing steps, yielding a 532,167-ha study domain (Figure 14, right), hereafter referred to as the San Diego County study area. USGS three-dimensional (3D) Elevation Program (EP) (3DEP) data and OpenStreetMap (OSM) data were used to derive information about terrain, elevation, and infrastructure.

California Department of Forestry and Fire Protection (CAL FIRE) Fire and Resource Assessment Program (FRAP) (CAL FIRE FRAP) historical fire polygons (1910 to 2020) were used to identify and exclude from analysis areas that burned four years before and the year of image acquisition (a five-year burn mask for each analyzed image date) to ensure more established herbaceous cover was not confused with immediate post-fire annual vegetation. The five-year period was based on chamise chaparral regrowth trajectories and postfire recovery results (Lippitt *et al.*, 2013; Storey *et al.*, 2016; Syphard *et al.*, 2019). Reference sampling grids were not sampled from within areas that burned between 2016 and 2020.

5. Landsat Data Preparation

Landsat image data were prepared and SMA was implemented using ENVI 5.7 + IDL 8.9 software. Processed satellite, aerial, and map data were analyzed with ENVI and ArcGIS Pro 2.8.3 software. Figure 16 shows the workflow for this study.

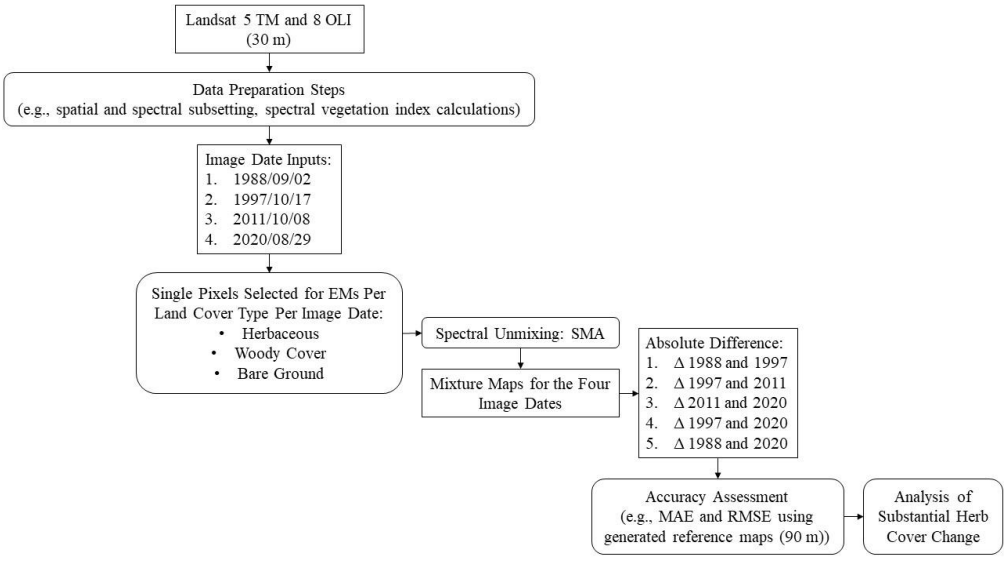

Figure 16. Image processing workflow for analyses focused on multi-year difference outputs. The list of tested image dates is shown, along with the number of EMs used. SMA unmixing steps yielded four cover maps (one per date). Absolute difference calculations yielded five difference results. Accuracy was assessed and sample patches of substantial change in herb cover were analyzed.

USGS-provided scale factors were applied to all four Landsat SR images, but no additional scale factors were applied to harmonize Landsat 5 TM to Landsat 8 OLI. Data were spatially subset to the smallest common areal extent of image coverage within the San Diego County study area. Landsat 8 data were spectrally subset to remove the Coastal band (resulting in six reflectance bands: Blue through the second shortwave infrared (SWIR 2) waveband) for a more direct comparison to Landsat 5 data.

6. Endmember (EM) Selection

Pixels representing the purest examples of a single land cover class (herbaceous, woody cover, or bare ground) were selected to derive EM signatures. The 30 m x 30 m Landsat pixels were selected based on interpretation of the Landsat, DOQ, NAIP, and Nearmap images, and by selecting apexes of feature space data clouds (Boardman, 1993; Peterson & Stow, 2003; Somers *et al.*, 2011). The DOQ (1996 and 1997) and NAIP and Nearmap (2020) orthoimages were used to identify herb, woody, and bare ground cover locations that displayed minimal change between the early and later time period. If reference data sampling grids generated from these orthoimages indicated -2 to 2% change in 1996 or 1997 versus 2020, the locations were flagged for consideration for in-image, single-pixel EM selection. Final EM combinations were selected for each image date based on accuracy assessment results.

7. Spectral Mixture Analysis (SMA)

Each Landsat image was modeled separately using SMA, with six wavebands and three EMs (one pixel per land cover type tested). A unit sum constraint with a weight of 1.00

(equating to 100% cover) was set. Four output images were generated per image date, with resulting herbaceous cover, woody cover, bare ground, and RMSE data.

8. Herbaceous Cover Change

Absolute difference images were generated to assess spatial variability in fractional cover change estimates for the entire mapped area between the different time steps (single years) (Lippitt *et al.*, 2017), as defined in Equation 1:

$$\Delta H_a = H_{t2} - H_{t1} \quad (1)$$

where: ΔH_a represents the absolute change in herbaceous cover, H_{t2} is the herbaceous cover of the later time, and H_{t1} is the herbaceous cover of the earlier time.

Three comparisons using the Landsat-derived fractional cover maps were analyzed to identify persistent shifts in cover and analyze herbaceous cover trends (Table 10). For each comparison, the absolute difference between each year or time step was calculated; these illustrated the fractional cover change between each interval. Every pairwise sequential combination was calculated, and five absolute difference images were generated for the entire study area at 30 m GRE with land use/land cover areas not of interest masked.

Table 10. Absolute difference comparisons analyzed. Comparison 1 calculated differences between each sequential year studied. Comparison 2 calculated the difference between the years closest to the available reference date years. Comparison 3 calculated the difference between the first and the last year studied.

Absolute Difference Comparisons	Process
Comparison 1. Each Sequential Year	Year 2 minus Year 1, Year 3 minus Year 2, Year 4 minus Year 3
Comparison 2. Reference Data Years	Year 4 minus Year 2
Comparison 3. First versus Last Year	Year 4 minus Year 1

9. Reference Data Generation

Reference data were generated by visual interpretation of the DOQ, NAIP, and Nearmap orthoimagery (Table 9). To estimate fractional cover, randomly sampled portions equivalent

to three-by-three Landsat pixels (90 m x 90 m or 0.81 ha) (hereafter referred to as a sampling grid) were interpreted. A sampling grid, which is larger than a single Landsat pixel, was used to account for uncertainty in the co-registration of the DOQ, NAIP, and Nearmap pixel groupings relative to Landsat pixels (Hogland & Affleck, 2019; Shih *et al.*, 2020). A regularly spaced grid was generated and overlaid on the Landsat data, and eight areas of interest (AOIs) (i.e., subareas within the study area, labeled based on nearby landscape features of interest) were designated. From within the eight AOIs, 100 systematically aligned individual sampling grids were created (Figure 17).

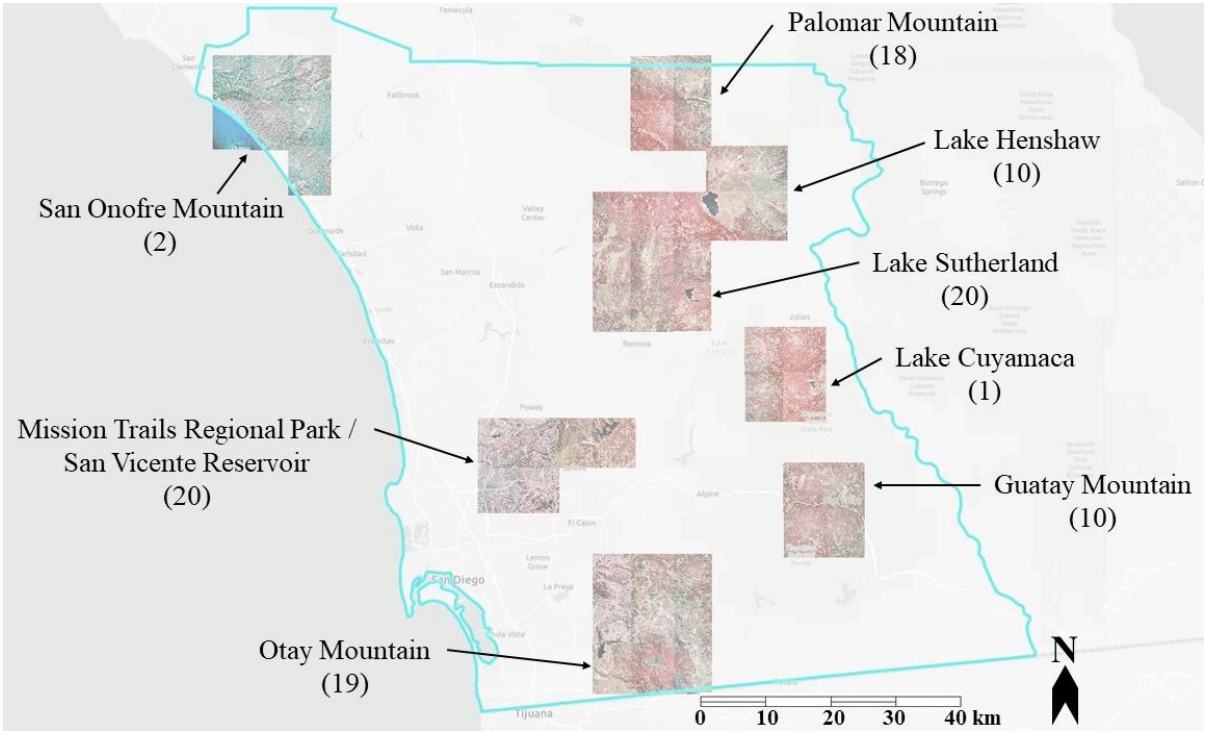

Figure 17. Locations of eight AOIs within the San Diego County study area used to assess the accuracy of herbaceous fractional cover estimates. The number following each AOI label represents the number of 90 m x 90 m sampling grids used to generate reference data. AOIs were selected based on the presence of locations with high herb, locations with a range of woody growth form cover, accessibility for field work, and different time-since-burn dates. Image data: CIR 1996 and 1997 DOQ orthoimages.

Sampling grids included a variety of landscape cover types, cover fraction values, and slope aspects, were representative of the study area, had burned in a wildfire incident anywhere between zero and four times between 1910 and 2021, and were separated by a

minimum distance of 100 m from one another. For each of the 100 sampling grids, a 100-point dot grid was created for visual image interpretation of the cover type located at each of the 100 points (Figure 18). Land cover type information for all points was recorded for both 1996 or 1997 (based on DOQ data) and 2020 (based on NAIP and Nearmap data) in an attribute table as herbaceous, woody cover, or bare ground. Reference data were used to assess the accuracy of Landsat-derived herb fraction maps, particularly those from Year 2 (1997) and Year 4 (2020).

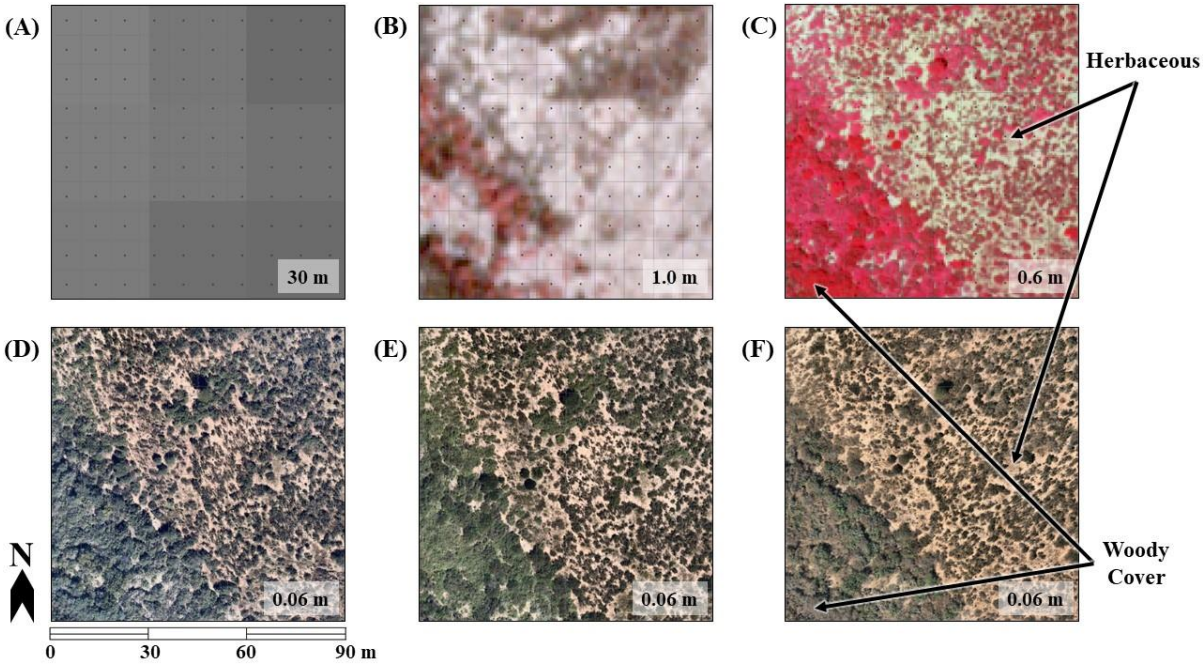

Figure 18. Examples of a single sampling grid with the 100-point dot grid and imagery. (A) Three-by-three Landsat pixels associated with the reference data sampling grid. (B) A false color DOQ image (1996/09/30). (C) A false color NAIP image (2020/05/20). (D) through (F) True color Nearmap images (left to right: 2020/01/04, 2020/05/01, and 2020/09/22). Arrows point to examples of herbaceous vegetation and woody cover in the scene.

10. Accuracy Assessment

Accuracy of herbaceous cover proportion maps for each year (1988, 1997, 2011, and 2020) was estimated using the generated reference data, according to MAE, RMSE, and R^2 metrics. Mixture model output values were not fully constrained to the set unit sum

constraint weight of 1.00 (100%), so negative values were set to 0.0001 (close to 0.00) and values greater than 1.00 were set to 1.00. Simple linear regression models were run, scatterplots depicting modeled versus reference cover were generated, and the 1:1 and best fit lines were delineated; the latter defines systematic error (Lippitt *et al.*, 2017; Peterson & Stow, 2003; Uyeda *et al.*, 2016).

The accuracy of the estimated change maps of herbaceous cover for 1988 to 2020 and 1997 to 2020 were calculated using reference data from 1996 and 1997 compared to 2020. The absolute difference was calculated for both the unmixed and reference data. MAE and RMSE were calculated for the 78 (out of the original 100) sampling grids that did not burn within five years of the 1988 image date and the 1996 and 1997 reference data orthoimagery; none of the sampling grids burned prior to 2020. Histograms of herbaceous fractional cover change were generated.

11. Analyses of Herbaceous Cover Distributions and Changes

A random sample of patches of 11 contiguous pixels exhibiting herbaceous cover change < -20% and > 20% were analyzed for possible vegetation type conversion from woody-to-herbaceous cover, or where woody cover re-established. The $\pm$ 20% value coincides with the uncertainty in the herb cover change map. DOQ and Nearmap image sets, along with NLCD land cover classification data, were analyzed to reconcile whether apparent herb changes were reliable. Percentages and histograms of herbaceous pixels were summarized for each Landsat date. The mean herb cover change for the four Landsat dates was analyzed, along with woody cover and bare ground fractional cover. The years a fire burned, the number of fires, and the time-since-fire were used to calculate fire frequency (and both minimum and average fire return interval). 3DEP data were used to determine elevation and aspect. DOQ

orthoimagery and OSM data were used to measure approximate distance from patch edges to roads and trails. Patch cover values from the estimated change map of woody cover for 1988 and 2020 were also compared to the chaparral recovery product from Storey *et al.* (2021) and woody cover loss points from Syphard *et al.* (2019).

C. Results

The most accurate Landsat SMA-estimated map is the 2020/08/29 image date with MAE = 9.55%, RMSE = 12.88%, and R^2 = 0.83 (Table 11). The best fit line in the associated scatterplot (Figure 19D) is very close to the 1:1 line, which communicates the map accurately and systematically estimated herb cover. Though high GRE orthoimage data that matched the 1988 (earliest) Landsat image date were unavailable, MAE = 10.99%, RMSE = 15.75%, and R^2 = 0.77 were lower when compared to the 1996 and 1997 reference data. Estimates of the 1997 Landsat product compared to 1996 and 1997 reference data (MAE = 19.11%, RMSE = 24.07%, and R^2 = 0.64) (Table 11) indicate that herb cover was overestimated in the 0 to 60% range and underestimated in the 80 to 100% range (Figure 19B).

Table 11. Herbaceous fractional cover error results for image date inputs compared to reference data. The number of sampling grids analyzed (out of 100) after omitting the grids within burned areas five years prior to the image date, and the MAE, RMSE, and R^2 results are displayed.

Image Dates	Number of Sampling Grids	MAE	RMSE	R^2
1988/09/22	94	10.99%	15.75%	0.77
1997/10/17	84	19.11%	24.07%	0.64
2011/10/08	74	13.55%	17.78%	0.78
2020/08/29	100	9.55%	12.88%	0.83

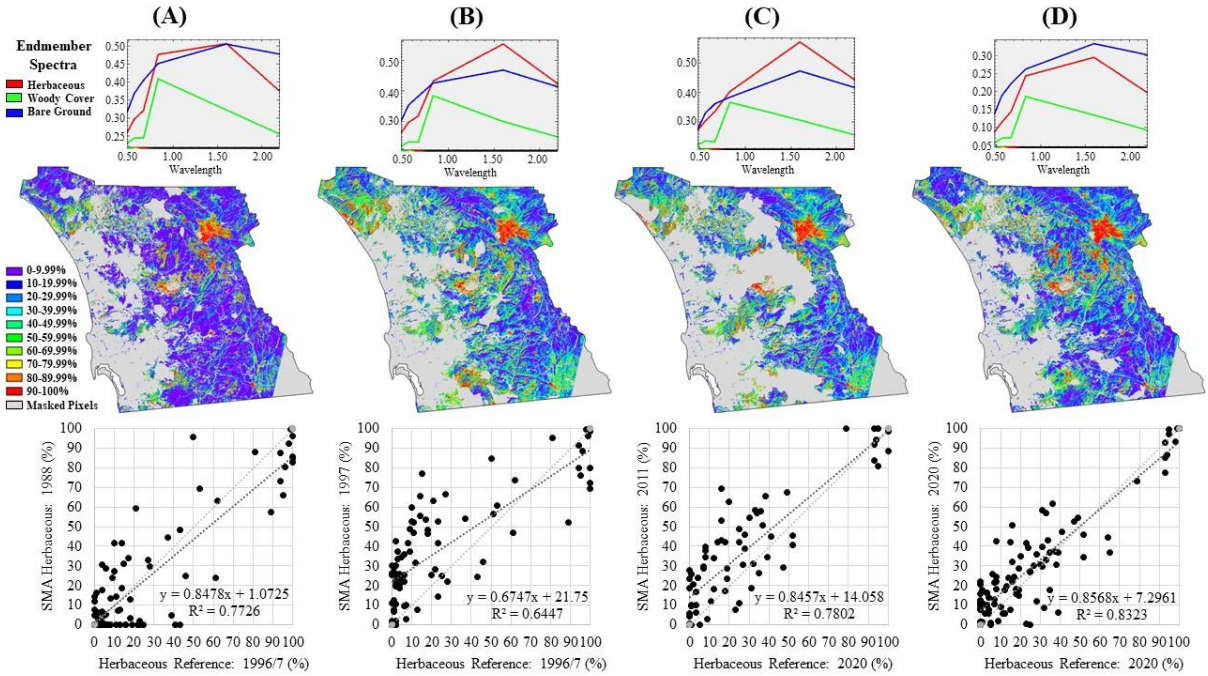

Figure 19. Herbaceous fractional cover maps and associated EM spectra and scatterplots from the four image dates: (A) 1988/09/22, (B) 1997/10/17, (C) 2011/10/08, and (D) 2020/08/29. First row: EM spectra. Second row: Herb cover maps. Areas that burned within five years of the image dates and reference data orthoimagery are masked. Third row: Scatterplots. The light gray dotted 1:1 line communicates each output's unsystematic estimation of herb cover (e.g., scatter), and the black dotted best fit line communicates the systematic error.

As a goal of this study was to capture fractional cover change from an early and present date from the available Landsat SR data archive, focus was placed on the longer time intervals. Herbaceous cover change was most accurately estimated for the 1988 and 2020 interval, for which recently burned sampling grids were omitted, with MAE = 12.17% and RMSE = 15.57% (Table 12). Therefore, mapped changes are represented as 20% intervals and changes between -20 and 20% are considered areas that experienced "minimal to no change" (or are at least within the range of uncertainty). Hereafter, the 1988 to 2020 multi-decadal period and 20% change intervals are the focus for this work. The 1997 and 2011 cover maps were treated as intermediate products to reconcile apparent fractional cover transitions between the end dates.

Table 12. Herbaceous fractional cover error results for cover maps resulting from the absolute differences of image dates compared to the absolute difference of the reference data. The number of sampling grids analyzed (out of 100) after omitting the grids within burned areas five years prior to the image date, and the MAE and RMSE results are displayed.

Absolute Difference	Number of Sampling Grids	MAE	RMSE
Δ 1988 and 2020	94	12.17%	15.57%
Δ 1997 and 2020	84	14.97%	18.83%

Histograms of herbaceous fractional cover values, at 20% intervals, from the 1988 and 2020 absolute difference cover map are shown in Figure 20. The results portray an agreement between the cover proportions of the reference data and Landsat-derived cover maps, and certainly within the 12.17% error range reported by the absolute difference of the 1988 and 2020 MAE metric. Both estimates communicate that more than 50% of the sampling grids (Figure 20A) and Landsat pixels within the full San Diego County study area (Figure 20B) experienced a 0 to 20% increase in herb cover over time; 79.49% of the sampling grid area and 68.42% of the map are within the "minimal to no change" range (-20 to 20%).

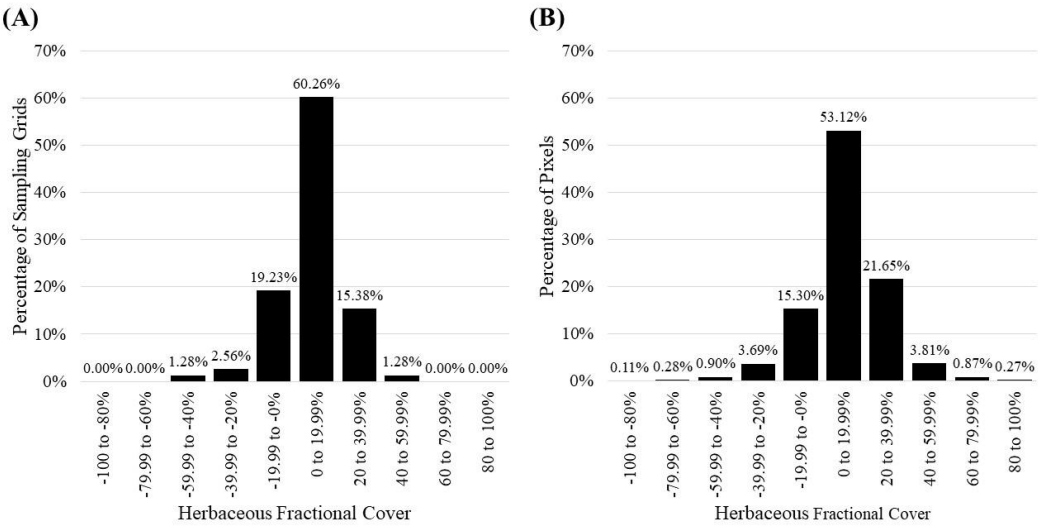

Figure 20. Histograms of herbaceous fractional cover change from the 1988 and 2020 absolute difference cover maps. (A) 78 reference data sampling grids (out of 100) that did not burn within five years of the 1988 image date and the 1996 and 1997 reference orthoimagery. Outside of the -20 to 20% uncertainty range, the sampling grids show a 3.85% decrease and 16.67% increase in herb cover. (B) Pixels from the full study area (with the NLCD land cover mask applied and areas that burned before 1988 and 2020 masked). Outside of the -20 to 20% uncertainty range, the map shows a 4.98% decrease and 26.60% increase in herb cover.

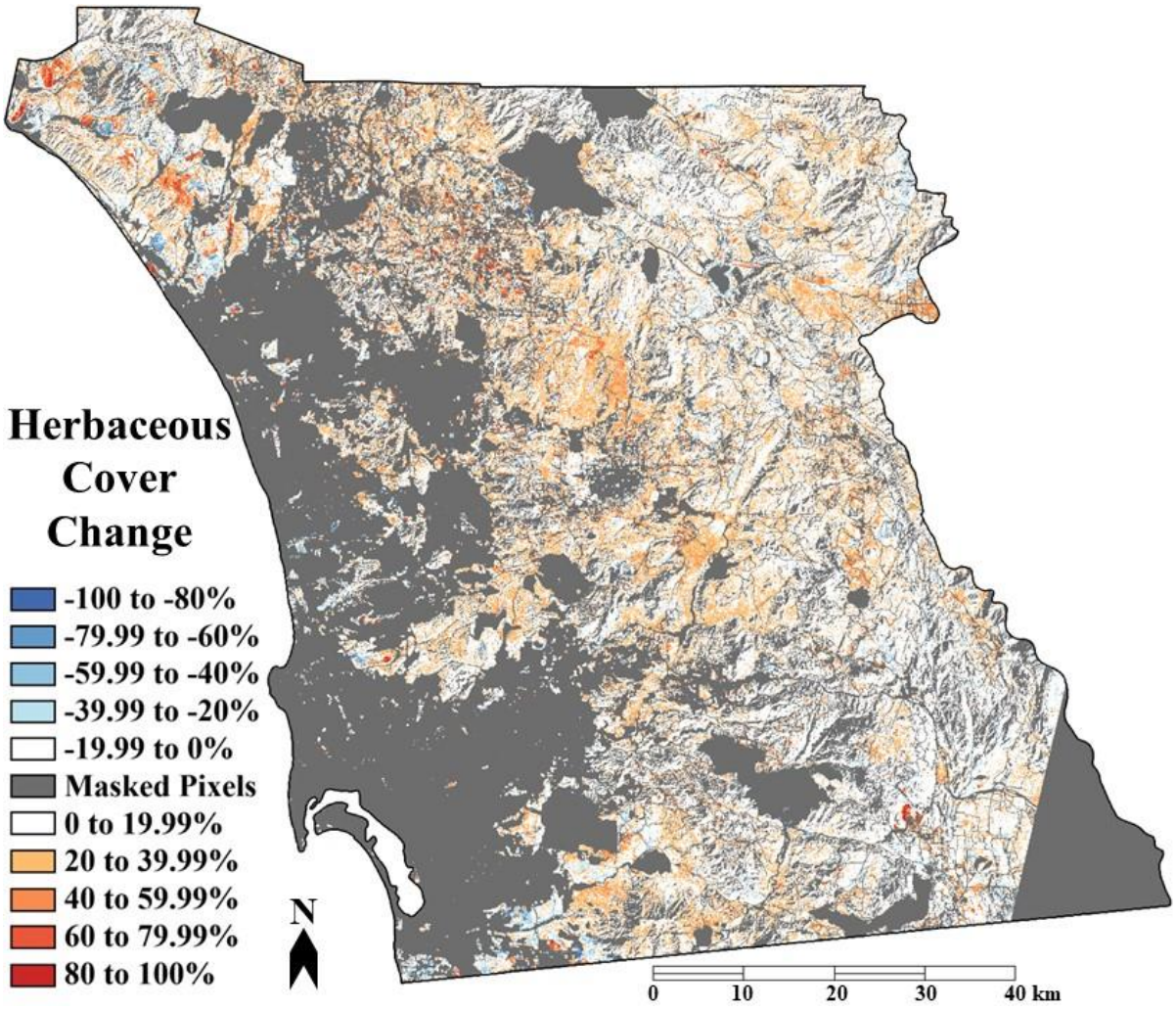

Figure 21. Absolute difference fractional cover map highlighting areas with change in herbaceous fractional cover < -20 and > 20% between 1988 and 2020. Areas that burned within five years of the image dates and the NLCD land cover types not of interest are masked.

A map depicting absolute herbaceous cover change between 1988 and 2020 for the San Diego County study area is shown in Figure 21. Again, emphasis is placed on cover change < -20 and > 20% to account for the uncertainty and error (Table 12). Less than a third (31.58%) of the study area had an absolute difference < -20 and > 20%; 26.60% of the study area exhibited an increase in herb > 20% and 4.98% experienced a decrease in herb < -20% (Figure 20B). Although pixels of substantial herb increase and decrease are scattered

throughout the study area, the greatest concentration are located in WUI areas in the Diegan Coastal Hills and Valleys, Diegan Western Granitic Foothills, and Santa Ana Mountains (Level IV) Ecoregions (refer back to Figure 14).

Contiguous 11-pixel patches belonging to the same 20% interval class were segmented to generate 50,104 patches that were analyzed for general trends in associated fire disturbance and environmental factors (Table 13). Despite the use of the NLCD 2019 data to mask land cover types not of interest, almost all patches that decreased by < -60% were associated with mechanical landscape disturbances or land cover changes associated with cultivated crops (agricultural areas). Many of the -59.99 to -40% change patches were pasture/grazing lands (defined by NLCD 2019 data as herbaceous cover). The decline in herb cover over time associated with this interval class may be related to the specific phenology associated with the image date, soil moisture, or drought. Most of the -39.99 to -20% change patches were areas of actual decrease in herb cover in heterogeneous wildland areas. The majority of the 20 to 39.99% patches were composed predominantly of subshrubs and grasses that experienced an increase in herb cover in wildland areas and are commonly associated with higher fire frequency (shorter fire return intervals). Similar to patches mapped as exhibiting large decreases in herb cover, patches that increased by > 40% were mostly found in agricultural areas (not masked by NLCD data), associated with changes in reservoir levels, or areas that had been mechanically cleared prior to building and development projects.

A sample of 50 patches was identified for more detailed qualitative analysis (Table 13, Figure 22). The number of patches selected per 20% interval was based on the area (ha) that experienced each interval of change over time, the number of patches identified within each

interval, and the total area of patches per interval (Table 13). Individual patches ranged from 11 to 372 pixels (0.99 to 33.5 ha) in size. The 20 to 39.99% interval class was represented by the largest number of patches (23) because I observed that the most herb expansion occurred within this interval (outside of the "minimal to no change" range), and this class had the largest number of patches (out of 50,104). Ten patches from the "minimal to no change" range (-20 to 20%) were included as a control group.

Table 13. Percentage and areal information, as well as patch information, associated with each 20% herbaceous change interval. The percentage and the area (ha) of the study area represented by pixels calculated from each interval are reported. The number of patches represented by each interval, the patch area (ha), and the number of patches qualitatively analyzed per interval are listed. The seven -39.99 to -20% and 23 20 to 39.99% interval class patches were selected for further descriptive analysis (highlighted rows).

Interval (%)	Percentage of the Study Area (%)	Area of the Study Area (ha)	Number of Total Patches	Total Area of Patches (ha)	Number of Sample Patches
-100 to -80	0.11	434	78	190	1
-79.99 to -60	0.28	1,164	131	320	1
-59.99 to -40	0.90	3,716	422	838	3
-39.99 to -20	3.69	15,218	2,247	5,044	7
-19.99 to -0 (Control)	15.30	63,122	10,347	33,807	5
0 to 19.99 (Control)	53.12	219,154	19,935	181,245	5
20 to 39.99	21.65	89,342	13,956	54,640	23
40 to 59.99	3.81	15,701	2,303	5,201	3
60 to 79.99	0.87	3,609	499	1,080	1
80 to 100	0.27	1,134	186	566	1
Total	100.00	412,594	50,104	282,940	50

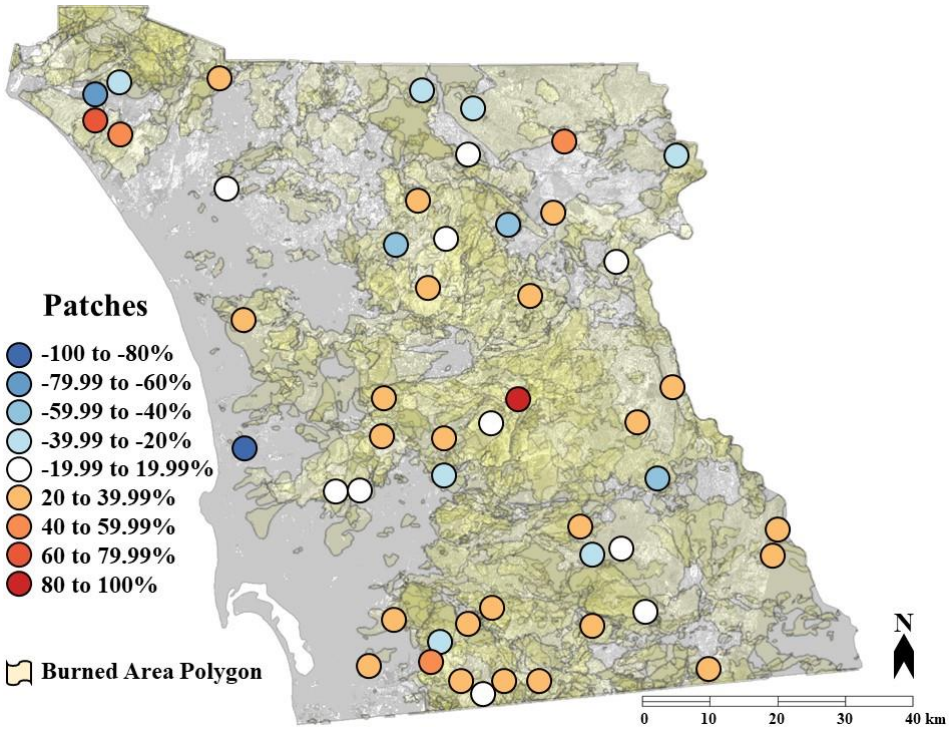

Figure 22. The locations of patches used for qualitative analysis overlaid on burned area polygons. The 50 circles represent the approximate location of each 20% interval patch (patches are not to scale). Pale yellow, transparent polygons represent areas that burned between 1910 and 2020 (CAL FIRE FRAP, 2021); brighter yellow indicates multiple fires in the same area (and therefore a lower average fire interval and higher fire frequency over time).

Following comparison to orthoimage data, I focused on the 30 patches within the -39.99 to -20% (seven patches) and 20 to 39.99% (23 patches) interval classes because they represented the most realistic examples of herbaceous change in wildland areas. One patch was predominantly herb covered throughout the study period, and the other 29 contained heterogeneous mixes of varying herb, woody, and bare ground cover values. Temporal relationship to wildfire over the 111-year period from 1910 to 2020 (Figure 23) and characteristics about the land cover were evaluated.

The seven patches that experienced a decrease in herbaceous cover burned between one and four times from 1910 to 2020 (an average of 2.57 fires per patch), had an averaged minimum fire interval of 13 years, an averaged average fire interval of 15.93 years, an average fire frequency of 58.14, and burned between nine and 92 years prior to 2020 (an

average of 32.71 years). Three of the seven patches (42.86%) had a minimum interval between fires < 15 years (Figure 23). These seven patches were in four of the seven Level IV Ecoregions, and on southeast- or east-facing slopes. Their average elevation ranged from 260 to 1,745 m and the average range in elevation within patches was 180 m. Patch edges ranged from 10 to 3,200 m from a road (an average of 2066.43 m) and 0 to 2,750 m from a trail or access road (an average of 713.33 m). All seven patches were classified by the NLCD program as predominantly Shrub/Scrub.

The 23 patches that experienced an increase in herbaceous cover burned between zero and seven times from 1910 to 2020, with an average of 2.35 fires per patch, had an averaged minimum return fire interval of 21.18 years, an averaged average fire interval of 29.02 years, an average fire frequency of 58.63, and burned between three and 76 years before 2020 (an average of 22.81 years). Eight of the 23 patches (34.78%) had a minimum interval between fires < 15 years (Figure 23). These patches were in all seven Level IV Ecoregions, were found on different slope aspects, on ridgelines, in valleys, and over flat terrain, the average elevation of patches ranged from 165 to 1,480 m (an average of 663.70 m, and the average change in elevation within patches was 90.74 m). Patch edges ranged from 0 to 4,130 m from a road (an average of 865.65 m) and 0 to 980 m from a trail or access road (an average of 175.65 m). Two patches were classified by the NLCD program as predominantly Herbaceous or Emergent Herbaceous Wetlands, and 21 were predominantly Shrub/Scrub.

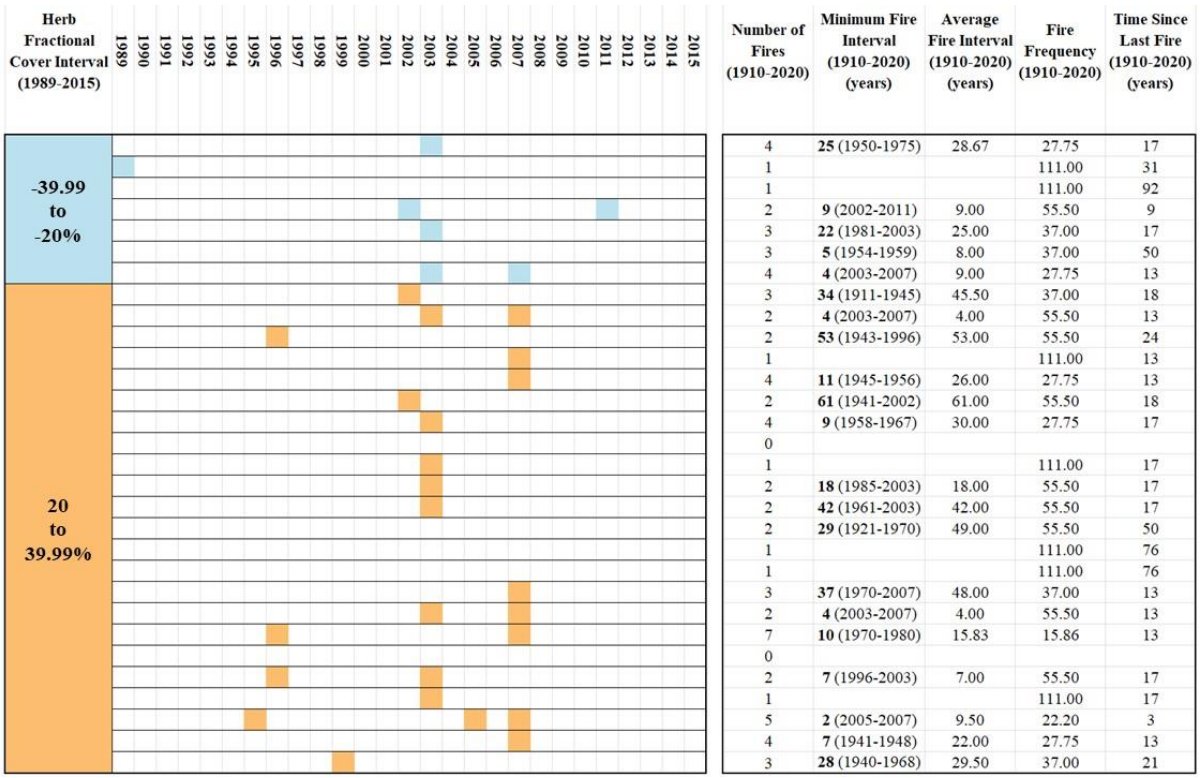

Figure 23. Wildfire information per sample patch. Left: Each of the 30 sample patches (one per row) are organized by -39.99 to -20% (seven sample patches) and 20 to 39.99% (23 sample patches) intervals, and the associated wildfire incidents are labeled by year (columns) with a square of the same color. Visualization is for the study period (1988 to 2020) with years prior to 1988 and 2020 masked, resulting in a focus on 1989 to 2015. Right: CAL FIRE FRAP fire information from 1910 through 2020 for each sample patch – the number of fires that burned a single patch over time, the minimum fire interval in time, the average fire interval at each patch, the frequency (111 years divided by the number of fire incidents), and the time since the patch last burned in a wildfire.

D. Discussion

1. Reliability and Accuracy of Herbaceous Cover Change Map

A standard SMA model applied to four dates of Landsat imagery captured over a 33-year period yielded maps of herbaceous fractional cover change that are reasonably reliable and accurate. The four herb cover maps produced for each fall image date over the study period (1988, 1997, 2011, and 2020) portray location-specific change in herb over time. Herb cover was most accurately estimated by the 2020/08/29 date with MAE = 9.55%, RMSE = 12.88%, and R^2 = 0.83 (Figure 19D, Table 11).

The 100 sampling grid locations were selected based on location, landscape heterogeneity, and areas that did not burn between 2016 and 2020. However, once grids that had been affected by wildfire between 1984 to 1988 and 1993 to 1997 were omitted, only 78 sampling grids remained. This lowered the number of available sampling grids for accuracy assessment and change analysis and may have introduced a discrepancy in representativeness of herb cover fractions observed, compared to the full study area.

The herbaceous fractional cover change map produced using the first and last years of the study (the absolute difference of 1988 and 2020) portrays the spatial distribution of herbaceous cover change < -20 and > 20% in the San Diego County study area (Figure 21). The change map depicts a 4.98% decrease and 26.60% increase in herb cover (Figure 20B), which is consistent with Syphard *et al.* (2019). When compared to 78 sampling grids, 90 m x 90 m in size, scattered throughout the study area, error in the change map was estimated to be MAE = 12.17% and RMSE = 15.57% (Table 12). This level of error is corroborated by the qualitative analysis of 30 sample patches, for which actual change (both decrease and increase) of herb was observed.

The estimated errors for the fractional cover maps (single dates and change) are reasonable and render the maps useful for assessing the broad-scale distributions of herbaceous change. However, two methodological recommendations stem from application of the SMA model for this study. First, validation of the Landsat-derived change map using reference data generated from orthoimage-based sampling grids is challenging. Despite use of DOQ, NAIP, and Nearmap orthoimagery from 1996 through 2020 at a GRE of $\leq$ 1.0 m and collected during multiple phenological cycles, comparison of the 78 sampling grids to the 1997 and 2020 cover map yielded an MAE = 14.97% and RMSE = 18.83% (Table 12).

Both reference data and SMA-derived maps should be considered model-based estimates of herbaceous cover, and the reference data are not "ground truth." Nevertheless, that the cover maps agree to the sampling grids within the level of estimated agreement is encouraging and yields confidence in the utility of the change map.

Second, selection and intermediate fine-tuning of EMs is critical for accurate unmixing based on SMA (Roberts *et al.*, 1998; Somers *et al.*, 2011; Tompkins *et al.*, 1997). The vegetation growth form and bare ground cover classes are not necessarily true EMs, which makes unmixing challenging (from Chapter II). The EMs incorporated in the SMA model that yielded the most accurate results were specific to each image date and were based on the results of testing iterative mixture analysis cycles. This makes sense when factors that contribute to land cover changes are considered (e.g., soil moisture related to precipitation or drought prior to image acquisition and vegetation phenology, particularly for green versus non-photosynthetic vegetation, causing spectral confusion (Dudley *et al.*, 2015; Hamada *et al.*, 2009; Roberts *et al.*, 1993; Rogan *et al.*, 2002; Roth *et al.*, 2012; Storey *et al.*, 2016), and recent wildfire effects (Quintano *et al.*, 2005; Quintano *et al.*, 2017; Röder *et al.*, 2008; Veraverbeke & Hook, 2013)). Similar to machine learning processes, datasets and parameters should be validated after each adjustment in the EM selection process based on independent testing (reference) data (Allred *et al.*, 2021; Jones *et al.*, 2018). However, SMA methods require substantially less training data and effort than machine learning and can still produce accurate fractional cover estimates without the need to generate large amounts of reference data for training.

Ancillary datasets were used to mask portions of Landsat images associated with land cover/land use types not of interest for the study (e.g., developed and agricultural lands)

from SMA modelling. However, errors and artifacts in those data sets resulted in substantial portions of developed and agricultural lands not being masked. In particular, NLCD data did not accurately represent all locations with urban development or cultivated crops. Similarly, fire incidents to which CAL FIRE were not engaged in fire suppression efforts (e.g., originating on military bases or too small to fit the guidelines for inclusion) were not mapped and therefore, not masked. These tended to emerge in the herb cover ranges of -100 to -60% and 40 to 100% change and were omitted from the sample patches. It is important to reconcile the reliability of initial results and manually mask locations like these to exclude all areas not of interest.

2. Areas Exhibiting Substantial Change in Herbaceous Fractional Cover

Products from this study were used to identify locations of herbaceous change over the multi-decadal study period, particularly to infer areas that experienced woody vegetation recovery or type conversion from woody-to-herb-dominated landscapes indicative of a grass-fire cycle. More than a quarter (26.60%) of the undeveloped portion of the San Diego County study area exhibited > 20% increase in herb cover (Figure 20). A sample of 50 patches was identified for further descriptive analysis (Figure 22, Table 13). Of the sample patches identified as experiencing an increase in herbaceous cover > 20% over time (28 out of 50, or 56%) (Figure 22, Table 13), 23 patches (82.14%) indicated a simultaneous decrease in woody cover (ranging in cover loss between 0.51 and 56.11%). The 23 patches ranged in size from 0.99 to 33.5 ha, which provides strong evidence for substantial shifts in growth form cover. However, none of the 50 sample patches were identified as having experienced full replacement of woody cover by herb. This reinforces that change in vegetation growth form cover is a gradual process that often occurs cumulatively over

multiple fire cycles (Syphard *et al.*, 2019); thus, the relatively short 33-year period of this study may not have bracketed the timing of 100% conversion.

A map depicting absolute woody cover change between 1988 and 2020 for the study area was also produced to explore the relationship between herbaceous and woody cover over time. The woody cover change values from the same 30 patch locations of apparent herb change ($\pm$20 to $\pm$39.99%) were compared to the woody cover change results from Storey *et al.* (2021) and Syphard *et al.* (2019). Twenty-four of the 30 sample patches (80%) (six that decreased and 18 that increased in herb cover) were in the same location as results from the Storey *et al.* (2021) recovery map. Comparison of mean woody cover values of each of the 24 patches to the mean of the same patch areas in the work of Storey *et al.* (2021) yielded MAE = 13.26% and RMSE = 18.71%. For the six patches that decreased in herb, MAE = 29.41% and RMSE = 32.25%; for the 18 patches that increased in herb, MAE = 7.87% and RMSE = 9.92%. This agrees with Storey *et al.* (2021) between woody cover estimates, particularly for those patches that exhibited herb increase over time (and a simultaneous decrease in woody cover), despite the slight difference in time period and variation in methodology for creating H_{t1} and H_{t2} (Equation 1).

Eighteen of the 30 sample patches (60%) from this study (four that decreased and 14 that increased in herb cover) were within 5,000 m of at least one point identified by Syphard *et al.* (2019) as exhibiting woody cover decrease > 25% between 1953 and 2016. However, only one of the sample patches exhibited a change in woody cover < -25%. Between 1988 and 2020 (and with areas that burned prior to those years masked), the Landsat SMA-estimated map indicated that some areas experienced a decrease in woody cover by 8.32%, and other areas an increase by 14.46%, which is not comparable to results from Syphard *et*

al. (2019). This may be due to the difference in studied time period, the variations in slope aspect and elevation within the 5,000 m range between the sample patch and associated point from Syphard *et al.* (2019), the fact that woody cover estimates in Syphard *et al.* (2019) were constrained to chaparral (and did not consider other woody vegetation growth form types), or by the selection of EMs, which may not have represented woody cover as accurately as herb.

The parsimonious modeling approach of standard SMA enables monitoring of change of herbaceous cover by satellite for wildfire-prone locations – both for short-term seasonal change as well as for long-term change. Results from this work may be used for monitoring purposes and to inform users about locations where herbaceous cover is expanding and where vegetation type conversion may be occurring. This is important not only due to biodiversity and carbon loss when woody shrubs convert to herbaceous cover, but also because grass ignites readily, and grassland fires are fast and dangerous. On average, grass fires were attributed to 6% of firefighter injuries between 2011 and 2015 alone, and an additional 52% of injuries are attributed to fire suppression in brush or a brush/grass mixture in the same five-year period (Ahrens, 2018). In December 2021, the Marshall Fire (first reported on 2021/12/30) ignited on an unseasonably warm and windy day in dry grass and brush in Boulder County, CO, ultimately burning nearly 1,000 homes and structures (Steinberg, 2022). In August 2023, the invasive grass-fueled and wind-driven wildfires that devastated Lahaina, Maui, HI (first reported on 2023/08/08) led to just under 100 fatalities, ranking among the top five deadliest wildfires in the U.S. since 1871 (Carli, 2023). Use of herbaceous cover maps can aid communities in identifying locations that require mitigation before the next ignition.

3. Factors Influencing Substantial Change in Herbaceous Fractional Cover

Based on the descriptive analysis of the 23 of 50 sample patches that indicated herbaceous increase between 20 and 39.99% (Table 13), the factors that yielded the greatest impact on substantial herb increase and subsequent woody cover decrease were fire return interval, drought, proximity to development, and elevation. Almost half (46.67%) of the 23 patches had fire return intervals less than 15 years, which is consistent with Syphard *et al.* (2019). The patches that experienced the shortest fire-return interval burned during drought-affected years or experienced a drought into the year following the fire (1996, 2002, 2003, and 2007). This may have impacted post-fire recovery (Pratt *et al.*, 2014; Syphard *et al.*, 2019) and mortality of woody resprouts or seedlings, as well as adult shrub mortality (Jacobsen & Pratt, 2018; Paddock *et al.*, 2013; Syphard *et al.*, 2019; Ventura *et al.*, 2016), which could allow for non-native annual herbs to invade more readily. The two short-interval fire incidents that burned most of the sample patches, as well as large areas of the study area – the Cedar Fire (first reported on 2003/10/25) and the Witch Fire (first reported on 2007/10/21) – are both associated with human-caused ignitions (CAL FIRE FRAP, 2021), further substantiating the role of proximity to development on high fire frequency and low fire return interval, particularly in WUI areas. This also supports the framework that explicitly recognizes a "human grass-fire cycle" (Fusco *et al.*, 2021). The average elevation range of the 23 patches (500 to 1,000 m) corresponds to findings from Safford and Van de Water (2014), who reported that some Southern California foothill elevation areas have burned more frequently over the last century than during any comparable (average) pre-settlement period within their reference period.

Out of the sample of 50 patches, the most notable differences between the 30 with ±20 to ±39.99% change and the remaining 20 representing the other interval classes were their relationships to fire return interval, distance to roads and trails, and elevation. Twenty-one out of 30 patches (70%) experienced more than one wildfire between 1910 and 2020; 36.67% of these 30 patches had an instance of at least one fire interval < 15 years. When compared to annual precipitation data per water year (Figure 15), the years in which multiple patches were affected by fires (1996, 2002, 2003, and 2007) (Figure 23) were also years that experienced lower than average precipitation, were recovering from low precipitation the previous year, or were followed by another year of low precipitation. Patches that were closer to roads (over 200% closer) and trails or access roads (over 400% closer) also exhibited an increase in herb cover. Patches that increased in herb occurred on slopes that were 50% flatter and 40% lower in elevation than those patches that decreased in herb. In summary, patches of substantial herb change tended to be associated with short fire return intervals compounded by drought conditions, elevations between 500 and 1,000 m, and in close proximity to roads, trails, and access roads.

E. Conclusions

To my knowledge, this is the first study to use SMA applied to multi-decadal Landsat image data to provide empirical evidence of the extent and amount of landscape-scale herbaceous change in San Diego County shrublands. With a focus on herb cover estimation over a 33-year period, I explored the accuracy of SMA applied to Landsat 5 TM and 8 OLI SR data acquired over the San Diego County study area. The resulting herb cover maps from the earliest (1988) and recent (2020) image dates were used to map absolute cover change (Figure 21), with an estimated error of MAE = 12.17% and RMSE =15.57%, respectively

(Table 12). High GRE orthoimagery supported evidence of herb cover increase and woody cover decline depicted in the cover change map, particularly where herb cover increased between 20 and 39.99%. This change interval most accurately depicted locations experiencing vegetation type conversion, possibly indicating grass-fire cycle effects. Satellite-derived herb cover change maps provide a useful data source to be used in conjunction with ground data, expert knowledge, and land use history data to support actionable and operational decisions (Allred *et al.*, 2021; Jones *et al.*, 2018).

Landsat data were used because of the long record length of archived data necessary for a multi-decadal study. For projects focused on a time period after 2015 and moving forward, other satellite sensor options with higher GRE such as the European Space Agency's Sentinel program, may be useful (Maestas *et al.*, 2020; Sousa & Davis, 2020). Incorporation of aerial hyperspectral image (HSI) or imaging spectroscopy data could also improve reference data generation and assessment of results (Jarocińska *et al.*, 2023). However, due to infrequent collects and smaller areal extents covered by airborne HSI, this option is not as tractable as use of spaceborne sensor data for a large area study.

The results of this study indicate potential for application of the SMA model combined with historical wildfire data to inform users of fractional cover conditions before the start of the next wildfire. Incorporation of additional EMs that differentiate between subshrubs, true shrubs, and trees may be beneficial for studies that extend beyond San Diego County and into other parts of Southern California. In Chapter IV, I will integrate historical ignition points with herb cover maps to analyze the effects of herbaceous cover and its change on wildfire starts in San Diego County shrublands.

IV. Evaluation of herbaceous cover fraction and wildfire ignition association in San Diego County, California, USA shrublands (1992-2020)

A. Introduction

Invasion and expansion of non-native grasses and forbs (herbaceous vegetation or herbs) can promote and increase landscape flammability and alter an ecosystem's fire regime (Brooks *et al.*, 2004; D'Antonio & Vitousek, 1992). Ecosystems are partly defined based on disturbance regimes, and wildfire is an important type of disturbance (Brooks *et al.*, 2004; Sousa, 1984). The invasion of vegetation growth forms can affect native ecosystems by changing fuel properties, which can then affect fire behavior and alter fire regime characteristics (e.g., frequency, intensity, extent, type, and seasonality) (Pickett & White, 1985). Although fire regimes are affected by spatial and temporal variations in fuel (which can change within a day following a major disturbance), climate (which can potentially shift within the scale of centuries to decades), and topography (which tend to change over long geologic time scales), fuels are the ecosystem component that is linked with fire regimes by feedback loops through other ecosystem properties and plants (Brooks *et al.*, 2004).

A complex relationship exists between fuels and a fire regime. Fuel amount is defined as the available combustible biomass, and it accounts largely for ignition propensity (Chen & Jin, 2022). An altered fire regime creates favorable conditions for invasive herbaceous species, which recover and spread quickly following a fire incident, resulting in a grass-fire cycle (D'Antonio & Vitousek, 1992; Fusco *et al.*, 2019). This directional shift in fire behavior and regime properties may result in localized conversion or replacement of species that are unable to persist under the new fire regime (Brooks *et al.*, 2004). Grasslands

invading shrublands are the cause of significant negative ecosystem effects (Brooks *et al.*, 2004; Mack *et al.*, 2001). However, there is no single driver that can be viewed as the "silver bullet" for type conversion prediction or restoration potential. Therefore, it is recommended that species with a high potential to alter fire regimes and contribute to the grass-fire cycle should be prioritized for control (Park & Jenerette, 2019). It is important to manage invasive species that alter ecosystem processes over large areas because they could feed back to alter other components of global change, such as climate, atmospheric composition, and land use (D'Antonio & Vitousek, 1992).

Numerous studies have investigated the effect of the presence and expansion of invasive herbaceous growth forms on fire regime (Balch *et al.*, 2013; Brooks *et al.*, 2004; Fusco *et al.*, 2019; Jin *et al.*, 2015b). Fusco *et al.* (2019) examined 12 species of non-native grasses and documented regional-scale alteration of fire regimes for eight species across 29 U.S. Environmental Protection Agency (EPA) level III ecoregions. They found invasive grasses increased fire occurrence by up to 230% and fire frequency by up to 150%, which suggested many ecosystems are vulnerable to the effects of a novel grass-fire cycle (Fusco *et al.*, 2019). Jin *et al.* (2015b) reported that greater grassy fuels accumulated during two or three wet years in Mediterranean climates can promote fire occurrence.

Balch *et al.* (2013) analyzed the effect of expanding and invading non-native cheatgrass (*Bromus tectorum*) cover on the Great Basin fire regime by quantifying fire ignition points from 1980 to 2009. The authors combined Moderate Resolution Imaging Spectroradiometer (MODIS) satellite and U.S. Geological Survey (USGS) burned area and historic fire perimeter data to determine the dates of fire detection and compare fire regimes. The proportion of ignitions in cheatgrass grassland was compared to the fraction of cheatgrass

area burned for each multi-date fire (fires that burned more than one day). They found that multi-date fires were significantly more likely to have burned in cheatgrass cover on their first day compared to other vegetation types (65% of 247 fires between 2000 and 2009). They also calculated the total number and mean area of individual fires that burned within each analyzed land cover class.

Increases in fire ignitions, historical fire cycle, altered fire dynamics, land fragmentation, rodent herbivory, and altered nitrogen deposition and cycling are examples of drivers that have lowered the resistance of native vegetation growth forms (e.g., chaparral) to the advances of competitive non-native vegetation species (Park & Jenerette, 2019). Anthropogenic development and land use change involves such activities as landscaping with exotic and invasive species, constructing firebreaks (intending to aid wildfire control) (Merriam *et al.*, 2006; Park & Jenerette, 2019), and mechanically removing fuel (intending to mitigate vegetation prior to a wildfire ignition) (Brennan & Keeley, 2015; Park & Jenerette, 2019). Recently, most fire ignitions in California chaparral shrublands are attributed to human activity (Conard & Weise, 1998; Park & Jenerette, 2019; Syphard *et al.*, 2007), and too-frequent burns do not allow chaparral to reach maturity or may even preclude the reseeding of chaparral shrubs, with especially deleterious effects on obligate seedlings (Zedler *et al.*, 1983; Park & Jenerette, 2019).

The wildland-urban interface (WUI), reported to be the fastest-growing land use type in the conterminous U.S., raises additional concerns (Radeloff *et al.*, 2005; Radeloff *et al.*, 2018) because more wildfires due to human ignitions are anticipated. When wildfires do occur, they will pose a risk to the growing human population and number of structures and

will be harder to fight. Additionally, naturally ignited (e.g., by lightning) fires will be less likely to be left to burn (Radeloff *et al.*, 2018).

In addition to the impacts of larger and more frequent fires, climate change and invading vegetation species will drive further disruptions to fire regimes (Dennison *et al.*, 2014). Based on projected changes in temperature and precipitation, climate change is expected to increase the potential for fire occurrence by 150% by the end of the century (Liu *et al.*, 2010; Fusco *et al.*, 2019). Analyses encompassing longer time periods are necessary to properly understand the influence of climate, weather, and disturbance factors on fractional cover of herbaceous vegetation in shrubland habitats (Lippitt *et al.*, 2017) and the potential impacts of herb change on the fire regime.

Remote sensing offers an approach to effectively map and monitor vegetation cover fractions over large areas and long timescales. The archive of Landsat Surface Reflectance (SR) data provides imagery acquired at regular time intervals over large geographic extents dating back to 1984; it is an ideal source of data for observing multi-decadal vegetation change and can be used in combination with imagery analysis methodologies to infer effects on fire regime. However, due to Landsat's moderate spatial resolution, an approach that can be used to estimate vegetation growth form and land cover fractions of distinct surface types at a sub-pixel level is required. This requirement is met by spectral mixture analysis (SMA), an image processing approach used to estimate material cover fractions based on the assumption that the ground area sampled by a pixel, the ground resolution element (GRE), can be reasonably approximated by a fractional mixture of a small number of spectrally distinct materials. During the unmixing process, the radiance (or reflectance) of a mixed GRE is considered to be an area-weighted linear combination of spectral endmember (EM)

materials, which represent homogeneous or "pure" materials, plus error (Adams *et al.*, 1986; Gillespie *et al.*, 1990; Roberts *et al.*, 1998; Settle & Drake, 1993; Smith *et al.*, 1990). Vegetation fractions produced by SMA have been used to describe vegetation growth form change (Dennison & Roberts, 2003; Roberts *et al.*, 2002; Rogan *et al.*, 2002) and vegetation regeneration after disturbance (Dennison & Roberts, 2003; Riano *et al.*, 2002).

Remotely sensed imagery and fractional cover maps derived from such imagery combined with historical fire data yield information about fire regimes. Balch *et al.* (2013) provided the first quantitative basin-wide support for widespread belief that cheatgrass increases fire activity across the Great Basin and, at the time of publication, fire cycle and cheatgrass relationships had not been evaluated at a regional scale, nor had the fire cycle and comparable herbaceous cover relationships been evaluated within Southern California shrubland ecoregions. An understanding of historical fire regimes in herbaceous vegetation is poor (Safford & Van de Water, 2014), and any shift outside of the typical range of fuel conditions for native plants will affect fire behavior and regime properties (D'Antonio & Vitousek, 1992; Keeley, 2001; Brooks *et al.*, 2004; Halsey & Syphard, 2015). Therefore, it is important to determine the effects of herb expansion regarding potential changes in fire regime (e.g., ignition potential, fire spread, and suppression potential) on San Diego County, California, USA shrublands.

The objective of this research was to analyze historical wildfire ignition data and assess the spatial-temporal association between herbaceous fractional cover and ignition distributions. Herbaceous vegetation cover maps from Chapter III were used to investigate the relationship between herb cover and the proportion of ignitions (the number of ignitions per total ignitions). I sought to examine and answer the question: Are differences in the

spatial distribution of wildfire ignitions associated with differences in herbaceous fractional cover in San Diego County shrublands for 1992 to 2020?

B. Data and Methods

1. Study Area

The study domain is the intersection of the 783,290 ha of the Southern California Mountains and Southern California/Northern Baja Coast U.S. Environmental Protection Agency (EPA) level III ecoregions (U.S. EPA, 2013) within San Diego County (Figure 24). Areas under agricultural, urban, and built land use were considered as "Developed" and masked from analysis, as was an area in the southeast portion of the study domain that is not covered by Landsat scenes used in this study.

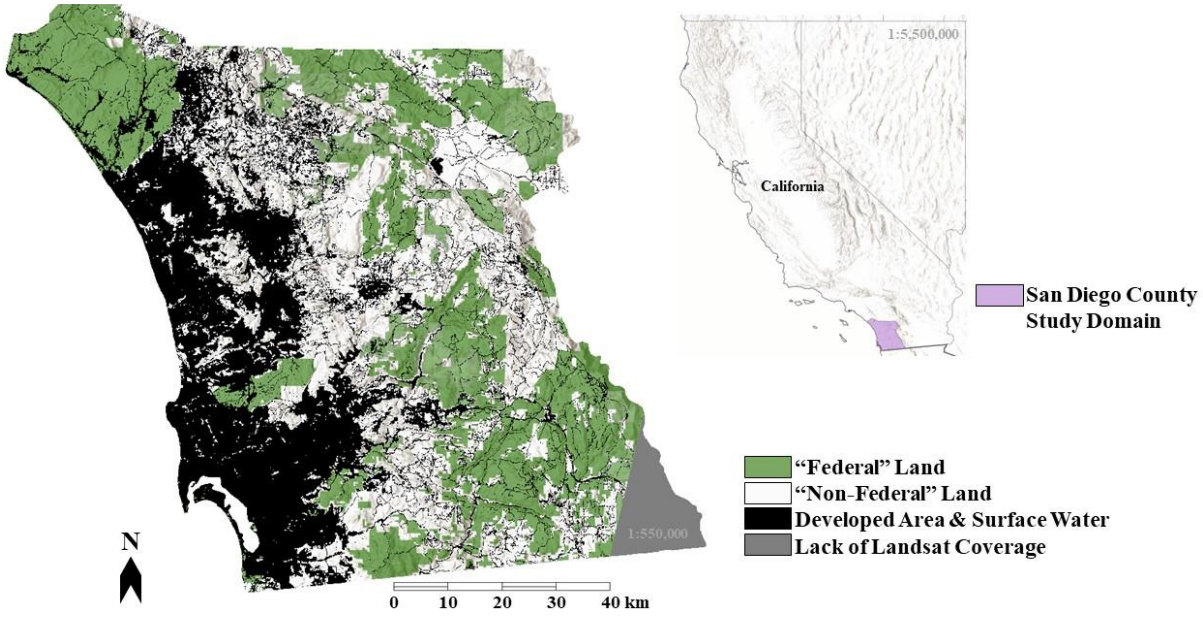

Figure 24. Study area location within San Diego County, California. Left: The San Diego County study domain (783,290 ha) with National Land Cover Database (NLCD) developed areas and surface water, as well as the southeast portion not covered by Landsat, masked (resulting in a study area of 532,167 ha). National Forest System ("Federal") lands (U.S. Department of Defense, U.S. Department of Interior – Bureau of Land Management, U.S. Fish & Wildlife Service, U.S. Forest Service, and Federal American Indian Reservations) are delineated by green over a topographic relief map (Source: Living Atlas). "Non-Federal" lands are white over a topographic relief map. Right: The study domain is delineated by a purple polygon.

The study domain mostly has a semi-arid Mediterranean-type climate and experiences hot, dry summer seasons (26 to 37 °C) and moderate winter precipitation (250 to 450 mm) (Rundel, 1998). The topographic and climatic heterogeneity contribute to high levels of biodiversity (Syphard *et al.*, 2019a). The most extensive vegetation types are true shrubs such as chamise (*Adenostoma fasciculatum*) chaparral and mixed chaparral communities (Keeley, 2000; Pryde, 2004; Syphard *et al.*, 2019a). Shrubs within these communities are often distributed in a mosaic with both native and non-native herbaceous cover and subshrubs (e.g., drought-deciduous coastal sage scrub like *Artemisia californica*, *Eriogonum fasciculatum*, and *Salvia* species (Rundel, 2007)). Oak woodlands and mixed conifer forest communities occur in higher elevation areas (Syphard *et al.*, 2019a).

The natural fire regime of San Diego County and most of the Southern California coastal shrubland area is characterized by periodic large, high-intensity crown (which includes shrubs) fires driven by hot, dry Santa Ana wind events that recur each autumn, in addition to smaller fires in the summer (Jin *et al.*, 2015b; Keeley & Syphard, 2019). Fire frequency has increased across much of the landscape in response to a variety of factors, but primarily population growth and urban expansion (Syphard *et al.*, 2019). The population of San Diego County increased by 27.2%, from 2.6 million people in 1992 to 3.3 million in 2020 (USAFACTS, 2022). More than 90% of fires in two-thirds of California counties are attributed to humans (Keeley & Syphard, 2018; Li & Banerjee, 2021). Thus, intervals between fires are now shorter than pre-Euro-American settlement conditions (Safford & Van de Water, 2014). Conversion of native shrubs to herbs has been documented in parts of San Diego County (Keeley & Brennan, 2012; Lippitt *et al.*, 2013, Syphard *et al.*, 2019a).

2. Herbaceous Fractional Cover Data

To examine the spatial association between ignitions and herbaceous growth form cover interval classes (based on Chapter III results), fire occurrence (ignition point) data sets were overlaid on a time sequence of maps of herb fractional cover. The maps were derived from single-date, fall season images (based on Chapter II results) from four years – three spectrally unmixed NASA/USGS Landsat 5 Thematic Mapper (TM) images (1988/09/22, 1997/10/17, 2011/10/08) and one spectrally unmixed Landsat 8 Operational Land Imager (OLI) image (2020/08/29) (Figure 25). The Landsat SR images were acquired from USGS EarthExplorer, Collection 2, Level-2, path/row 40/37, have a spatial resolution of 30 m, and exhibit less than 10% cloud cover. Each Landsat image was modeled separately using SMA, with six wavebands and three EMs (one pixel per herbaceous, woody cover, and bare ground was tested). A unit sum constraint with a weight of 1.00 (equating to 100% cover) was applied, and four output images were generated per image date (cover maps of herbaceous, woody, bare ground, and RMSE data). Refer to Chapters II and III for further details.

USGS National Land Cover Database (NLCD) 2019 data were used to create a mask of urban and built land cover (developed and cultivated crops) and surface water (lakes, reservoirs, and woody wetlands) classes. Application of the NLCD cover mask to the Landsat data resulted in an area of 532,167 ha, hereafter referred to as the San Diego County study area.

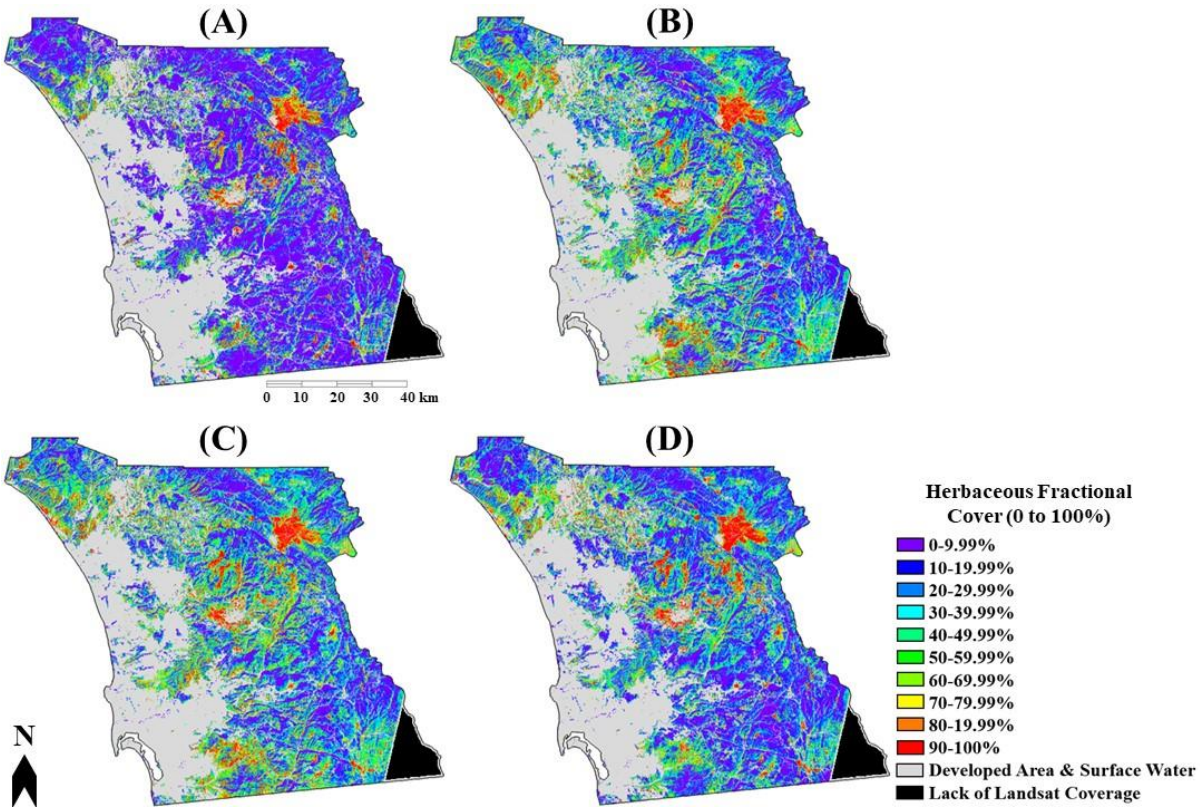

Figure 25. Herbaceous fractional cover maps from the four Landsat image dates: (A) 1988/09/22, (B) 1997/10/17, (C) 2011/10/08, and (D) 2020/08/29 with NLCD developed areas and surface water, as well as the southeast portion not covered by Landsat, masked.

3. Historical Ignition Data

Two historical fire ignition point data sets were used for this study (Table 14). Points from the U.S. Forest Service (USFS) Fire Statistics System (FIRESTAT) database (1981 through 2021) represent ignition points, or points of origin, from which individual wildfires started on National Forest System lands. Points from the U.S. Department of Agriculture (USDA)/USFS Fire Program Analysis (FPA) fire-occurrence database (FOD) (FPA FOD) (1992 through 2020) (Short, 2014; Short, 2022) include records acquired from the reporting systems of federal, state, and local fire organizations. Ignition types include actionable fire types (i.e., suppression efforts or management response were required), fires that ignited and went out naturally, and unplanned ignitions related to fuels management for which agency

units had protection responsibility for the fire resulting from the ignition (Short, 2014). Hereafter, FIRESTAT data are referred to as "Federal" and FPA FOD data as "Non-Federal."

Table 14. Sources of fractional land cover and fire occurrence (ignition point) data. Symbol indicates that a data set had the attribute listed under the column title. (Website links were verified on 09/30/2023, 1: https://data.fs.usda.gov/geodata/edw/datasets.php, 2: https://www.fs.usda.gov/rds/archive/catalog/RDS-2013-0009.6).

Data	Fire Name	Ignition Discovery Date	Ignition Location (Latitude/ Longitude)	Ignition Cause	Ignition Fuel/ Cover Type	Ignition Herb Fraction	Fire Containment Date	Ignition Slope, Aspect, Elevation	Fire Size (Area)
Herb Cover Maps						🔥			
FIRESTAT [1] (Federal)	🔥	🔥	🔥	🔥	🔥		🔥	🔥	🔥
FPA FOD[2] (Non-Federal)	🔥	🔥	🔥	🔥			🔥		🔥

A challenge when working with historical ignition data points is the high degree of error and uncertainty related to the positional information associated with each point (Brown *et al.*, 2002; Schmidt *et al.*, 2002; Short, 2014). The reasons for this positional uncertainty include but are not limited to the way data were collected in the field at an incident, constraints of dispatch applications, data entry by agencies in jurisdictions with different recording standards (e.g., state, national, intra-agency, interagency), and the reality that not all data were reconciled post-incident (Short, 2014). It is also challenging to gather reliable and complete data on smaller fires and those quickly suppressed by firefighting (Chen & Jin, 2022).

In an assessment of federal wildland fire occurrence data, Brown *et al.* (2002) examined 657,949 fire occurrence reports acquired over the entire U.S. (1970 to 2000) and found that 10% of USFS and 30% of U.S. Department of Interior (DOI) records were unusable due to reporting issues; they cited numerous quality, control, and assurance aspects of fire data

observation and recording. However, Brown *et al.* (2002) found USFS data to be the only series that showed a high percentage of usable records consistently each year (0.94 to 0.99%), and there was a slight improvement (approximately 0.02 to 0.05%, depending upon the perspective) over time.

Even though Non-Federal ignition point locations from FPA FOD are standardized, screened for obvious errors, and checked for redundancy, Short (2014) cautioned against presuming that reference estimates reflected actual wildfire activity. Short (2014) cited published estimates of annual wildfire numbers and area burned that differed considerably among sources due to inconsistencies and errors in measurement and reporting (Urbanski *et al.*, 2009). Although Non-Federal points are at least as precise as a Public Land Survey System (PLSS) section (1 mi^2 grid) (Short, 2022), they are gridded, which reduces the positional precision of the data and therefore increases uncertainty when attempting to co-locate herbaceous cover estimates at the ignition location (Figure 26). Other discrepancies were identified in the data collected for federal incidents from FPA FOD. For example, over 300 ignition points from one year were associated with the same latitude/longitude, despite all other attributes being different. Positional inaccuracies may be a result of prior Township-Range-Section (TRS) or Universal Transverse Mercator (UTM) conversions to latitude/longitude (Brown *et al.*, 2002), which resulted in several fire incidents being plotted at an identical location. For this reason, only non-federal data from the FPA FOD (Non-Federal) data set were included in this study.

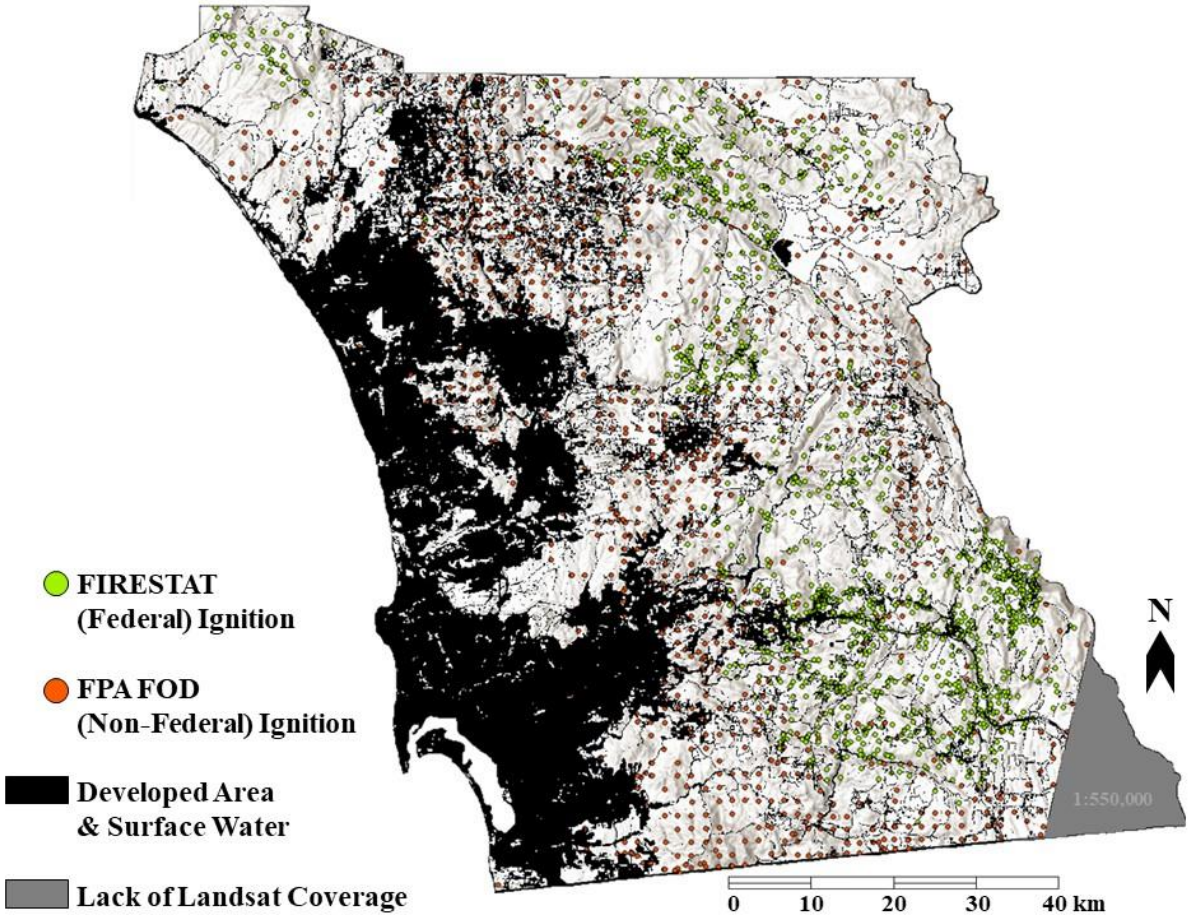

Figure 26. San Diego County study area with ignition points overlaid. The 3,132 ignitions points (1,031 FIRESTAT (Federal) and 2,101 FPA FOD (Non-Federal)) overlaid on a topographic relief map. NLCD developed areas and surface water, as well as the southeast portion not covered by Landsat, are masked.

Ignition points from both the Federal and Non-Federal sources were spatially subset to the San Diego County study area (e.g., points were excluded from NLCD developed areas and the area lacking Landsat coverage) and Federal points were temporally subset to match Non-Federal points (1992 to 2020). Points for ignitions were checked for records that were missing either spatial or temporal information, as well as redundant, identical, or duplicate records (Brown *et al.*, 2002); duplicate points were identified and removed. This resulted in 3,132 ignition points in the San Diego County study area: 1,031 from Federal and 2,101 from Non-Federal (Figure 26).

4. Evaluation of Herbaceous Cover Fraction and Ignition Association

To assess whether ignitions tended to be more associated with particular cover ranges of herbaceous growth forms, historical fire ignition data and herb cover maps were analyzed with ArcGIS Pro 2.8.3 software. Ignition point data from the combined Federal and Non-Federal sets were overlaid on the four single-date herb fractional cover maps derived from Landsat data and spectral unmixing methods. The herb fractional cover values from the Landsat pixel and grid cell for each ignition point location were recorded. Herb cover estimates were extracted from the temporally closest maps, meaning, for 1992 ignition points from the 1988/09/22 cover map, for ignitions from 1993 through 2003 from the 1997/10/17 cover map, for ignitions from 2004 through 2015 from the 2011/10/08 cover map, and for ignitions from 2016 through 2020 from the 2020/08/29 cover map. I assumed that fractional cover did not change substantially over the nine-to-14-year periods between fractional cover maps. All calculations were executed for five herb cover interval classes (low (0 to 19.9%), intermediate (20 to 39.9, 40 to 59.9, and 60 to 79.9%), and high (80 to 100%)). These interval classes stem from accuracy assessment results from Chapter III, for which mean absolute error (MAE), root mean square error (RMSE), and coefficient of determination (R^2) values for each cover map were 1988 = 10.99%, 15.75%, and 0.77; 1997 = 19.11%, 24.07%, and 0.64; 2011 = 13.55%, 17.78%, and 0.78; and 2020 = 9.55%, 12.88%, and 0.83.

Federal ignition data points include 15 fuel/cover type attributes that provide a general cover classification, but do not take fractional cover of herbaceous vegetation into consideration. To evaluate the degree of correspondence between herb cover map pixel values and the predominant fuel/cover type recorded at ignition locations, herb cover values

were identified for a sample set of ignitions classified as three types of woody cover (sagebrush with grass (e.g., subshrub), intermediate brush, and mature brush (chaparral)), as well as one herbaceous cover type (western annual grasses). The sample was comprised of 483 ignitions from woody cover and 183 ignitions from herbaceous from all years of the study period (46% and 18% of total Federal ignitions, respectively).

Statistical tests were used to examine the association between herbaceous cover and the location of ignitions. All 3,132 ignition herb cover values from 1992 through 2020 (derived from the temporally closest four single-date herb cover maps from 1988, 1997, 2011, and 2020) were compared to the sample (comprised of 100 ignitions following the 1997 Landsat image acquisition date, 100 ignitions following the 2011 image date, and the remaining seven ignitions following the 2020 image date). These 207 sample ignition points were selected because they were temporally closest to the herb cover maps and, therefore, herb values at the points were assumed to be as accurate as possible. Two chi-square goodness of fit tests were used to determine whether the proportion of observed ignitions within herb cover classes was significantly different when compared to proportions of the study area represented by the same herb cover class (Agresti, 2007; Syphard *et al.*, 2014), which is what one would expect, for the full set of ignitions and for the sample set. A third chi-square goodness of fit test was executed to assess whether the proportion of all observed ignitions was significantly different compared to the observed sample set of 207 ignition points.

I hypothesized a significant relationship between herbaceous fractional cover and proportion of ignitions by interval class per year, and that ignitions per area would be higher in higher herb growth forms compared to chance alone. To determine whether fires ignited in low, intermediate, or high cover interval classes of herb, the (1) proportion of ignitions

per year per cover class interval per proportion of area (Schwartz & Syphard, 2021) and the (2) proportion of ignitions per cover class interval per proportion of area were calculated. Analyses included comparisons of Federal versus Non-Federal sets for (1) all ignitions, as well as four additional exploratory analyses: (2) human-caused ignitions, (3) naturally-caused ignitions, (4) ignitions that resulted in a multi-date fire (a fire that burned more than one day), and (5) ignitions that resulted in a large fire (a fire that burned $\geq$ 4.05 ha).

C. Results

1. Ignition Trends and Distributions

An obvious downward trend in the number of individual ignitions per year is evident for the 29-year period. However, Federal ignitions per unit area burned decreased over time and Non-Federal ignitions per area burned increased (Figure 27A and B, respectively). A plot of Federal versus Non-Federal ignitions exhibits a nonlinear, positive association (Figure 27C).

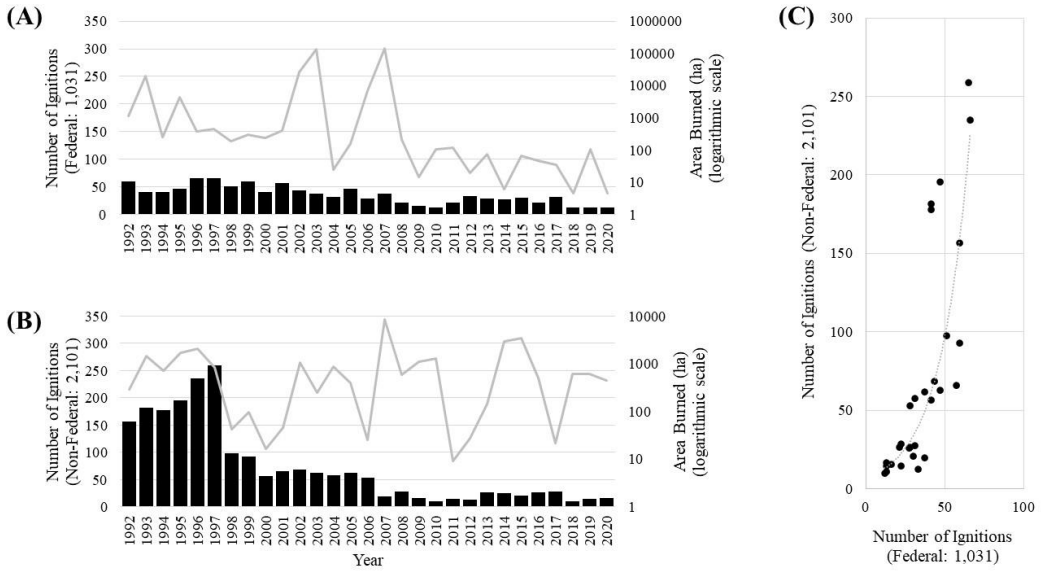

Figure 27. Federal and Non-Federal ignitions and area burned during the study time period for 1992 to 2020. (A) Histogram: Number of Federal ignitions per year (1,031). Line: Area burned per year (total: 340,907 ha). (B) Histogram: Number of Non-Federal ignitions per year (2,101). Line: Area burned per year (total: 30,335 ha). (C) Number of ignitions reported by Federal versus Non-Federal data sets.

Federal ignition points comprise 39.92% of the total of 3,132 points, with 67.08% of the total from the Non-Federal data set (Table 15). Human-caused ignition points represent 80.30% of the total (of the 80.30%, Federal = 24.10%, Non-Federal = 75.90%). Naturally-caused ignitions make up 8.49% of the total (of the 8.49%, Federal = 68.42%, Non-Federal = 31.58%). Ignition points resulting in a multi-date fire represent 3.99% of the total (of the 3.99%, Federal = 92.80%, Non-Federal = 7.20%). Ignitions resulting in a large fire characterize 8.43% of total points (of the 8.43%, Federal = 38.26%, Non-Federal = 61.74%).

Table 15. Ignition sample sets. Number of ignitions per Federal and Non-Federal data sets and the tests executed to analyze the relationship of herbaceous cover fraction and ignitions.

	Federal	Non-Federal
(1) All	1,031	2,101
(2) Human-Caused	606	1,909
(3) Naturally-Caused	182	84
(4) Multi-Date Fire	116	9
(5) Large Fire	101	163

The herbaceous fractional values agree reasonably well with the 483 Federal fuel/cover type woody vegetation growth form point classifications. Corresponding herb cover interval data show a slight trend from more to less herb when transitioning from the light to heavy brush fuels. The percentage of points with herb cover values between 40 and 100% is: sagebrush with grass = 33.62%; intermediate brush = 33.88%; mature brush (chaparral) = 29.60%. Although intermediate herb cover interval classes are mapped in all levels of brush classifications, this result is not surprising since the San Diego County study area subshrub communities have intermixed grasses and chaparral communities tend to have low fractions of herb. The reasonable agreement between the SMA derived herb cover and coarse fuel/cover type descriptions provides some confidence regarding positional uncertainty concerns.

2. Association of Ignitions and Herbaceous Cover

A chi-square goodness of fit test was executed to compare the proportion of combined Federal and Non-Federal ignitions within each cover interval class to the proportion of the same cover interval class within the study area (per herb cover interval class). For the total combined ignitions, chi-square = 0.05, p = 1.00, n = 3,132 (Figure 28A), which indicates there is not a significant difference between the proportion of ignitions per herb interval classes within the study area extent. In another analysis, the proportion of the sample Federal and Non-Federal ignitions (6.60% of all points) that were temporally closest to the dates immediately following the 1997, 2011, and 2020 Landsat image acquisitions was compared to the proportions of the study area. For the sample of ignitions, chi-square = 0.01, p = 1.00, n = 207 (Figure 28B), revealing no significant difference between the proportion of ignitions per herb interval classes and the study area extent. Comparison of total combined ignitions to the sample of ignitions yielded chi-square = 0.27, p = 0.99, n = 3,339 (Figure 28C), suggesting that the combined and sample data sets were not significantly different. This implies that, when monitoring a large areal extent over a multi-decadal period, a small number of regularly (temporally) spaced herb cover maps is sufficient for determining fraction values at a 20% interval class for ignition points. All available ignition points from 1992 through 2020 are used for the rest of the analyses.

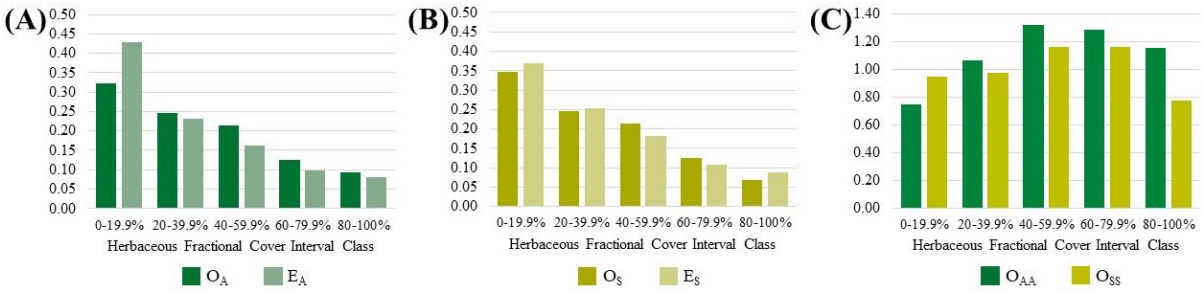

Figure 28. Histograms depicting chi-square test results. (A) Proportion of all 3,132 ignitions (O_A) (per herb cover class) based on ignitions from 1992 through 2020 compared to the proportion of the study area (E_A) (per herb cover class) derived from SMA herb cover map results from 1988, 1997, 2011, and 2020. (B) Proportion of the sample 207 ignitions (O_S) (per herb cover class) based on ignitions after 1997, 2011, and 2020 Landsat image dates compared to the proportion of the study area (E_S) (per herb cover class) derived from SMA herb cover map results from 1997, 2011, and 2020. (C) Proportion of all ignitions per the proportion of the study area (O_{AA}) (from (A)) compared to the proportion of sample ignitions per the proportion of the study area (O_{SS}) (from (B)).

3. Annual Proportion of Ignitions per Proportion of Area

Results of the chi-square analyses indicate that the observed proportion of ignitions per 20% herbaceous interval class for the full study time period are not significantly different than the expected amount based on areal coverage of each interval class. However, annual analyses emphasize the proportion of ignitions that exceed the expectation (e.g., the proportion of the study area attributed to an herb interval class) when the calculated value from a single year is > 1.00. Color-coded line charts in Figures 29 through 31 communicate the fluctuations for each 20% herb cover interval class per year. Trends of increasing ignitions, particularly in intermediate (20 to 39.9, 40 to 59.9, and 60 to 79.9%) and high (80 to 100%) cover interval classes are observed, as well as trends of decreasing ignitions in low (0 to 19.9%) cover intervals. This may indicate grass-fire cycle occurrence and support evidence for a changing fire regime. Federal ignitions exhibit increasing proportions of ignitions in the 40 to 59.9 and 60 to 79.9% herb cover intervals over time (Figure 29A). Non-Federal points show slightly increasing proportions of ignitions in the 20 to 39.9, 60 to 79.9, and 80 to 100% intervals (Figure 29B).

Figure 29. Annual proportion of all Federal and Non-Federal ignitions per proportion of the study area (1992 through 2020). Line charts represent the fluctuations in the proportion of ignitions per associated proportion of the area represented by (from left to right): 0 to 19.9, 20 to 39.9, 40 to 59.9, 60 to 79.9, and 80 to 100% herbaceous fractional cover interval classes. Dotted trendlines indicate whether the proportion of ignitions increased or decreased over time. (A) All Federal ignitions (1,031). (B) All Non-Federal ignitions (2,101).

The Federal human-caused proportion of ignitions increased most substantially over the study period in the 40 to 59.9 and 60 to 79.9% herb cover classes, and slightly in the 80 to 100% class (Figure 30A). The proportion of Non-Federal human-caused ignitions increased in the 60 to 79.9 and 80 to 100% interval classes (Figure 30B). The proportion of Federal naturally-caused ignitions increased over time in the 40 to 59.9% cover class (Figure 30C). The Non-Federal naturally-caused proportion of ignitions show an increase in the 80 to 100% herb cover class (Figure 30D).

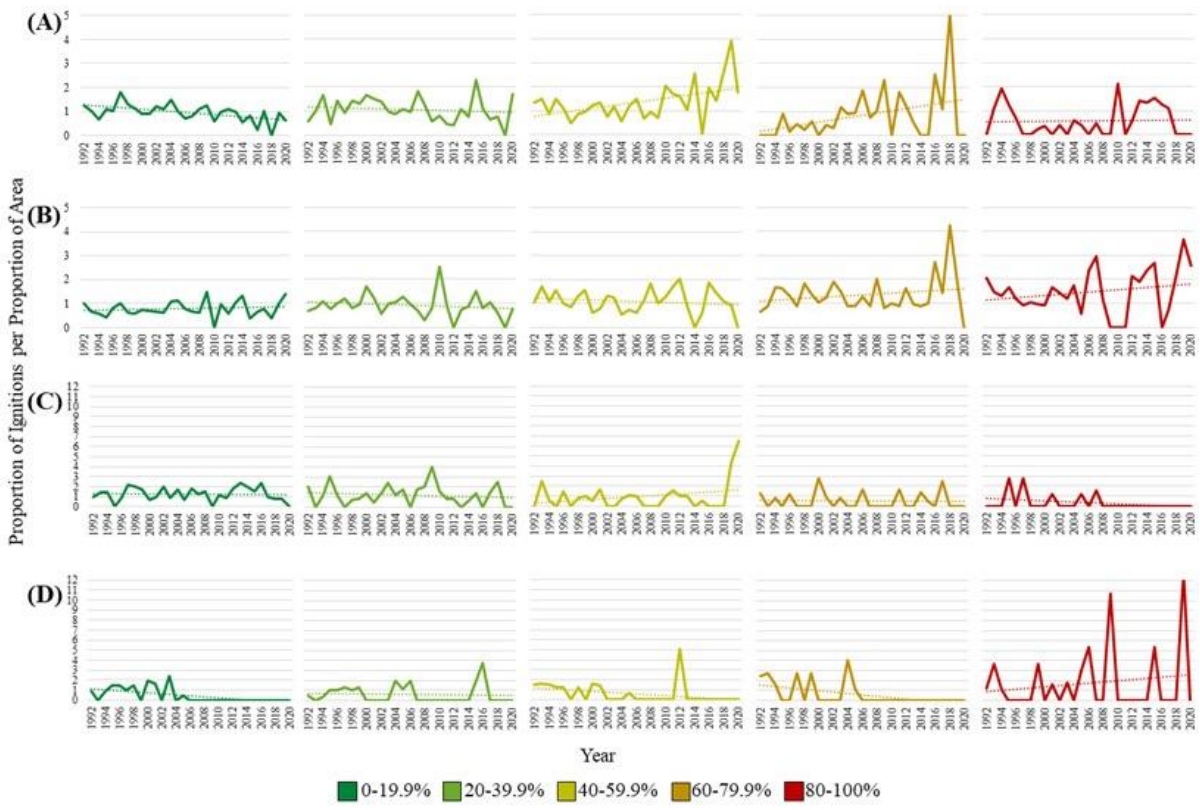

Figure 30. Annual proportion of Federal and Non-Federal human-caused and naturally-caused ignitions per proportion of the study area (1992 through 2020). (A) Human-caused Federal ignitions (606). (B) Human-caused Non-Federal ignitions (1,909). (C) Naturally-caused Federal ignitions (182). (D) Naturally-caused Non-Federal ignitions (84).

The proportion of Federal ignitions resulting in a multi-date fire increased in the 40 to 59.9, 60 to 79.9, and 80 to 100% cover intervals over time (Figure 31A). The small sample of Non-Federal ignitions resulting in a multi-date fire are not sufficient to draw definitive conclusions regarding which cover classes experienced the largest proportion of ignitions (Figure 31B). The proportion of Federal ignition points resulting in a large fire increased in the 60 to 79.9 and 80 to 100% herb cover interval classes (Figure 31C). The Non-Federal proportion of ignitions resulting in a large fire increased slightly in the 20 to 39.9% cover class (Figure 31D).

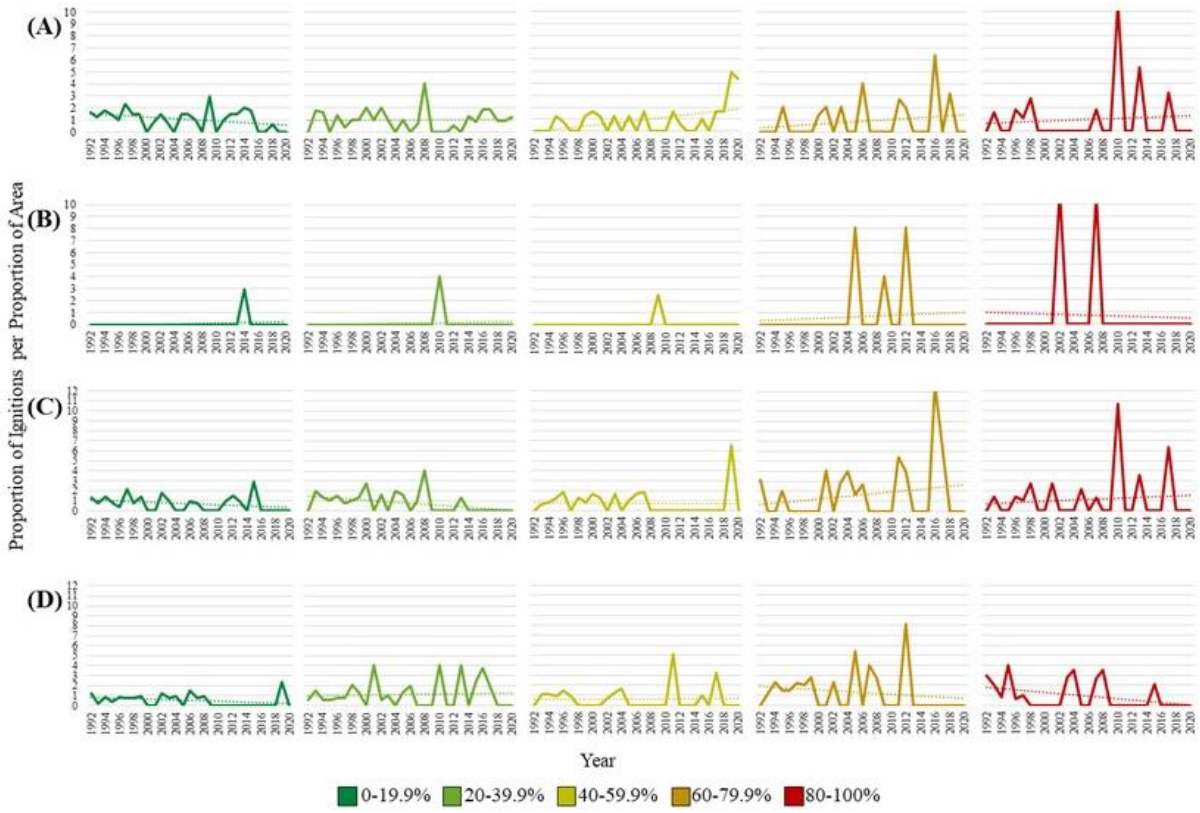

Figure 31. Annual proportion of Federal and Non-Federal ignitions resulting in multi-date and large fires per proportion of the study area (1992 through 2020). (A) Federal ignitions resulting in a multi-date fire (> 1 day) (116). (B) Non-Federal ignitions resulting in a multi-date fire (9). (C) Federal ignitions resulting in a large fire (≥ 4.05 ha) (101). (D) Non-Federal ignitions resulting in a large fire (163).

Of importance, 13 Federal and Non-Federal ignitions (of the total 3,132) resulted in the largest fires that burned ≥ 2,023 ha. Eleven of the 13 (84.62%) ignitions occurred in areas mapped as having > 20% herb fractional cover (Table 16). Ten of the 11 ignited following water years (WY) (measured from 01 October to 30 September) with higher precipitation compared to the WY corresponding to the ignition date (refer to Chapter III for historical average WY precipitation values). For example, the five wildfires that ignited in 2007 (and burned a combined total of 149,034 ha) ignited after a higher-than-average annual precipitation 2005 WY and a high 2006 WY. This reinforces results showing strong associations ($p < 0.01$ per Faivre *et al.*, 2014) between precipitation during the preceding year with grass fire size and the number of fires (Balch *et al.*, 2013; Keeley *et al.*, 2022;

Keeley & Syphard, 2018). Additionally, 10 of the 11 fires ignited on days classified by the Santa Ana Winds Regional Index as Santa Ana wind events (Guzman-Morales & Gershunov, 2019; Guzman-Morales *et al.*, 2016).

Table 16. Year and herbaceous fractional cover interval class in which the 13 Federal and Non-Federal ignition points resulting in large fires (≥ 2,023 ha) occurred (1992 through 2020). Years with a water year (WY) designator indicate the previous water year received higher annual precipitation. The numbers in the cells indicate the number of ignitions per cover class, followed by the ignition or discovery date and abbreviated month, a Federal (F) or Non-Federal (NF) designator, and a Santa Ana wind (SAW) event designator.

Year	Herbaceous Fractional Cover Interval Class				
	0-19.9%	20-39.9%	40-59.9%	60-79.9%	80-100%
1993^{WY}		2 (27 Oct^{F,SAW}; 27 Oct^{F,SAW})			
1995				1 (27 Aug^{F})	
2002^{WY}	1 (29 Jul^{F})				
2003^{WY}			1 (25 Oct^{F,SAW})	1 (26 Oct^{F,SAW})	
2006^{WY}				1 (23 Jul^{F})	
2007^{WY}	1 (22 Oct^{F,SAW})		2 (21 Oct^{F,SAW}; 23 Oct^{F,SAW})		2 (21 Oct^{F,SAW}; 23 Oct^{NF,SAW})
2014^{WY}		1 (14 May^{NF})			

4. Proportion of Ignitions per Proportion of Area

Histograms shown in Figure 32A through J depict a noticeable difference in proportions of ignitions between the Federal and Non-Federal data sets for the 1992 to 2020 study period. The proportion of ignitions is considered disproportionate and exceeds the expectation (e.g., the proportion of the study area attributed to an herb interval class) when the calculated value is > 1.00. The largest proportion of ignitions from the Federal data set occurred in the 40 to 59.9% herb cover interval class, closely followed by the 20 to 39.9% cover class (Figure 32A). Federal ignition points are almost entirely located in foothill, montane, and mountain areas (Figure 26), with approximately 60% of ignitions reported at > 1,000 m elevation. About 70% of the Federal ignition point fuel/cover type attributes

indicate that fires occurred in either woody or a woody/herb cover mix, having intermediate herb cover (e.g., 20 to 39.9, 40 to 59.9, and 60 to 79.9%).

The largest proportion of Non-Federal ignitions occurred in high herb cover interval classes – 60 to 79.9%, closely followed by 80 to 100% herb cover (Figure 32B). Ignition points are in all landscape types within the study area, ranging from the coastal to the high mountain locations (e.g., Hot Springs Mountain: 1,992 m), and capture the topographic and fuel heterogeneity found in San Diego County. Additionally, more Non-Federal ignitions are within the WUI or abutting the populated urban areas (compared to Federal ignition points).

Because human-caused ignitions represent just over 80% of the total ignitions, the resulting values visualized in the histograms closely resemble those in Figure 32A and B. Federal human-caused ignitions disproportionately occurred in the 40 to 59.9% herb cover class (Figure 32C). Non-Federal human-caused ignitions started in 60 to 79.9% herb cover (Figure 32D). Federal naturally-caused ignitions disproportionately occurred in 20 to 39.9% herb cover (Figure 32E), and Non-Federal naturally-caused ignitions disproportionately started in the 80 to 100% herb cover interval class (Figure 32F).

The largest proportion of Federal ignitions that resulted in a multi-date fire occurred in 20 to 39.9% herbaceous cover, but not disproportionately so – proportions of ignitions are similar for all cover classes (Figure 32G). The very low number of Non-Federal ignitions is too small of a sample size for a definitive assessment (Figure 32H). The largest proportion of Federal ignitions resulting in a large fire occurred in 60 to 79.9% herb cover (Figure 32I). Like the Federal ignition points, the Non-Federal ignitions resulting in a large fire occurred in 60 to 79.9% herbaceous cover (Figure 32J).

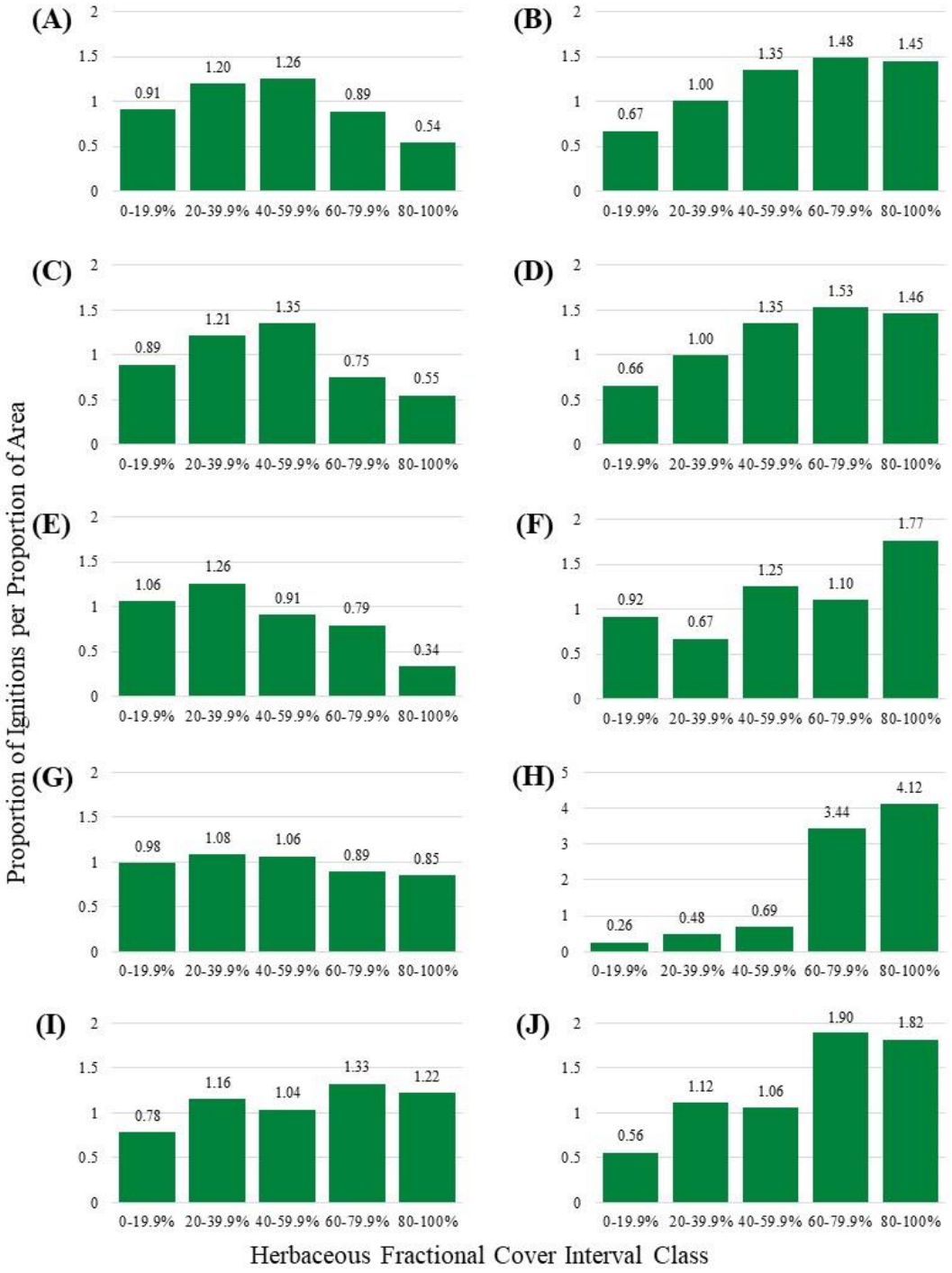

Figure 32. Proportion of Federal and Non-Federal ignition points per proportion of the study area (1992 through 2020) separated by 20% herbaceous fractional cover interval classes. (A) All Federal ignitions. (B) All Non-Federal ignitions. (C) Human-caused Federal ignitions. (D) Human-caused Non-Federal ignitions. (E) Naturally-caused Federal ignitions. (F) Naturally-caused Non-Federal ignitions. (G) Federal ignitions resulting in a multi-date fire (> 1 day). (H) Non-Federal ignitions resulting in a multi-date fire. (I) Federal ignitions resulting in a large fire (≥ 4.05 ha). (J) Non-Federal ignitions resulting in a large fire.

D. Discussion

I used SMA-derived herbaceous fractional cover maps from four Landsat image dates and a combined 3,132 ignition points from two historical fire occurrence data sets to evaluate the spatial association of ignition occurrence for 20% herb cover interval classes from 1992 through 2020 in the San Diego County study area. The 29-year study period is too short to draw conclusions about regional climate changes but is long enough to capture change in herbaceous fuels (Brooks *et al.*, 2004). Annual proportions of ignitions per proportion of area analysis results show increasing proportions of ignitions, particularly in > 40% herb cover over time (Figures 29A and B, 30A, and 31A and C). This reinforces findings that herbaceous vegetation, particularly expanding invasive grass, increases fire occurrence (Balch *et al.*, 2013; Brooks *et al.*, 2004; D'Antonio & Vitousek, 1992; Fusco *et al.*, 2019). When the entire study time period is evaluated, results of all analyses show the largest proportion of ignitions occurred in > 20% cover (Figure 32).

1. Spatial Association Between Ignitions and Herbaceous Cover

Despite the overall decline in the number of ignitions (Figure 27), herbaceous cover has increased in the study area over time (Chapter III). Separation of the Federal and Non-Federal data points provides the opportunity to assess within which herbaceous fractional cover interval class ignitions were more strongly associated. With human-caused ignition points representing 58.78% of the Federal points and 90.86% of the Non-Federal points and, considering that impacts of larger and more frequent fires are expected to drive disruptions to fire regimes (Dennison *et al.*, 2014), greater focus is placed on the explanatory variables garnered from the exploratory analyses associated with human-caused ignitions and ignitions resulting in a large fire.

Evaluation of Federal human-caused ignition points reveal a disproportionate number of occurrences in the 40 to 59.9% herbaceous cover class (Figure 32C). Large fires disproportionately ignited on Federal land in the 60 to 79.9% herb cover class (Figure 32I). Brown *et al.* (2002) noted that changes in vegetation characteristics on Federal land may have increased the probability of human-caused fire occurrence whether or not substantial changes in human activity had occurred. This is supported by results from the annual analyses showing increasing proportions of human-caused ignitions in > 40% herb (Figure 30A), and ignitions resulting in large fires in > 60% herb (Figure 31C).

Non-Federal human-caused ignitions and ignitions resulting in large fires show a disproportionate number of occurrences in the 60 to 79.9% herbaceous cover class (Figure 32D and J). However, assessment of exploratory analysis results shows increasing proportions of human-caused ignitions in low (0 to 19.9%) and intermediate-to-high (60 to 79.9 and 80 to 100%) cover (Figure 30B), and proportions of ignitions resulting in a large fire increasing over time in 20 to 39.9% herb cover (Figure 31D). Compared to Federal data points that show increasing and large proportions of ignitions in intermediate-to-high herb interval classes, Non-Federal ignition points exhibit change and disproportionate ignitions in nearly all herb classes. Despite this difference in the fraction of cover in which Federal versus Non-Federal ignitions occurred, points from both sets indicate spatial similarities and common causes of a high percentage of ignitions.

Federal ignition points tend to be clustered near roads (Deluz (DeLuz Road), Palomar Mountain (Highway 76, State Park Road, East Grade Road, South Grade Road), Kumeyaay Highway (Interstate 8), Mount Laguna (Sunrise Highway)) and, although associated with the PLSS grid, Non-Federal points are also observed near travel corridors and urban areas

(Figure 26). Equipment/vehicle use and arson/incendiarism are attributed to 19.47% and 13.86% of human-caused Federal ignitions and 33.37% and 11.52% of human-caused Non-Federal ignitions, respectively. These statistics corroborate similar findings that ignition occurrence is significantly affected by distance to roads and housing in Southern California's National Forest System lands ($p < 0.0001$ per Faivre *et al.*, 2014) (Chen & Jin, 2022) and proximity to urban areas (Syphard *et al.*, 2019b). Much of the vegetation growth forms along transportation corridors in the San Diego County study area contain herbs. Considering the relationship between prior-year rainfall and increased fuel production in grass-dominated ecosystems (Crimmins & Comrie, 2004; Keeley & Syphard, 2016), the rising human population in the study area, and the ability of the entire exhaust system of a vehicle (muffler, catalytic converter, and exhaust pipe) to ignite a fire in roadside vegetation (Downey, 2016), it is not surprising to observe increasing proportions of human-caused ignitions in > 40% (Figure 30A) and > 60% herb cover (Figure 30B) over time.

The 13 Federal and Non-Federal ignitions resulting in the largest fires that burned > 2,023 ha correspond to results from Balch *et al.* (2013). The authors reported that the largest fire events, particularly from 2000 to 2009, were disproportionately represented by fires that burned on cheatgrass-dominated landscapes. They calculated that, of the 50 largest fires between 2000 and 2009, 78% were associated with cheatgrass. Of the 13 ignitions that resulted in the largest fire sizes from 1992 to 2020, 84.62% occurred in herbaceous fractional cover > 20% (Table 16).

2. Data Set Reliability and Accuracy

The accuracy and uncertainty associated with the Landsat-derived fractional cover maps and ignition point locations have serious implications for the objective of this study. Despite

knowledge of the local landscape, use of high spatial resolution orthoimagery acquired during multiple seasons for reference data generation and EM selection, and reasonable MAE and RMSE values associated with herbaceous cover estimates, the extraction of pure spectral signatures of herb cover for EMs from Landsat image data with 30 m spatial resolution is challenging (Chapters II and III). Both the orthoimage-based reference data and moderate spatial resolution Landsat fractions are model-based estimates and measurements of comparative model agreement, rather than predicted outputs compared to "ground truth." Additionally, even if the unmixed cover maps for 1988, 1997, 2011, and 2020 were perfectly accurate, ignitions from years between (or just prior to the Landsat acquisition dates) may not have been well represented by herb fractions from the four image dates. However, use of a small number of herb cover maps is justified by the results of the chi-square analysis comparing the combined ignitions to the sample set (Figure 28). Thus, I assumed herb cover values did not change substantially between image dates (and not more than the interval class amounts) for this study.

Federal and Non-Federal ignition occurrence point records were checked "row-by-row" to identify redundant, identical, or duplicate records, which were removed (Brown *et al.*, 2002). However, this does not mean that the record was necessarily error free, but only that no obvious errors remained in the final data set of 3,132 ignition points (Brown *et al.*, 2002). A high number of ignitions prior to 1998, followed by a substantial decrease in ignitions, (Figure 27) raised questions and concerns about data reliability. However, this decrease is supported by Keeley and Syphard (2018), who identified a decrease in fire occurrence between 1980 and 2016, and Chen and Jin (2022), whose model predictions suggested a slight decrease in ignition probability between circa 2000 and 2010 in coastal Southern

California. By calculating the proportion of ignitions, the effects of the high number of ignitions in the early- to mid-1990s compared to the 2000s were partially normalized for non-herb cover influences, and focus was placed on the relationship between ignitions and the herb cover interval classes. A century ago, Show and Kotok (1923) argued that "successful [wildfire] protection depends on a critical study of past performances. For this purpose, the importance of accurate and complete records of fires cannot be overestimated" (Short, 2014). Conversations regarding a continued need to assess and improve fire occurrence data are important (Brown *et al.*, 2002; Short, 2014) and incorporation of fractional cover information such as from this work should benefit future studies.

3. Information for Mitigation and Management Strategies

As is the nature of cycles such as the grass-fire cycle, uncertainties associated with the true drivers of change can be substantial. Potential interactions between changing fire regimes, native vegetation, and invasive plants are still not well understood (Chornesky, 2015). Therefore, any plant species that demonstrates potential to alter fire regimes should be prioritized for control, and restoration of pre-invasion plant communities and ecosystem properties may be necessary (Brooks *et al.*, 2004).

This study reinforces the importance of prioritizing mitigation, fuels reduction, habitat management, and ecological restoration practices based on available data and the observed adaptations of dominant plant species in a given fire regime (Syphard & Keeley, 2015). Variations in spatial patterns and importance of predictor variables have implications for understanding why, where, and how ignitions are generated in the region and can inform decisions for developing strategies that would focus fire prevention efforts (Syphard & Keeley, 2015). Results of the proportions of ignitions per herbaceous cover interval class per

year (Figures 29 through 31) are useful for comparing past and recent ignition proportions to infer risk. These charts alone do not account for effects of other explanatory variables such as small temporal scale weather (e.g., days, weeks, or months) or spatial proximity to human populations but, when combined with these data from other sources, can lead to interesting observations. For example, six of the 13 (46.15%) ignitions resulting in a large fire ($\geq$ 2,023 ha) occurred during a Santa Ana wind event in a year preceded by a higher annual precipitation WY in areas with > 40% herb cover (Table 16). The proportions of ignitions per herb cover interval class per proportion of area (Figure 32) can inform practitioners regarding priority herb cover classes for pre-fire mitigation and can be combined with management recommendations per land ownership type (such as from Brooks *et al.*, 2004; Chen & Jin, 2021; Fusco *et al.*, 2021). When combined with herb cover maps (such as from Chapter III), these data will improve upon existing ignition point sets, which only include coarse fuel/cover type classifications, and can be used to better prepare San Diego County shrubland communities for fire-related emergencies in Federal and Non-Federal areas at local scales (Chen & Jin, 2022).

E. Conclusions

To my knowledge, this is the first study to focus exclusively on the association between herbaceous fractional cover and the proportion of wildfire ignitions in San Diego County shrublands to inform observations of a possibly changing fire regime. Landsat-derived herbaceous fractional cover maps from 1988, 1997, 2011, and 2020 (30 m) were combined with 3,132 historical ignition points to determine the 20% herb cover interval classes in which the largest proportions of ignitions occurred in San Diego County shrublands between 1992 and 2020. Results show annual changes within each herb cover class and highlight

trends of herb increase or decrease over the 29-year period, which can be used to define the study area fire regime. Results also show the herb cover class in which a disproportionate number of ignitions occurred for the entire study time period, which can be used to determine ignition potential dependent on herb fractions. Differences are observed in the spatial distribution of Federal and Non-Federal wildfire ignitions within the different herb fractional cover interval classes. The results emphasize the importance of monitoring landscapes for evidence of grass-fire cycles, and can be used to inform prioritization of fire mitigation and management efforts.

Although the effects of climate and weather were briefly discussed, only annual average precipitation data from one centrally located weather station were used in this study (Chapter III). Follow-on work should incorporate spatial locations of known wind corridors, seasonal weather statistics, and detailed Santa Ana wind event data for all ignition dates as opposed to just the dates associated with ignitions resulting in the largest fire sizes (Cayan *et al.*, 2022; Jin *et al.*, 2015b; Syphard & Keeley, 2015). Due to changing climate, Keeley and Syphard (2019) discussed the likelihood that warmer spring temperatures will alter the competitive balance of post-fire environments such that invasive herbs are favored over native shrub seedling recruitment, thus increasing the dominance of the more flammable fuel types and changing the fire regime in Southern California coastal shrublands. Therefore, analyses exploring proportions of ignitions and the relationship between herbaceous fraction per meteorological season could also be pursued. Another logical next step beyond fire occurrence is evaluation of the association between herbaceous fractional cover and fire frequency. Comparisons between past and current fire frequencies (Safford & Van de Water,

2014) should be combined with herb cover maps to address the association between herb cover variability and fire frequency, another important fire regime variable.

V. Conclusion

A. Summary and Synthesis

The overall goal of this study is to compare and implement procedures for locating and quantifying fractional cover of herbaceous vegetation growth forms, and to understand the relationship between herb cover and ignitions through time in San Diego County, California, USA. I accomplish this goal by executing spectral unmixing techniques applied to Landsat multispectral data from four image dates between 1988 and 2020. To my knowledge, this is the first study to apply these methods in a spatially explicit manner with the intent to monitor herb expansion as indicators of the grass-fire cycle and a changing fire regime in San Diego County coastal shrublands.

Results presented in Chapter II demonstrate the most parsimonious approach – simple spectral mixture analysis (SMA) using a spectral library applied to surface reflectance data from a fall date – yields the highest accuracy output. The advantage of SMA applied to Landsat is that it provides a framework for monitoring herbaceous growth forms using multiple decades of archived data, for a large area, and on a frequent basis. The disadvantage of SMA is the critical step of identifying accurate endmembers for dominant vegetation growth forms per image; it is an iterative process that requires great attention to data in spectral feature space and vegetation phenology in the image. Findings from the Chapter II accuracy assessments of 2020 outputs are used to develop the herb cover maps output in Chapter III and used in Chapter IV.

Application of the SMA approach to additional Landsat image dates in Chapter III, for a 33-year study period from 1988 to 2020, provides a framework for evaluating change in

herbaceous vegetation cover. Results show areas that experienced shifts from woody- to herb-dominated cover due to successional changes and suggest that a grass-fire cycle has been established in the San Diego County study area. Combining herb cover values and historical wildfire attribute data provides the opportunity to analyze the factors most strongly associated with the increase in herb over time – fire return interval, drought, proximity to development, and elevation.

In Chapter IV, I evaluate the association between herbaceous fractional cover (based on the maps produced for Chapters II and III) and the proportion of ignitions for a 29-year study period from 1992 to 2020. I separate ignitions that occurred on Federal lands from Non-Federal and execute exploratory analyses to yield information about the herb cover interval classes in which human- and naturally-caused ignitions, as well as ignitions resulting in a multi-date fire and a large fire, occurred. This work builds upon other studies that have explored ignitions in the entire state of California and the Great Basin region. However, this research further expands on previous studies and wildfire data sets that only include coarse vegetation classifications by incorporating and addressing herbaceous fractional cover values.

Use of open-source, pre-processed Landsat surface reflectance data results in efficient image acquisition and at a low cost. This will enable detection of at-risk locations and areas that require immediate post-fire action on a faster and more frequent basis. This study provides a framework for identifying the location and monitoring the spread of flammable herbaceous vegetation and determines the herb cover classes in which disproportionate amounts of ignitions occurred over time. The approaches developed in this study will be useful for identifying target areas for combating the grass-fire cycle. Results from this study

have benefits for a diverse range of fields, including geography, remote sensing, emergency response, hazard and risk mitigation, ecology, biodiversity, and regional planning. Ecologists and land managers will be able to use the results to assess vegetation community health and decide whether to implement preservation or restoration techniques. Emergency response personnel will find the derived products and findings useful for incorporation into fire management, mitigation, and preparation plans prior to the start of the next wildfire season.

B. Future Directions

Follow-on work should include production of SMA-derived herbaceous fractional cover maps for additional areas, such as to other Mediterranean-type ecosystems around the globe. Landsat data were used for this research due to the ability to acquire archived data with large areal coverage and imagery dating back to the mid-1980s. However, because it was difficult to generate reference data from high spatial resolution multispectral orthoimagery as well as select accurate endmembers (Chapters II and III), future work focused on post-2015 dates should pursue other data acquisition options. For example, use of higher spatial resolution satellite sensor data as well as incorporation of aerial hyperspectral imagery or imaging spectroscopy data will result in improved reference data generation and endmember selection opportunities for better herb cover maps.

Another logical next step beyond fire occurrence is evaluation of the association between herb fractional cover and other fire regime variables (e.g., frequency, intensity, type, and seasonality). A comprehensive analysis of fire frequency (or minimum fire interval) should be executed for all ignitions (as opposed to only a sample set, as was done in Chapter III) to determine whether there has been change over time. Additionally, future

studies should explore proportions of ignitions and the relationship between herbaceous fraction per meteorological season to evaluate the effects of phenology and prior-year precipitation on ignitions through time. Assessment of seasonal effects, particularly when combined with extreme wind event data, could yield spatial and temporal insight into ignition risk. To further the utility of these methods, slope, aspect, and elevation data should be considered to gain a more thorough understanding about the association between herb cover and ignitions in known wind corridors and steep terrain abutting the wildland-urban interface.

References

1. Adams, J. B., & Gillespie, A. R. (2006). *Remote Sensing of Landscapes with Spectral Images: A Physical Modeling Approach.* Cambridge University Press.

2. Adams, J. B., Smith, M. O., & Gillespie, A. R. (1993). Imaging spectroscopy: Interpretation based on spectral mixture analysis. In C. M. Pieters, & P. Englert (Eds.), *Remote Geochemical Analysis: Elemental and Mineralogical Composition* (pp. 145-166). New York: Cambridge University Press.

3. Adams, J. B., Smith, M. O., & Johnson, P. E. (1986). Spectral mixture modeling - A new analysis of rock and soil types at the Viking Lander-1 site. *Jounral of Geophysical Research, Solid Earth and Planets, 91*, 8098-8112. doi:10.1029/JB091iB08p08098

4. Agresti, A. (2007). *An Introduction to Categorial Data Analysis* (Second ed.). New York.

5. Ahrens, M. (2018). *Brush, Grass and Forest Fires - Firefighter Injuries (Supporting Tables).* National Fire Protection Association (NFPA). Quincy, MA: NFPA Research. Retrieved from https://www.nfpa.org/-/media/Files/News-and-Research/Fire-statistics-and-reports/WUI/osBrushGrassForestSupportingTablesFFInjuries.ashx

6. Allred, B. W., Bestelmeyer, B. T., Boyd, C. S., Brown, C., Davis, K. W., Duniway, M. C., . . . Uden, D. R. (2021). Improving Landsat predictions of rangeland fractional cover with multitask learning and uncertainty. *Methods in Ecology and Evolution, 12*(5), 841-849. doi:10.1111/2041-210X.13564

7. Araki, R., Branger, F., Wiekenkamp, I., & McMillan, H. (2022). A signature-based approach to quantify soil moisture dynamics under contrasting land uses. *Hydrological Processes, 36*(4), 1021. doi:10.22541/au.162435676.61345839/v1

8. Arroyo, M. T., Zedler, P. H., & Fox, M. D. (1995). *Ecology and Biogeography of Mediterranean Ecosystems in Chile, California, and Australia.* London: Springer.

9. Baez, S., & Collins, S. L. (2008). Shrub invasion decreases diversity and alters community stability in northern Chihuahuan Desert plant communities. *PloS one, 3*(6), e2332. doi:10.1371/journal.pone.0002332

10. Balch, J. K., Bradley, B. A., D'Antonio, C. M., & Gomez-Dans, J. (2013). Introduced annual grass increases regional fire activity across the arid western USA (1980-2009). *Global Change BIology, 19*(1), 173-183. doi:10.1111/gcb.12046

11. Bartolome, J. W. (1989). Local temporal and spatial structure. In L. F. Huenneke, & H. A. Mooney (Eds.), *Grassland structure and function: California annual grassland* (pp. 73-80). Dordrecht: Kluwer Academic Publishers.

12. Bartolome, J. W., Barry, W. J., & Griggs, T. H. (2007). Valley Grassland. In M. G. Barbour, W. J. Barry, & T. H. Griggs (Eds.), *Terrestrial Vegetation of California* (Third ed., p. 22). University of California Press. Retrieved from www.jstor.org/stable/10.1525/j.ctt1pnqfd

13. Boardman, J. W. (1993). Automated spectral unmixing of AVIRIS data using convex geometry concepts. *Proceedings Summary of the Fourth Annual JPL Airborne Geoscience Workshop 25-29 October 1993. 1*, pp. 11-14. Arlington, Virginia: JPL Publication 93-26.

14. Brennan, T. J., & Keeley, J. E. (2015). Effect of mastication and other mechanical treatments on fuel structure in chaparral. *International Journal of Wildland Fire, 24*, 949-963.

15. Brooks, M. L., D'Antonio, C. M., Richardson, D. M., Grace, J. B., Keeley, J. E., DiTomaso, J. M., . . . Pyke, D. (2004). Effects of invasive alien plants on fire regimes. *BioScience, 54*(7), 677. doi:10.1641/0006-3568(2004)054[0677:EOIAPO]2.0.CO;2

16. Brown, T. J., Hall, B. L., Mohrle, C. R., & Reinbold, H. J. (2002). *Coarse Assessment of Federal Wildland Fire Occurrence Data: Report for the National Wildfire Coordinating Group.* Desert Research Institute (DRI) Program for Clilmate, Ecosystem and Fire Applications (CEFA).

17. California Department of Forestry and Fire Protection (CAL FIRE) Fire and Resource Assessment (FRAP). (n.d.). GIS database of fire perimeter polygons. Retrieved August 08, 2022, from https://frap.fire.ca.gov/mapping/gis-data/

18. Carli, L. (2023, August 12). *Maui wildfire one of deadliest in U.S. history.* Retrieved from National Fire Protection Association (NFPA): https://www.nfpa.org/News-and-Research/Publications-and-media/Blogs-Landing-Page/NFPA-Today/Blog-Posts/2023/08/12/Maui-wildfire-one-of-deadliest-in-US-history

19. Cayan, D. R., DeHaan, L. L., Gershunov, A., Guzman-Morales, J., Keeley, J. E., Mumford, J., & Syphard, A. D. (2022). Autumn precipitation: the competition with Santa Ana winds in determining fire outcomes in southern California. *International Journal of Wildland Fire, 31*(11), 1056-1067. doi:10.1071/WF22065

20. Chen, B., & Jin, Y. (2022). Spatial patterns and drivers for wildfire ignitions in California. *Environmental Research Letters, 17*, 055004. doi:10.1088/1748-9326/ac60da

21. Chornesky, E. A., Ackerly, D. D., Beier, P., Davis, F. W., Flint, L. E., Lawler, J. J., . . . Weiss, S. (2015). Adapting California's ecosystems to a changing climate. *BioScience, 65*, 247-262. doi:10.1093/biosci/biu233

22. Christensen, N. L. (1994). Fire and soil in Mediterranean shrublands. In J. M. Moreno, & W. C. Oechel (Eds.), *The role of fire in Mediterranean-type ecosystems* (pp. 79-95). New York: Springer.

23. Clemente, R. C., Cerrillo, R. M., & Gitas, I. Z. (2009). Monitoring post-fire regeneration in Mediterranean ecosystems by employing multispectral satellite imagery. *International Journal of Wildland Fire, 18*, 648-658.

24. Conard, S. G., & Weise, D. R. (1998). Management of fire regime, fuels and fire effects in southern California chaparral: lessons from the past and thoughts for the future. *Tall Timbers Fire Ecology Conference Proceedings. 20.* Tallahassee: Tall Timber Research Station.

25. Crimmins, M. A., & Comrie, A. C. (2004). Interactions between antecedent climate and wildfire variability across south-eastern Arizona. *International Journal of Wildland Fire, 13*, 455-466. doi:10.1071/WF03064

26. D'Antonio, C. M., & Vitousek, P. M. (1992). Biological invasion by exotic grasses, the grass/fire cycle, and global change. *Annual Review of Ecology, Evolution, and Systematics, 23*, 63-87. Retrieved from https://www.jstor.org/stable/2097282

27. D'Antonio, C. M., Malmstrom, C., Reynolds, S. A., & Gerlach, J. (2007). Ecology of invasive species in California grassland. In M. R. Stromberg, J. D. Corbin, & C. M. D'Antonio (Eds.), *California grasslands: Ecology and management* (pp. 67-86). Berkeley, California: University of California Press.

28. Davis, G. W., & Richardson, D. M. (1995). *Mediterranean-type Ecosystems: the Function of Biodiversity.* London: Springer.

29. Dennison, P. E., & Roberts, D. A. (2003). Endmember selection for multiple endmember spectral mixture analysis using endmember average RMSE. *Remote Sensing of Environment, 87*, 123-135. doi:10.1016/S0034-4257(03)00135-4

30. Dennison, P. E., Brewer, S. C., Arnold, J. D., & Mortiz, M. A. (2014). Large wildfire trends in the western United States, 1984-2011. *Geophysical Research Letters, 41*(8), 2928-2933. doi:10.1002/2014GL059576

31. Dennison, P. E., Halligan, K. Q., & Roberts, D. A. (2004). A comparison of error metrics and constraints for multiple endmember spectral mixture analysis and spectral angle mapper. *Remote Sensing of Environment, 93*, 359-367. doi:10.1016/j.rse.2004.07.013

32. Di Castri, F., Goodall, D. W., & Specht, R. L. (1981). *Mediterranean-type Shrublands.* Amsterdam: Elsevier.

33. Diaz-Delgado, R., Lloret, F., Pons, X., & Terradas, J. (2002). Satellite evidence of decreasing resilience in Mediterranean plant communities after recurrent wildfires. *Ecology, 83*(8), 2293-2303. doi:10.2307/3072060

34. Downey, D. (2016, September 06). Here's how to avoid accidentally starting the next firestorm. The Press-Enterprise. Retrieved November 01, 2023, from https://www.pressenterprise.com/2016/09/06/heres-how-to-avoid-accidentally-starting-the-next-firestorm/

35. Dudley, K. L., Dennison, P. E., Roth, K. L., Roberts, D. A., & Coates, A. R. (2015). A multitemporal spectral library approach for mapping vegetation species across spatial and temporal phenological gradients. *Remote Sensing of Environment, 167*, 121-134. doi:10.1016/j.rse.2015.005.004

36. Elmore, A. J., Mustard, J. F., Manning, S. J., & Lobell, D. B. (2000). Quantifying vegetation change in semiarid environments: Precision and accuracy of spectral mixture analysis and the normalized difference vegetation index. *Remote Sensing of Environment, 73*, 87-102.

37. Faivre, N., Jin, Y., Goulden, M. L., & Randerson, J. T. (2014). Controls on the spatial pattern of wildfire ignitions in Southern California. *International Journal of Wildland Fire, 23*, 799-811. doi:10.1071/WF13136

38. FGDC [Federal Geographic Data Committee]. (1997). *Vegetation Classification Standard.* Vegetation Subcommittee, Federal Geographic Data Committee, FGDC Secretariat. Reston, Virginia: U.S. Geological Survey.

39. Fusco, E. J., Balch, J. K., Mahood, A. L., Nagy, R. C., Syphard, A. D., & Bradley, B. A. (2021). The human-grass-fire cycle: how people and invasives co-occur to drive fire regimes. *Frontiers in Ecology and the Environment, 20*(2), 117-126. doi:10.1002/fee.2432

40. Fusco, E. J., Finn, J. T., Balch, J. K., Nagy, R. C., & Bradley, B. A. (2019). Invasive grasses increase fire occurrence and frequency across US ecoregions. *PNAS*. doi:10.1073/pnas.1908253116

41. Gillespie, A. (1990). Interpretation of residual images: spectral mixture analysis of AVIRIS images, Owens Valley, California. *Second Airborne Visible/Infrared Imaging Spectrometer (AVIRIS) Workshop* (pp. 243-270). Pasadena, California: NASA.

42. Griffith, G. E., Omernik, J. M., Smith, D. W., Cook, T. D., Tallyn, E., Moseley, K., & Johnson, C. B. (2016). *Ecoregions of California (poster).* U.S. Geological Survey Open File Report 2016-1021.

43. Guzman-Morales, J., & Gershunov, A. (2019). Climate change suppresses Santa Ana winds of Southern California and sharpens their seasonality. *Geophysical Research Letters, 46*(5), 2772-2780. doi:10.1029/2018GL080261

44. Guzman-Morales, J., Gershunov, A., Theiss, J., Li, H., & Cayan, D. (2016). Santa Ana Winds of Southern California: Their climatology, extremes, and behavior spanning six and a half decades. *Geophysical Research Letters, 43*(6), 2827-2834. doi:10.1002/2016GL067887

45. Halsey, R. W. (2008). *Fire, Chaparral, and Survival in Southern California.* Chula Vista, California: Sunbelt Productions Inc.

46. Halsey, R. W., & Syphard, A. D. (2015). High-severity fire in chaparral: cognitive dissonance in the shrublands. In D. A. DellaSala, & C. T. Hanson (Eds.), *The Ecological Importance of Mixed-Severity Fires: Nature's Phoenix* (pp. 177-209). Elsevier Publications Inc.

47. Hamada, Y., Stow, D. A., & Franklin, J. (2009). Quantifying biological integrity of California sage scrub communities using plant life-form cover. *Journal of Mediterraean Ecology, 10*, 19-32.

48. Hamada, Y., Stow, D. A., & Roberts, D. A. (2011). Estimating life-form cover fractions in California sage scrub communities using multispectral remote sensing. *Remote Sensing of Environment, 115*(12), 3056-3068. doi:10.1016/j.rse.2011.06.008

49. Hamada, Y., Stow, D. A., Roberts, D. A., Franklin, J., & Kyriakidis, P. C. (2012). Assessing and monitoring semi-arid shrublands using object-based image analysis and multiple endmember spectral mixture analysis. *Environmental Monitoring and Assessment, 185*, 3173-3190. doi:10.1007/s10661-012-2781-z

50. Hardinsky, M. A., Klemas, V., & Smart, R. M. (1983). The influence of soil salinity, growth form, and leaf moisture on the spectral radiance of Spartina alterniflora canopies. *Photogrammetric Engineering and Remote Sensing, 49*(1), 77-83.

51. Heady, H. F. (1956). Evaluation and measurement of the California annual type. *Journal of Range Management, 9*, 25-27.

52. Hernandez-Clemente, R., Navarro-Cerrillo, R. M., & Gitas, I. Z. (2009). Monitoring post-fire regeneration in Mediterranean ecosystems by employing multitemporal satellite imagery. *International Journal of Wildland FIre, 18*, 648-658. doi:10.1016/j.rse.2011.04..036

53. Hogland, J., & Affleck, D. L. (2019). Mitigating the impact of field and image registration errors through spatial aggregation. *MDPI: Remote Sensing, 11*(3), 222. doi:10.3390/rs11030222

54. Huenneke, L. F. (1989). Grassland structure and function: California annual grasslands. In L. F. Huenneke, & H. A. Mooney (Eds.), *The California Annual Grassland: An Overview* (pp. 1-12). Dordrecht, The Netherlands: Kluwer Academic Publishers.

55. Jackson, R. D., & Bartolome, J. W. (2002). A state-transition approach to understanding nonequilibrium plant community dynamics in California grasslands. *Plant Ecology, 162,* 49-65.

56. Jacobsen, A. L., & Pratt, R. B. (2019). Extensive drought-associated plant mortality as an agent of type-conversion in chaparral shrublands. *New Phytologist, 219*, 498-504.

57. Jain, M., Mondal, P., DeFries, R. S., Small, C., & Galford, G. L. (2013). Mapping cropping intensity of smallholder farms: a comparison of methods using multiple sensors. *Remote Sensing of Environment, 134*, 210-223. doi:10.1016/j.rse.2013.02.029

58. Jarocinska, A., Kopec, D., Niedzielko, J., Wylazlowska, J., Halladin-Dabrowska, A., Charyton, J., . . . Kaminski, D. (2023). The utility of airborne hyperspectral and satellite multispectral images in identifying Natura 2000 non-forest habitats for conservation purposes. *Scientific Reports, 13*(4549). doi:10.1038/s41598-023-31705-6

59. Jensen, J. R. (2016). *Introductory Digital Image Processing: A Remote Sensing Perspective* (Fourth ed.). Pearson Education Inc.

60. Jin, J., Li, M., & Jin, L. (2015a). Data normalization to accelerate training for linear neural net to predict tropical cyclone tracks. *Mathematical Problems in Engineering, 2015*(5), 1-8. doi:10.1155/2015/931629

61. Jin, Y., Goulden, M., Faivre, S., Veraverbeke, V., Hall, A., Hand, M., . . . Randerson, J. (2015b). Identification of two distinct fire regimes in southern California: implications for economic impact and future change. *Environmental Research Letters*, 10:094005.

62. Jones, M. O., Allred, B. W., Naugle, D. E., Maestas, J. D., Donnelly, P., Metz, L. J., . . . McIver, J. D. (2018). Innovation in rangeland monitoring: annual, 30 m, plant functional type percent cover maps for U.S. rangelands, 1984-2017. *Ecosphere, 9*(9), e02430. doi:10.1002/ecs2.2430

63. Jones, M. O., Robinson, N. P., Naugle, D. E., Maestas, J. D., Reeves, M. C., Lankston, R. W., & Allred, B. W. (2021). Annual and 16-day rangeland production estimates for the Western United States. *Rangeland Ecology & Management, 77*, 112-117. doi:10.3390/rs9080863

64. Keeley, J. E. (2000). Chaparral. In M. G. Barbour, & W. D. Billings (Eds.), *North American Terrestrial Vegetation* (Second ed., pp. 203-254). Cambridge University Press.

65. Keeley, J. E. (2001, November). Fire and invasive species in Mediterranean-climate ecosystems of California. *Proeedings of the Invasive Species Workshop: The role of fire in the control and spread of invasive species, Fire Conference 2000, The First*

National Congress on Fire Ecology, Prevention, and Management 27, 81-94. (K. E. Galley, & T. P. Wilson, Eds.) San Diego, California: Tall Timbers Research Station Tallahassee, Florida.

66. Keeley, J. E., & Brennan, T. J. (2012). Fire-driven alien invasion in a fire-adapted ecosystem. *Oecologia, 169*, 1043-1052.

67. Keeley, J. E., & Davis, F. W. (2007). Chaparral. In M. G. Barbour, T. Keeler-Wolf, & A. A. Schoeenherr (Eds.), *Terrestrial Vegetation of California* (pp. 339-366). Berkeley, California: University of California Press.

68. Keeley, J. E., & Syphard, A. D. (2016). Climate change and future fire regimes: examples from California. *Geoscience Canada*. doi:10.3390/GEOSCIENCES6030037

69. Keeley, J. E., & Syphard, A. D. (2018). Historical patterns of wildfire ignition sources in California ecosystems. *International Journal of Wildland Fire, 27*, 781-799. doi:10.1071/WF18026

70. Keeley, J. E., & Syphard, A. D. (2019). Twenty-first century California, USA, wildfires: fuel-dominated vs. wind-dominated fires. *Fire Ecology*, 15-24. doi:10.1186/s42408-012-0041-0

71. Keeley, J. E., Brennan, T. J., & Syphard, A. D. (2022). The effects of prolonged drought on vegetation dieback and megafires in southern California chaparral. *Ecosphere, 13*(8), e4203.

72. Kellman, M. (1980). *Plant Geography* (Second ed.). New York: St. Martin's Press.

73. Keshava, N., & Mustard, J. (2002). Spectral unmixing. *IEEE Signal Processing Magazine, 19*, 44-57. doi:10.1109/79.974727

74. Knapp, P. A. (1998). Spatio-temporal patterns of large grassland fires in the Intermountain West, USA. *Global Ecology and Biogeography, 7*, 259-272. doi:10.2307/2997600

75. Lavorel, S. (1999). Ecological diversity and resilience of Mediterranean vegetation to disturbance. *Diversity and Distributions, 5*, 3-13. doi:10.1046/J.1472-4642.1999.00033.X

76. Li, S., & Banerjee, T. (2021). Spatial and temporal pattern of wildfires in California from 2000 to 2019. *Scientific Resports, 11*(8779). doi:10.1038/s41598-021-88131-9

77. Lieth, H. (1974). *Phenology and Seasonality Modeling* (First ed.). London, England: Chapman and Hall.

78. Link, S. O., Keeler, C. W., Hill, R. W., & Hagen, E. (2006). Bromus tectorum cover mapping and fire risk. *International Journal of Wildland Fire*, 113-119. doi:10.1071/WF05001

79. Lippitt, C. L., Stow, D. A., O'Leary, J. F., & Franklin, J. (2013). Influence of short-interval fire occurrence on post-fire recovery of fire-prone shrublands in California, USA. *International Journal of Wildland Fire, 22*, 184-193. doi:10.1071/WF10099

80. Lippitt, C. L., Stow, D. A., Roberts, D. A., & Coulter, L. L. (2017). Multidate MESMA for monitoring vegetation growth forms in southern California shrublands. *International Journal of Remote Sensing, 39*(3), 655-683. doi:10.1080/01431161.2017.1388936

81. Liu, Y., Stanturf, J., & Goodrick, S. (2010). Trends in global wildfire potential in a changing climate. *Forest Ecology and Management, 259*(4), 685-697. doi:10.1016/j.foreco.2009.09.002

82. Lobell, D. B., & Asner, G. P. (2004). Cropland distributions from temporal unmixing of MODS data. *Remote Sensing of Environment, 93*, 412-422.

83. Mack, M. C., & D'Antonio, C. M. (1998). Impacts of biological invasions on disturbance regimes. *Trends in Ecology and Evolution, 13*, 195-198.

84. Mack, M. C., D'Antonio, C. M., & Ley, R. (2001). Pathways through which exotic grasses alter N cycling in a seasonally dry Hawaiian woodland. *Ecological Applications, 11*, 1323-1335.

85. Maestas, J., Jones, M., Pastick, N. J., Rigge, M. B., Wylier, B. K., Garner, L., . . . Witacre, B. (2020). *Annual Herbaceous Cover across Rangelands of the Sagebrush Biome.* U.S. Geological Survey data release. doi:10.5066/P9VL3LD5

86. McMichael, C. E., Hope, A. S., & Roberts, D. (2004). Post-recovery of leaf area index in California chaparral: a remote sensing-chronosequence approach. *International Journal of Remote Sensing, 25*, 4743-4760.

87. Merriam, K. E., Keeley, J. E., & Beyers, J. L. (2006). Fuel breaks affect nonnative species abundance in Californian plant communities. *Ecological Applications, 16*(2), 515-527. doi:10.1890/1051-0761(2006)016[0515:FBANSA]2.0.CO;2

88. Nill, L., Grunberg, I., Ullmann, T., Gessner, M., Boike, J., & Hostert, P. (2022). Arctic shrub expansion revealed by Landsat-derived multitemporal vegetation cover fractions in the Western Canadian Arctic. *Remote Sensing of Environment, 281*, 113228. doi:10.1016/j.rse.2022.113228

89. Olsson, A. D., Van Leeuwen, W. J., & Marsh, S. E. (2011). Feasbility of invasive grass detection in desertscrub community using hyperspectral field measurements and Landsat TM imagery. *MDPI: Remote Sensing, 3*(10), 2283-2304. doi:10.3390/rs3102283

90. Paddock III, W. A., Davis, S. D., Pratt, R. B., Jacobsen, A. L., Tobin, M. F., Lopez-Portillo, J., & Ewers, F. W. (2013). Factors determining mortality of adult chaparral shrubs in an extreme drought year in California. *Aliso: A Journal of Systematic and Floristic Botany, 31*, 49-57. doi:10.5642/aliso.20133101.08

91. Park, I. W., & Jenerette, G. D. (2019). Causes and feedbacks to widespread grass invasion into chaparral shrub dominated landscapes. *Landscape Ecology, 34*(3), 459-471. doi:10.1007/s10980-019-00800-3

92. Park, I. W., Hooper, J., Flegal, J. M., & Jenerette, G. D. (2018). Impacts of climate, disturbance and topography on distribution of herbaceous cover in Southern California chaparral: Insights from a remote-sensing method. *Diversity and Distributions, 24*(4), 497-508. doi:10.1111/ddi.12693

93. Peddle, D. R., Brunke, S. P., & Hall, F. G. (2001). A comparison of spectral mixture analysis and ten vegetation indices for estimating boreal forest biophysical information from airborne data. *Canadian Journal of Remote Sensing, 27*, 627-635.

94. Pena-Barragan, J. M., Ngugi, M. K., Plant, R. E., & Six, J. (2011). Object-based crop identification using multiple vegetation indices, textural features and crop phenology. *Remote Sensing of Environment, 115*(6), 1301-1316. doi:10.1016/j.rse.2011.01.009

95. Peterson, S. H., & Stow, D. A. (2003). Using multiple endmember spectral mixture analysis to study chaparral regrowth in southern California. *International Journal of Remote Sensing, 24*(22), 4481-4504. doi:10.1080/0143116031000082415

96. Pickett, S. T., & White, P. S. (1985). *The Ecology of Natural Disturbance and Patch Dynamics.* New York: Academic Press.

97. Piwowar, J. M., Peddle, D. R., & LeDrew, E. F. (1998). Temporal mixture analysis of arctic sea ice imagery: a new approach for monitoring environmental change. *Remote Sensing of Environment, 63*(3), 195-207. doi:10.1016/S0034-4257(97)00105-3

98. Powell, R. L., Roberts, D. A., Dennison, D. E., & Hess, L. L. (2007). Sub-pixel mapping of urban land cover using multiple endmember spectral mixture analysis: Manaus, Brazil. *Remote Sensing of Environment, 106*(2), 253-267. doi:10.1016/j.rse.2006.09.005

99. Pratt, R. B., Jacobsen, A. L., Ramirez, A. R., Helms, A. M., Traugh, C. A., Tobin, M. F., . . . Davis, S. D. (2014). Mortality of resprouting chaparral shrubs after a fire and during a record drought: physiological mechanisms and demographic consequences. *Global Change Biology, 20*, 893-907.

100. Pryde, P. R. (2004). *San Diego: An Introduction to the Region* (Fourth ed.). San Diego: Sunset Publications/Pearson Custom Publishing.

101. Quarmby, N. A. (1992). Towards continental scale crop area estimation. *International Journal of Remote Sensing, 13*(5), 981-989. doi:10.1080/01431169208904172

102. Quarmby, N. A., Townshend, J. R., Settle, J. J., White, K. H., Milnes, M., Hindle, T. L., & Silleos, N. (1992). Linear mixture modelling applied to AVHRR data for crop area estimation. *International Journal of Remote Sensing, 13*(3), 415-425. doi:10.1080/01431169208904046

103. Quintano, C., Fernandez-Manso, A., & Roberts, D. A. (2017). Burn severity mapping from Landsat MESMA fraction images and Land Surface Temperature. *Remote Sensing of Environment, 190*, 83-95.

104. Quintano, C., Shimabukuro, Y. E., Fernandez, A., & Delgado, J. A. (2005). A spectral unmixing approach for mapping burned areas in Mediterranean countries. *International Journal of Remote Sensing, 26*(7), 1493-1498. doi:10.1080/01431160412331330220

105. Radeloff, V. C., Hammer, R. B., Stewart, S. I., Fried, J. S., Holcomb, S. S., & McKeefry, J. F. (2005). The wildland-urban interface in the United States. *Ecological Applications, 15*(3), 799-805.

106. Radeloff, V. C., Helmers, D. P., Kramer, H. A., Mockrin, M. H., Alexandre, P. M., Bar-Massada, A., . . . Stewart, S. I. (2018). Rapid growth of the US wildland-urban interface raises wildfire risk. *PNAS*. doi:10.1073/pnas.1718850115

107. Riano, D., Chuvieco, E., Ustin, S., Zomer, R., Dennison, P., Roberts, D., & Salas, J. (2002). Assessment of vegetation regeneration after fire through multitemporal analysis of AVIRIS images in the Santa Monica Mountains. *Remote Sensing of Environment, 79*, 60-71.

108. Roberts, D. A., Dennison, P. E., Gardner, M. E., Hetzel, Y., Ustin, S. L., & Lee, C. T. (2003). Evaluation of the potential of Hyperion for fire danger assessment by comparison to the airborne visible/infrared imaging spectrometer. *IEEE Transactions on Geoscience and Remote Sensing, 41*, 1297-1310. doi:10.1109/TGRS.2003.812904

109. Roberts, D. A., Gardner, M., Church, R., Ustin, S., Scheer, G., & Green, R. O. (1998). Mapping chaparral in the Santa Monica Mountains using Multiple Endmember Spectral Mixture Models. *Remote Sensing of Environment, 65*(3), 267-279. doi:10.1016/S0034-4257(98)00037-6

110. Roberts, D. A., Halligan, K., Dennison, P., Dudley, K., Somers, B., & Crabbe, A. (2019a). Viper Tools User Manual (Version 2.1).

111. Roberts, D. A., Numata, I., Holmes, K., Batista, G., Krug, T., Monteiro, A., . . . Chadwick, O. A. (2002). Large area mapping of landcover change in Rondonia

using multitemporal spectral mixture analysis and decision tree classifiers. *Journal of Geophysical Research - Atmospheres, 107*, 8073.

112. Roberts, D. A., Roth, K. L., Wetherley, E. B., Meerdink, S. K., & Perroy, R. L. (2019b). Hyperspectral Vegetation Indices. In P. S. Thenkabail, J. G. Lyon, & A. Huete (Eds.), *Hyperspectral Remote Sensing of Vegetation* (Second ed., Vol. II). CRC Press.

113. Roder, A., Hill, J., Duguy, B., Alloza, J., & Vallejo, R. (2008). Using long time series of Landsat data to monitor fire events and post-fire dynamics and identify driving factors. A case study in the Ayora region (eastern Spain). *Remote Sensing of Environment, 112*(1), 259-273. doi:10.1016/j.rse.2007.05.001

114. Rogan, J., Franklin, J., & Roberts, D. A. (2002). A comparison of methods for monitoring multitemporal vegetation change using Thematic Mapper imagery. *Remote Sensing of Environment, 80*(1), 143-156.

115. Roth, K. L., Dennison, P. E., & Roberts, D. A. (2012). Comparing endmember selection techniques for accurate mapping of plant species and land cover using imaging spectrometer data. *Remote Sensing of Environment, 127*, 139-152. doi:10.1016.j.rse.2012.08.030

116. Rouse, J. W., Haas, R. H., Schell, J. A., & Deering, D. W. (1973). Monitoring vegetation systems in the Great Plains with ERTS. *Proceedings of the Earth Resources Technology Satellite Symposium. 1*, pp. 309-317. NASA SP-351 Washington DC.

117. Rundel, P. W. (1998). *Landscape disturbance and biodiversity in Mediterranean-type ecosystems.* Springer.

118. Rundel, P. W. (2007). Sage Scrub. In M. G. Barbour, T. Keeler-Wolf, & A. A. Schoenherr (Eds.), *Terrestrial Vegetation of California* (Third ed., pp. 208-228). Berkeley, California: University of California Press.

119. Safford, H. D., & Van de Water, K. M. (2014). *Using fire return interval depature (FRID) analysis to map spatial and temporal changes in fire frequency on national forest lands in California.* PSW-RP-266, U.S. Department of Agriculture, Forest Service, Pacific Southwest Research Station, Albany, CA.

120. Schmidt, K. M., Menakis, J. P., Hardy, C. C., Hann, W. J., & Bunnell, D. L. (2002). *Development of coarse-scale spatial data for wildland fire and fuel management.* Fort Collins: USDA Forest Service, Rocky Mountain Research Station.

121. Schwartz, M. W., & Syphard, A. D. (2021). Fitting the solutions to the problems in managing extreme wildfire in California. *Environment Research Communications, 3*, 081005. doi:10.1088/2515-7620/ac15e1

122. Settle, J. J., & Drake, N. A. (1993). Linear mixing and the estimation of ground cover proportions. *International Journal of Remote Sensing, 14*(6), 1159-1177. doi:10.1080/01431169308904402

123. Shih, H., Stow, D. A., Tsai, Y., & Roberts, D. A. (2020). Estimating the starting time and identifying the type of urbanization based on dense time series of landsat-derived Vegetation-Impervious-Soil (V-I-S) maps - A case study of North Taiwan from 1990 to 2015. *International Journal of Applied Earth Observation and Geoinformation, 85*, 101987. doi:10.1016/j.jag.2019.101987

124. Short, K. C. (2014). A spatial database of wildfires in the United States, 1992-2011. *Earth System Science Data, 6*, 1-27. doi:10.5194/essd-6-1-2014

125. Short, K. C. (n.d.). Spatial wildfire occurrence data for the United States, 1992-2020 [FPA FOD 20221014]. (Sixth). Fort Collins, CO: Forest Service Research Data Archive. doi:10.2737/RDS-2013-0009.6

126. Show, S. B., & Kotok, E. I. (1923). Forest fires in California, 1911-1920: an analytical study. 83. Washington, DC: Government Printing Office.

127. Singh, K. K., & Gray, J. (2020). Mapping understory invasive plants in urban forests with spectral and temporal unmixing of Landsat imagery. *Photogrammetric Engineering & Remote Sensing, 86*(8), 509-518. doi:10.14358/PERS.86.8.509

128. Small, C. (2012). Spatiotemporal dimensionality and time-space characterization of multitemporal imagery. *Remote Sensing of Environment, 124*, 793-809. doi:10.1016/j.rse.2023.05.031

129. Small, C., & Sousa, D. (2019). Spatiotemporal characterization of mangrove phenology and disturbance response. *Remote Sensing, 11*, 2063. doi:10.3390/rs11172063

130. Smith, M. O., Ustin, S. L., Adams, J. B., & Gillespie, A. R. (1990). Vegetation in deserts: I. A regional measure of abundance from multispectral images. *Remote Sensing of Environment, 31*, 1-26. doi:10.1016-0034-4257(90)90074-V

131. Somers, B., Asner, G. P., Tits, L., & Coppin, P. (2011). Endmember variability in Spectral Mixture Analysis: A review. *Remote Sensing of Environment, 115*(7), 1603-1616. doi:10.1016/j.rse.2011.03.003

132. Sousa, D., & Davis, F. W. (2020). Scalable mapping and monitoring of Mediterranean-climate oak landscapes with temporal mixture models. *Remote Sensing of Environment, 247*, 111937. doi:10.1016/j.rse.2020.111937

133. Sousa, D., & Small, C. (2019). Mapping and monitoring rice agriculture with multisensor temporal mixture models. *Remote Sensing, 11*, 181. doi:10.3390/rs11020181

134. Sousa, D., Small, C., Spalton, A., & Kwarteng, A. (2019). Coupled spatiotemporal characterization of monsoon cloud cover and vegetation phenology. *Remote Sensing, 11*, 1203. doi:10.3390/rs11101203

135. Sousa, W. P. (1984). The role of disturbance in natural communities. *Annual Review of Ecology and Systematics, 15*, 353-391.

136. South Dakota Grassland Coalition. (2017). Healthy Grasslands. In A. J. Smart, P. J. Bauman, & J. Lefers (Eds.), *Greener Pastures* (Second ed., pp. 1-40).

137. Steinberg, M. (2022, January 03). *Hard truths about a hard time: Marshall Fire devastation illustrates conditions leading to wildfire disaster.* Retrieved from National Fire Protection Association (NFPA): https://www.nfpa.org/News-and-Research/Publications-and-media/Blogs-Landing-Page/Fire-Break/Blog-Posts/2022/01/03/Hard-truths-about-a-hard-time-Marshall-Fire-devastation-illustrates-conditions

138. Storey, E. A., Stow, D. A., & O'Leary, J. F. (2016). Assessing postfire recovery of chamise chaparral using multi-temporal spectral vegetation index trajectories derived from Landsat imagery. *Remote Sensing of Environment, 183*, 53-64. doi:10.1016/j.rse.2016.05.018

139. Storey, E. A., Stow, D. A., O'Leary, J. F., Davis, F. W., & Roberts, D. A. (2021). Does short-interval fire inhibit postfire recovery of chaparral across southern California? *Science of the Total Environment, 751*, 142271.

140. Syphard, A. D., & Keeley, J. E. (2015). Location, timing, and extent of wildfire vary by cause of ignition. *International Journal of Wildland Fire, 24*(1), 37-47. doi:10.1071/WF14024

141. Syphard, A. D., & Keeley, J. E. (2019). Factors associated with structure loss in the 2013-2018 California wildfires. *Fire, 2*(3), 49. doi:10.3390/fire2030049

142. Syphard, A. D., Brennan, T. J., & Keeley, J. E. (2014). The role of defensible space for residential structure protection during wildfires. *International Journal of Wildland Fire, 23*, 1165-1175. doi:10.1071/WF13158

143. Syphard, A. D., Brennan, T. J., & Keeley, J. E. (2018). Chaparral Landscape Conversion in Southern California. In E. C. Underwood, H. D. Safford, N. A. Molinari, & J. E. Keeley (Eds.), *Valuing Chaparral* (pp. 323-346). Springer International Publishing. doi:10.1007/978-3-319-68303-4_12

144. Syphard, A. D., Brennan, T. J., & Keeley, J. E. (2019a). Extent and drivers of vegetation type conversion in Southern California chaparral. *Ecosphere, 10*(7), e02796. doi:10.1002/ecs2.2796

145. Syphard, A. D., Radeloff, V. C., Keeley, J. E., Hawbaker, T. J., Clayton, M. K., Stewart, S. I., & Hammer, R. B. (2007). Human influence on California fire regimes. *Ecological Applications, 17*(5), 1388-1402. doi:10.1890/06-1128.1

146. Syphard, A. D., Rustigian-Romsos, H., Mann, M., Conlisk, E., Moritz, M. A., & Ackerly, D. (2019b). The relative influence of climate and housing development on current and projected future fire patterns and structure loss across three California landscapes. *Global Environmental Change, 56*, 41-55. doi:10.1016/j.gloenvcha.2019.03.007

147. Tompkins, S., Mustard, J. F., Pieters, C. M., & Forsyth, D. W. (1997). Optimization of endmembers for spectral mixture analysis. *Remote Sensing of Environment, 59*(3), 472-489.

148. U.S. Department of Agriculture (USDA) and U.S. Forest Service (USFS), Southwestern Region, Regional GIS Coordinator. (n.d.). Fire Occurrence Point. Vector digital data. Retrieved September 30, 2023, from https://data.fs.usda.gov/geodata/edw/datasets.php?xmlKeyword=ignition

149. U.S. Environmental Protection Agency (EPA). (2013). Level III ecoregions of California. U.S. EPA Office of Research and Development (ORD), National Health and Environmental Effects Research Laboratory (NHEERL).

150. Urbanski, S. P., Salmon, J. M., Nordgren, B. L., & Hao, W. M. (2009). A MODIS direct broadcast algorithm for mapping wildfire burned area in the western United States. *Remote Sensing of Environment, 113*, 2511-2523. doi:10.1016/j.rse.2009.07.007

151. USAFACTS. (2022, July). *Our Changing Population: San Diego County, California*. Retrieved October 26, 2023, from USAFACTS: https://usafacts.org/data/topics/people-society/population-and-demographics/our-changing-population/state/california/county/san-diego-county/?endDate=2020-01-01&startDate=1992-01-01

152. Uyeda, K. A., Stow, D. A., O'Leary, J. F., Schmidt, I. T., & Riggan, P. J. (2016). Spatial variation of fuel loading within varying aged stands of chaparral. *Applied Vegetation Science, 19*(2), 267-279. doi:10.1111/avsc.12209

153. Ventura, M., MacKinnon, E., Dario, H., Jacobsen, A., Pratt, R., & Davis, S. (2016). Chaparral shrub hydraulic traits, size, and life history types relate to species mortality during California's historic drought of 2014. *PLoS ONE, 11*, e0159145.

154. Veraverbeke, S., & Hook, S. J. (2013). Evaluating spectral indices and spectral mixture analysis for assessing fire severity, combustion completeness and carbon emissions. *International Journal of Wildland Fire, 22*, 707-720. doi:10.1071/WF12168

155. Whittaker, R. H. (1975). *Communities and Ecosystems* (Second ed.). New York: The Macmillan Company.

156. Zapisocki, Z., de Assis Murillo, R., & Wagner, V. (2022). Non-native plant invasions in prairie grasslands of Alberta, Canada. *Rangeland Ecology and Management, 83*(1), 20-30. doi:10.1016/j.rama.2022.02.011

157. Zedler, P. H., Gautier, C. R., & McMaster, G. S. (1983). Vegetation change in response to extreme events: the effect of a short interval between fires in California chaparral and coastal scrub. *Ecology, 64*(4), 809-818. doi:10.2307/1937204